Pseudotoothed Birds (Aves, Odontopterygiformes) from the Early Tertiary of Morocco

Authors: Bourdon, Estelle, Amaghzaz, Mbarek, and Bouya, Baâdi

Source: American Museum Novitates, 2010(3704) : 1-71

Published By: American Museum of Natural History

URL: https://doi.org/10.1206/3704.2

AMERICAN MUSEUM NOVITATES

Number 3704 December 20, 2010

Pseudotoothed Birds (Aves, Odontopterygiformes) from the Early Tertiary of Morocco

ESTELLE BOURDON,[1] MBAREK AMAGHZAZ,[2] AND BAÂDI BOUYA[2]

ABSTRACT

We describe here new specimens of pseudotoothed birds (Odontopterygiformes) from the Upper Paleocene and Lower Eocene of the Ouled Abdoun Basin, Morocco. These Lower Paleogene fossils are among the oldest representatives of the Odontopterygiformes and include braincases, beak fragments, and long bones. *Dasornis toliapica* (Owen, 1873) (2–3 m wingspan) and *Dasornis emuinus* (Bowerbank, 1854) (3.5–4.5 m wingspan) were initially described from the Lower Eocene London Clay of Sheppey, England. The new species *Dasornis abdoun* (1.5–1.7 m wingspan) constitutes the smallest species of pseudotoothed bird ever discovered. We partly revise the oversplit taxonomy of the odontopterygiforms: the two species from the Paleogene of England and Morocco are regarded as congeneric, the name *Dasornis* having priority over the name *Odontopteryx*. We also synonymize *Neptuniavis minor* Harrison and Walker, 1977, and *Macrodontopteryx oweni* Harrison and Walker, 1976, with *D. toliapica* (Owen, 1873). Moreover, the genera *Pelagornis* Lartet, 1857, and *Osteodontornis* Howard, 1957, are regarded as pertaining to one single taxonomic entity that corresponds to the *Pelagornis* morphotype. In *Dasornis*, the morphological peculiarities of the humerus that are related to gliding flight are less pronounced than in *Pelagornis*. The latter taxon includes exceedingly specialized gliders that were most likely unable of sustained flapping flight and relied almost entirely on winds to provide lift. Pseudotoothed birds pertaining to the *Dasornis* morphotype were more generalists and could probably undertake flapping flight, even if limited. The species of *Dasornis* were soaring pelagic feeders that could disperse over large territories like extant albatrosses. They formed large breeding colonies near the shore of the

[1]American Museum of Natural History, Dept of Ornithology, Central Park West at 79th St, New York, NY 10024, USA (ebourdon@amnh.org).
[2]Office Chérifien des Phosphates, Centre Minier de Khouribga, Khouribga, Morocco.

 ISSN 0003-0082

northeastern part of the Moroccan phosphate sea, some 55 million years ago. Our work provides evidence that *Dasornis* was widespread in the early Tertiary, as it is currently known from the Lower Paleogene deposits of Morocco, England, and Kazakhstan. Paleoenvironmental studies show that these marine deposits formed in a tropical climate. This could explain the occurrence of both *Dasornis* and prophaethontids in all three Paleogene localities.

INTRODUCTION

A convention between the Muséum National d'Histoire Naturelle (France) and the Moroccan authorities has led to the recent discovery of fossil neornithine birds in the Lower Paleogene phosphatic deposits of the Ouled Abdoun Basin, Morocco (Bourdon, 2005, 2006a, 2006b; Bourdon et al., 2005, 2008a, 2008b). So far, described taxa comprise two species of tropicbird-like seabirds, namely, the prophaethontid *Lithoptila abdounensis* Bourdon, 2005 (Bourdon et al., 2005, 2008b) and the possibly phaethontid *Phaethusavis pelagicus* Bourdon, 2008 (Bourdon et al., 2008a). We describe here new specimens of pseudotoothed birds (Odontopterygiformes, Pelagornithidae) from the Upper Paleocene and Lower Eocene of the Ouled Abdoun Basin.

Pseudotoothed birds had a worldwide distribution and wandered the seas for approximately 55.5 million years, from the Upper Paleocene to the latest Pliocene. In Eurasia, remains are known from the Upper Paleocene (Harrison, 1985), Lower Eocene (Harrison and Walker, 1976; Mayr, 2008), and possibly Lower Oligocene (Harrison and Walker, 1979) of England; Middle Eocene of Belgium (Mayr and Smith, 2010); Miocene of France (Lartet, 1857) and Portugal (Mayr et al., 2008); Upper Paleocene of Kazakhstan and Eocene of Uzbekistan (Averianov et al., 1991); Oligocene of Azerbaijan (Aslanova and Burchak-Abramovich, 1999); Oligocene (Hasegawa et al., 1986; Okazaki, 1989), Miocene (Ono, 1989; Matsuoka et al., 1998), and Pliocene (Ono et al., 1985) of Japan. In Africa, pseudotoothed birds were first described from the Middle Eocene of Nigeria (Andrews, 1916). Recently, Mourer-Chauviré and Geraads (2008) described some fossils from the latest Pliocene of Morocco.

Odontopterygiformes are also abundantly represented in the New World, with fossils described from the Eocene (Goedert, 1989; Olson, 1999), Oligocene (Shufeldt, 1916; Wetmore, 1917; Hopson, 1964; Olson, 1985), and Miocene (Howard, 1957, 1978; Howard and White, 1962; Olson, 1984, 1985; Rasmussen, 1998; Olson and Rasmussen, 2001; Stidham, 2004) of North America; Oligocene of Canada (Cope, 1894; Olson, 1985); Middle Eocene (González-Barba et al., 2002) and late Miocene (González-Barba et al., 2004) of Central America; and Miocene and Pliocene of South America (Cheneval, 1993; Walsh and Hume, 2001; Rincón and Stucchi, 2003; Chavez et al., 2007), including undescribed material from the Miocene of Peru (GoGeometry, 2009). Some remains were also recovered from the Middle Eocene (Stilwell et al., 1998) to late Eocene of Antarctica (Tonni, 1980; Tonni and Tambussi, 1985; Tambussi and Hospitaleche, 2007) and from the Miocene (Howard and Warter, 1969; Scarlett, 1972) to Pliocene (McKee, 1985) of New Zealand. Thus, the pseudotoothed birds from the Upper Paleocene/Lower Eocene phosphates of Morocco are among the oldest representatives of this group.

INSTITUTIONAL ABBREVIATIONS

AMNH, American Museum of Natural History, New York, USA; BMNH, Natural History Museum, London, United Kingdom; D1, Rhinopolis Association, Gannat, France; LACM, Natural History Museum of Los Angeles County, Los Angeles, USA; MEM, Ministry of Energy and Mines, Rabat, Morocco; MHNL, Muséum d'Histoire Naturelle de Lyon, Lyon, France; MHNM, Muséum d'Histoire Naturelle de Marrakech, Marrakech, Morocco; MNHN, Muséum National d'Histoire Naturelle, Paris, France; NHM, Natural History Museum, London, United Kingdom; NMNH, National Museum of Natural History, Washington, USA; OCP, Office Chérifien des Phosphates, Casablanca, Morocco; OCP.DEK/GE, Office Chérifien des Phosphates, Direction des Exploitations de Khouribga, Service de Géologie, Morocco; USNM, National Museum of Natural History, Washington, USA.

MATERIAL AND METHODS

The new material referred to *Dasornis* includes 233 fossil specimens deposited in four institutions: OCP (203 specimens), MHNL (24), D1 (5) and MHNM (1). Most specimens come from Grand Daoui, which is located in the northeastern part of the Ouled Abdoun Basin (fig. 1). A few of them come from southern Meraa El Arech and Sidi Chennane (fig. 1). Fossils are found in Upper Paleocene (Thanetian) and Lower Eocene (Ypresian) levels (fig. 2), and most of them are dated as lowermost Ypresian (Intercalary bed II/bed I of mining terminology). The

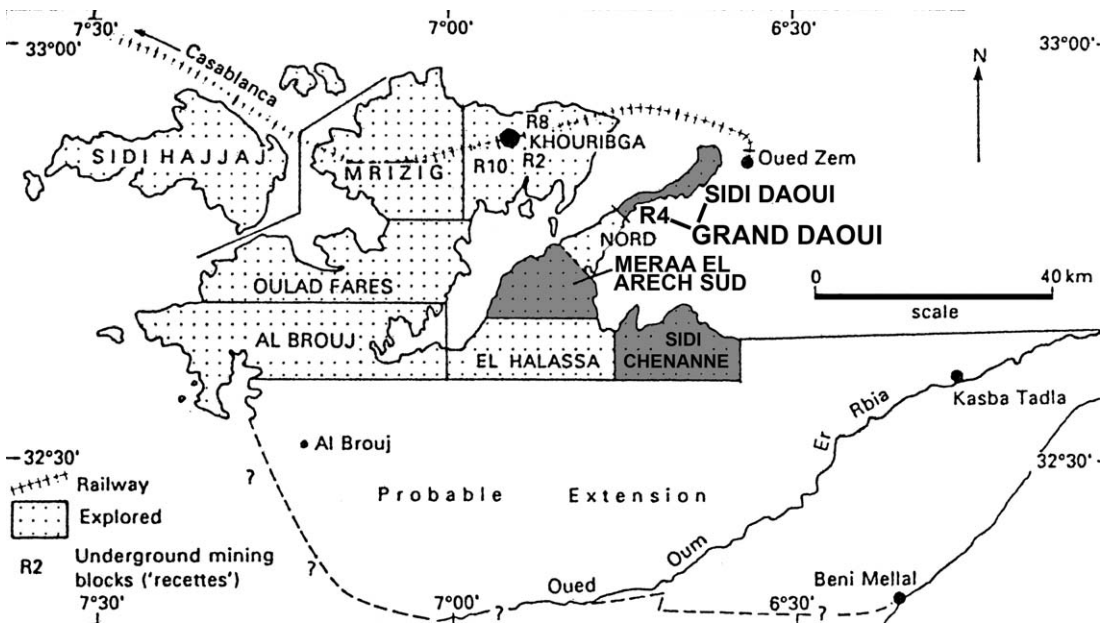

FIGURE 1. Ouled Abdoun Basin, Morocco. Gray areas indicate the localities where *Dasornis* was found (after Office Chérifien des Phosphates, 1989, modified).

Ouled Abdoun specimens include braincases, beak fragments, and postcranial elements including bones of the pectoral belt, forelimb, and hind limb. Fossils were prepared with 10% formic acid and mechanically. Measurements were made with dial caliper accurate to 0.1 mm. Anatomical terminology follows Baumel et al. (1993) and Livezey and Zusi (2006), unless stated otherwise.

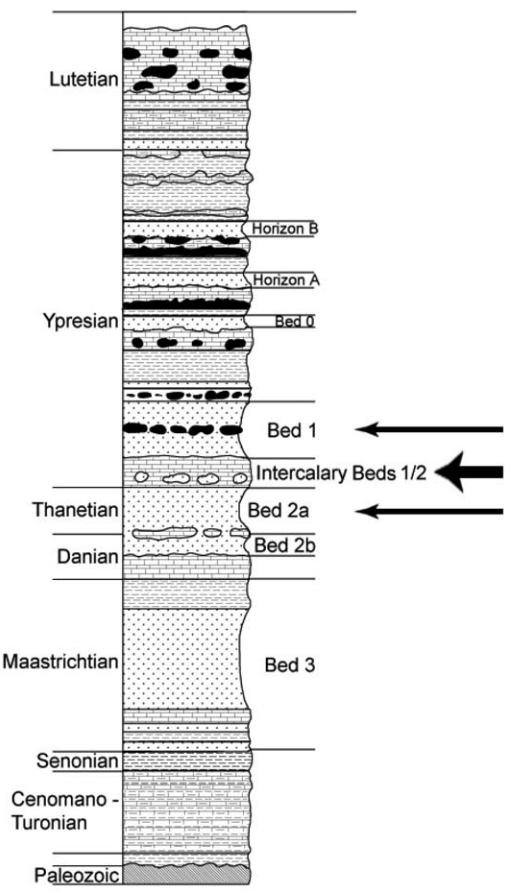

FIGURE 2. Stratigraphical column of the Phosphates Series in the Ouled Abdoun Basin, area of Grand Daoui (after Gharbi, 1998, and OCP, Khouribga mining service). Stratigraphy and mining terminology of the phosphate levels. Arrows indicate the horizons in which *Dasornis* was found.

SYSTEMATIC PALEONTOLOGY

Odontopterygiformes Howard, 1957
Pelagornithidae Fürbringer, 1888
Dasornis Owen, 1870

Odontopteryx Owen, 1873.
Macrodontopteryx Harrison and Walker, 1976.
See Mayr (2008) for a complementary list of synonymies.

Stratigraphic and Geographical Distribution: Upper Paleocene/Lower Eocene of Morocco (this study); Upper Paleocene of Kazakhstan (Nessov, 1992); Lower Eocene of England (Harrison and Walker, 1976; Mayr, 2008).

Amended Diagnosis (from Harrison and Walker, 1976): Small to large pseudotoothed birds that differ from *Pelagornis*/*Osteodontornis* in the following features: no distinct impressio glandulae nasalis; sulcus nervi olfactorii narrow and curved; facies articularis parasphenoidalis of os pterygoideum elongated and pedunculate; humerus, tuberculum dorsale smooth and distal to craniocaudally narrow caput; proximodistally elongated crista deltopectoralis showing evenly curved outer margin; fossa pneumotricipitalis very large, bearing one or two pneumatic foramina; large intumescentia humeri; corpus humeri not flattened in proximal region; epicondylus dorsalis very prominent and caudocranially flattened; ulna, cotyla ventralis round, smaller, and much less prominent ventrally; olecranon more prominent; tuberculum ligamenti collateralis ventralis prominent and proximodistally elongated; extremitas distalis ulnae shaped like isosceles triangle, with condylus dorsalis, condylus ventralis, and tuberculum carpale of same width; radius, cotyla humeralis more caudocranially flattened, with ventral border forming prominent, proximodistally short overhang; carpometacarpus, os metacarpale alulare less elongated; proxi-

mal synostosis of os metacarpale minus with os metacarpale majus shorter; spatium intermetacarpale present; femur more elongated and slender; tarsometatarsus, hypotarsus with three cristae hypotarsi and two sulci, devoid of canales hypotarsi; corpus tarsometatarsi longer, more slender, not dorsoplantarly compressed, almost square in transverse section; trochlea metatarsi II strongly displaced proximally.

Dasornis toliapica (Owen, 1873), new combination

Odontopteryx toliapica Owen, 1873.
Macrodontopteryx oweni Harrison and Walker, 1976.
Neptuniavis minor Harrison and Walker, 1977.

Referred Material: OCP.DEK/GE 534B, distal part of right tibiotarsus; OCP.DEK/GE 1001, fragments of cranium; OCP.DEK/GE 1002, proximal part of right ulna; OCP.DEK/GE 1003, incomplete proximal part of left humerus; OCP.DEK/GE 1005, proximal part of left ulna; OCP.DEK/GE 1011, distal part of left tibiotarsus; OCP.DEK/GE 1012, proximal part of left carpometacarpus; OCP.DEK/GE 1013, fragment of shaft of humerus + fragment of shaft of ulna + distal part of left tibiotarsus; OCP.DEK/GE 1017, distal part of left tibiotarsus; OCP.DEK/GE 1018, distal part of right ulna; OCP.DEK/GE 1020, incomplete distal end of right tarsometatarsus; OCP.DEK/GE 1024, fragment of shaft of left carpometacarpus; OCP.DEK/GE 1026, fragment of shaft of humerus; OCP.DEK/GE 1029, fragment of distal part of right tarsometatarsus; OCP.DEK/GE 1034, distal part of left ulna; OCP.DEK/GE 1035, distal part of right ulna; OCP.DEK/GE 1038, distal part of right carpometacarpus; OCP.DEK/GE 1039, incomplete proximal part of left ulna; OCP.DEK/GE 1042, incomplete cranium; OCP.DEK/GE 1043, incomplete cranium; OCP.DEK/GE 1044, incomplete cranium; OCP.DEK/GE 1045, shaft of right femur; OCP.DEK/GE 1048, proximal part of left ulna; OCP.DEK/GE 1051, fragment of shaft of ulna; OCP.DEK/GE 1055, fragment of shaft of left radius; OCP.DEK/GE 1056, fragment of shaft of right radius; OCP.DEK/GE 1058, distal end of right radius; OCP.DEK/GE 1068, fragment of shaft of right radius close to distal end; OCP.DEK/GE 1070, nearly complete right humerus; OCP.DEK/GE 1071, distal part of right ulna; OCP.DEK/GE 1073, fragments of right humerus; OCP.DEK/GE 1075, distal end of right humerus; OCP.DEK/GE 1076, incomplete cranium; OCP.DEK/GE 1079, distal part of left ulna lacking extremity; OCP.DEK/GE 1080, fragment of shaft of left ulna; OCP.DEK/GE 1081, fragment of shaft of left ulna; OCP.DEK/GE 1082, fragment of left carpometacarpus; OCP.DEK/GE 1083, proximal part of left ulna; OCP.DEK/GE 1086, proximal part of left humerus; OCP.DEK/GE 1088, three fragments of right coracoideum; OCP.DEK/GE 1090, fragments of distal part of left tibiotarsus; OCP.DEK/GE 1091, fragments of distal part of left tibiotarsus; OCP.DEK/GE 1092, fragment of shaft of radius; OCP.DEK/GE 1100, fragment of shaft of left carpometacarpus; OCP.DEK/GE 1101, distal part of right carpometacarpus; OCP.DEK/GE 1102, distal part of right carpometacarpus; OCP.DEK/GE 1105, proximal part of right humerus; OCP.DEK/GE 1107, fragment of shaft and incomplete distal part of right humerus; OCP.DEK/GE 1108, fragment of shaft of right ulna; OCP.DEK/GE 1110,

distal part of left ulna; OCP.DEK/GE 1112, fragment of major metacarpal of right carpometacarpus; OCP.DEK/GE 1114, fragments of shaft of left ulna; OCP.DEK/GE 1115, proximal part of right humerus; OCP.DEK/GE 1116, fragment of shaft of left humerus in proximal half; OCP.DEK/GE 1118, distal end of right radius; OCP.DEK/GE 1121, fragment of shaft of radius; OCP.DEK/GE 1122, fragment of shaft of carpometacarpus; OCP.DEK/GE 1124, fragment of shaft of left humerus; OCP.DEK/GE 1125, distal part of right ulna; OCP.DEK/GE 1126, proximal end of right ulna; OCP.DEK/GE 1128, fragment of shaft of right humerus; OCP.DEK/GE 1135, fragment of shaft of left ulna; OCP.DEK/GE 1137, fragment of left carpometacarpus; OCP.DEK/GE 1138, fragment of shaft of radius + distal part of right carpometacarpus; OCP.DEK/GE 1139, fragment of left carpometacarpus; OCP.DEK/GE 1140, distal end of left tibiotarsus; OCP.DEK/GE 1141, fragment of shaft of right humerus; OCP.DEK/GE 1142, fragment of shaft of left ulna; OCP.DEK/GE 1144, fragment of distal end of right femur; OCP.DEK/GE 1146, distal end of left tarsometatarsus; OCP.DEK/GE 1147, distal end of right ulna; OCP.DEK/GE 1148, fragment of shaft of right ulna; OCP.DEK/GE 1149, fragment of shaft of left ulna; OCP.DEK/GE 1150, fragment of shaft of left ulna close to proximal end; OCP.DEK/GE 1152, proximal end of left carpometacarpus; OCP.DEK/GE 1153, fragment of shaft of left ulna + fragment of shaft of radius; OCP.DEK/GE 1155, fragment of shaft of left tarsometatarsus close to distal end; OCP.DEK/GE 1157, fragment of shaft of right radius close to distal end; OCP.DEK/GE 1160, fragment of shaft of right ulna; OCP.DEK/GE 1161, fragment of shaft of left ulna; OCP.DEK/GE 1163, fragment of shaft of left ulna; OCP.DEK/GE 1164, several fragments of right humerus; OCP.DEK/GE 1166, portion of right mandible; OCP.DEK/GE 1168, fragment of shaft of humerus; OCP.DEK/GE 1171, incomplete distal part of left tibiotarsus; OCP.DEK/GE 1172, left carpometacarpus with incomplete extremities; OCP.DEK/GE 1173A, proximal part of left humerus with incomplete end; OCP.DEK/GE 1174, fragment of shaft of right tibiotarsus; OCP.DEK/GE 1175, proximal part of left radius with incomplete end; OCP.DEK/GE 1176, nearly complete right tarsometatarsus; OCP.DEK/GE 1179, proximal part of right humerus lacking extremity; OCP.DEK/GE 1180, fragment of right humerus close to proximal end; OCP.DEK/GE 1182, incomplete distal end of right tarsometatarsus; OCP.DEK/GE 1183, incomplete proximal part of right humerus + shaft of ulna; OCP.DEK/GE 1185, portion of maxilla close to proximal end; OCP.DEK/GE 1187, fragments of shaft of left humerus close to proximal end; OCP.DEK/GE 1188, fragments of proximal part of right humerus; OCP.DEK/GE 1190, shaft of right tarsometatarsus; OCP.DEK/GE 1192, distal end of left carpometacarpus; OCP.DEK/GE 1193, distal end of right ulna; OCP.DEK/GE 1194, proximal part of right humerus; OCP.DEK/GE 1195, distal part of right humerus and proximal part of left coracoideum; OCP.DEK/GE 1197, proximal part of right humerus; OCP.DEK/GE 1198, distal part of right ulna; OCP.DEK/GE 1199, fragment of shaft of right radius close to distal end; OCP.DEK/GE 1203, incomplete distal end of left humerus; OCP.DEK/GE 1204, distal part of right tibiotarsus lacking extremity; OCP.DEK/GE 1205, fragment of shaft of right humerus close to distal end; OCP.DEK/GE 1206, distal part of left carpometacarpus; OCP.DEK/GE 1207, fragment of shaft of right ulna; OCP.DEK/GE 1209, several fragments of incomplete left humerus; OCP.DEK/GE 1210, fragment of shaft of left humerus; OCP.DEK/GE 1212, proximal part of left radius; OCP.DEK/GE 1213, fragment of shaft of radius; OCP.

DEK/GE 1216, proximal end of left humerus; OCP.DEK/GE 1217, fragment of shaft of right femur; OCP.DEK/GE 1218, distal part of left humerus with incomplete end; OCP.DEK/GE 1219, fragment of shaft of ulna; OCP.DEK/GE 1222, fragment of shaft of right humerus; OCP.DEK/GE 1223, fragment of shaft of left ulna; OCP.DEK/GE 1227, fragment of shaft of left tibiotarsus; OCP.DEK/GE 1228, fragment of shaft of left humerus; OCP.DEK/GE 1229, proximal end of left humerus; OCP.DEK/GE 1230, fragment of cranium and fragment of maxilla embedded in matrix; OCP.DEK/GE 1233, complete right humerus embedded in matrix; OCP.DEK/GE 1235, distal end of right tarsometatarsus embedded in matrix; OCP.DEK/GE 1238, cranium embedded in matrix; OCP.DEK/GE 1240, complete right humerus embedded in matrix; OCP.DEK/GE 1241, complete right carpometacarpus embedded in matrix; OCP.DEK/GE 1243, fragment of shaft of right ulna embedded in matrix; OCP.DEK/GE 1244, fragment of shaft of ulna; OCP.DEK/GE 1246, distal end of left humerus + fragment of shaft of ulna; OCP.DEK/GE 1250, fragment of shaft of ulna; OCP.DEK/GE 1255, distal part of right carpometacarpus; OCP.DEK/GE 1256, distal part of left tibiotarsus; OCP.DEK/GE 1257, fragment of shaft of left ulna; OCP.DEK/GE 1258, fragment of shaft of right humerus; OCP.DEK/GE 1260, fragment of shaft of ulna; OCP.DEK/GE 1262, fragment of shaft of right ulna; OCP.DEK/GE 1264, fragment of shaft of humerus; OCP.DEK/GE 1265, fragment of shaft of left radius; OCP.DEK/GE 1270, fragment of shaft of right humerus; OCP.DEK/GE 1272, distal end of left tarsometatarsus; OCP.DEK/GE 1274, fragment of shaft of humerus; OCP.DEK/GE 1275, distal end of left ulna; OCP.DEK/GE 1283, proximal part of left ulna; OCP.DEK/GE 1287, cranium embedded in matrix; OCP.DEK/GE 1289, complete left humerus embedded in matrix; OCP.DEK/GE 1293, distal end of left tarsometatarsus; OCP.DEK/GE 1294, distal end of left tarsometatarsus; OCP.DEK/GE 1298, proximal part of right radius; OCP.DEK/GE 1299, distal part of right ulna lacking extremity; OCP.DEK/GE 1314, fragment of shaft of humerus; OCP.DEK/GE 1316, incomplete proximal part of right humerus; OCP.DEK/GE 1324, incomplete proximal part of right humerus; OCP.DEK/GE 1326, proximal part of left radius; OCP.DEK/GE 1327, distal part of right radius; MHNL 20-149211, distal part of right humerus; MHNL 20-149212, shaft of left humerus; MHNL 20-149213, fragment of shaft of left humerus; MHNL 20-149214, distal part of right humerus; MHNL 20-149215, left ulna + fragment of shaft of radius; MHNL 20-149216, fragments of shaft of left humerus with incomplete distal end; MHNL 20-149217, fragment of shaft of left ulna close to distal end; MHNL 20-149218, distal part of right ulna; MHNL 20-149219, fragment of shaft of left radius in proximal part; MHNL 20-149220, two fragments of distal part of left ulna; MHNL 20-149221, fragment of shaft of right ulna; MHNL 20-149227, fragment of shaft of right ulna; MHNL 20-149228, fragment of shaft of left humerus + fragment of shaft of ulna; MHNL 20-149229, incomplete proximal part of left humerus; MHNL 20-149231, partial left tarsometatarsus; MHNL 20-149234, fragment of shaft of left humerus; MHNL 20-149235, incomplete distal part of left ulna; MHNL 20-149236, fragments of shaft of humerus + fragment of distal end of left ulna; MHNL 20-149237, incomplete distal part of left ulna; MHNL 20-149238, complete right tibiotarsus; D1-0027B, incomplete cranium; D1-0027C, incomplete cranium with portion of proximal maxilla; D1-0027D, incomplete cranium; D1-0027E, distal end of maxilla; MHNM-Khg 10, left humerus embedded in matrix.

TABLE 1: Comparative measurements of the cranium in *Dasornis toliapica* and *Dasornis emuinus*. Lengths in mm. * = estimated measurements; ** = strong dorsoventral flattening.

	D. toliapica	*D. emuinus*
Length (rostral end-prominentia cerebellaris)	59 (BMNH 44096) 63* (OCP.DEK/GE 1043) 65* (OCP.DEK/GE 1238) 66.1 (OCP.DEK/GE 1287) 69 (OCP.DEK/GE 1076) 80* (OCP.DEK/GE 1044) 82* (BMNH A1)	102* (OCP.DEK/GE 1288) 105–110* (based on OCP.DEK/GE 324 and D1-0027A) 110 (BMNH 31929)
Width at rostral end (zona flexoria craniofacialis)	19 (BMNH 44096) 23 (OCP.DEK/GE 1043) 25* (OCP.DEK/GE 1238) 25 (OCP.DEK/GE 1287) 27* (OCP.DEK/GE 1076) 28* (OCP.DEK/GE 1044) 30 (BMNH A1)	36* (OCP.DEK/GE 324) 41* (BMNH 31929)
Minimal width in interorbital region	12 (BMNH 44096) 14 (OCP.DEK/GE 1076, 1238) 15* (OCP.DEK/GE 1287) 16 (OCP.DEK/GE 1044) 18 (BMNH A1)	25.7 (OCP.DEK/GE 1004) 26.8 (OCP.DEK/GE 324) 29* (D1-0027A) 30* (OCP.DEK/GE 1288) 32.1 (BMNH 31929)
Width at processus postorbitales	49* (OCP.DEK/GE 1043) 51* (OCP.DEK/GE 1076) 58* (OCP.DEK/GE 1230) 59.5* (OCP.DEK/GE 1044)	90* (OCP.DEK/GE 1004) 91* (OCP.DEK/GE 324) 95* (D1-0027A) 99* (BMNH A3691) 102* (BMNH 31929)
Lamina parasphenoidalis: width at tuberculi basilares	15.9 (BMNH 44096) 17 (OCP.DEK/GE 1043) 18 (OCP.DEK/GE 1042) 19 (OCP.DEK/GE 1076) 21.5 (OCP.DEK/GE 1044)	35.4 (BMNH A3691) 38* (OCP.DEK/GE 324) 39* (OCP.DEK/GE 1004) 41 (BMNH 31929) 41.5 (D1-0027A)
Height (apex-lamina parasphenoidalis)	24 (OCP.DEK/GE 1043) 24.5 (OCP.DEK/GE 1076) 31.5 (OCP.DEK/GE 1044) 32 (OCP.DEK/GE 1042) 33 (BMNH 44096) 41.3 (BMNH A1)	43.4** (D1-0027A) 51.3 (OCP.DEK/GE 1004) 58 (BMNH 31929) 64 (BMNH A3691)
Foramen magnum: width	7 (OCP.DEK/GE 1042) 8.2 (BMNH 44096)	11 (D1-0027A) 11.3 (BMNH 31929)
Foramen magnum: height	7.5* (BMNH 44096) 9 (OCP.DEK/GE 1042)	9** (D1-0027A) 13.3 (BMNH 31929)
Condylus occipitalis: width	6 (OCP.DEK/GE 1042, 1043) 6.2 (OCP.DEK/GE 1076) 7 (OCP.DEK/GE 1044)	11 (D1-0027A) 11.7 (OCP.DEK/GE 324) 12* (OCP.DEK/GE 1288) 12.5 (SMNK-PAL 4017; after Mayr, 2008) 12.6 (BMNH 31929)
Processus rostropterygoideus: length	10 (OCP.DEK/GE 1042) 10.5 (OCP.DEK/GE 1044) 12.2 (BMNH 44096)	16.5 (D1-0027A) 18.5 (OCP.DEK/GE 1004)

	D. toliapica	*D. emuinus*
Laterosphenoid hollow: width	12 (OCP.DEK/GE 1043) 13 (OCP.DEK/GE 1042) 14 (OCP.DEK/GE 1076, D1-0027B) 17 (OCP.DEK/GE 1044)	28* (OCP.DEK/GE 324, 1004) 29* (BMNH A3691) 34 (D1-0027A)
Height of maxilla at apertura nasi ossea	20* (OCP.DEK/GE 1185)	—
Maximum width of maxilla at apertura nasi ossea	17* (OCP.DEK/GE 1185)	—
Apertura nasi ossea: length/height	7*/2 (OCP.DEK/GE 1185)	—
Estimated whole length of maxilla	170* (based on BMNH 44096, OCP.DEK/GE 1185 and D1-0027E)	—
Ratio length of maxilla/length of cranium	2/5* (based on estimated length of maxilla and OCP.DEK/GE 1076)	—
Maximum height of mandibula as preserved	17.5 (OCP.DEK/GE 1166)	—

Localities: Ouled Abdoun Basin (Morocco): Sidi Daoui (including Krupp, PH2, RP13, TS and TZ5 areas); Recette IV; southern Meraa El Arech (Lahou area); Sidi Chennane (M1S2, M8, M11 and R6–R7 areas).

Stratigraphic Distribution: Bed IIa, Thanetian, Upper Paleocene; intercalary beds II/I, basal Ypresian, lowermost Eocene; bed I, Ypresian, Lower Eocene.

Amended Diagnosis (from Harrison and Walker, 1976): Albatross-sized odontopterygiform with a wingspan of 2 to 3 m; differs from *Dasornis emuinus* in the following features: much smaller size; cranium, sutura frontoparietalis less pronounced, forming barely distinguishable groove; lamina parasphenoidalis caudorostrally longer; caudal extension of cotyla quadratica otici shorter and not twisted ventrally; foramen pneumaticum dorsale larger; laterosphenoid hollow square in shape, bounded medially by conspicuous prominentia lobi optici; tibiotarsus with shorter sulcus musculi fibularis.

Measurements: See tables 1 and 2.

DESCRIPTION

Cranium (figs. 3–6)

Dorsal Part of Calvaria (fig. 3): The os frontale is narrowest just caudal to the os lacrimale and widens strongly and regularly toward the processus postorbitalis. The depressio frontalis deepens and widens toward the transverse rostral end of the cranium. The caudal part of the vault of the cranium is broadly rounded and devoid of marked eminence on either side. It shows a paired discontinuity that is best visible in the largest individuals as a faint groove (fig. 3A). Computed tomographic (CT) reconstruction of the endocranium of *Dasornis toliapica* has shown that the os frontale overlaps the os parietale caudally, and that the two bones are unfused at the caudal region of the os frontale (Milner and Walsh, 2009). In the light of these new data, the groove in the caudal part of the cranial vault is interpreted as an incom-

TABLE 2: Measurements of the postcranium in *Dasornis* spp. Lengths in mm. * = estimated measurements.

	D. abdoun	*D. toliapica*	*D. emuinus*
CORACOIDEUM			
Greatest width of processus procoracoideus	—	8 (OCP.DEK/GE 1195)	—
Length of processus procoracoideus	—	18.7 (OCP.DEK/GE 1195)	—
Estimated minimal width of corpus	—	13 (OCP.DEK/GE 1195)	—
Width of collum	—	6.5 (OCP.DEK/GE 1195)	—
HUMERUS			
Length	200* (OCP.DEK/GE 1033)	245* (OCP.DEK/GE 1289) 260* (OCP.DEK/GE 1240) 270 (OCP.DEK/GE 1233) 280* (based on OCP.DEK/GE 1173A and 1210) 300* (OCP.DEK/GE 1070) 370* (based on OCP.DEK/GE 1116, 1209 and MHNL 20-149229)	470* (based on OCP.DEK/GE 1109, 1072 and 1078) 540 (OCP.DEK/GE 1237) 545 (OCP.DEK/GE 1236)
Width at apex of extremitas proximalis	27* (OCP.DEK/GE 1031)	34.5* (OCP.DEK/GE 1289) 36.9 (OCP.DEK/GE 1229)	70* (OCP.DEK/GE 1236, 1237)
Depth of caput	—	8 (OCP.DEK/GE 1289) 8.7 (OCP.DEK/GE 1229) 9 (OCP.DEK/GE 1216) 10.5 (OCP.DEK/GE 1209)	12.8 (OCP.DEK/GE 1072) 15* (OCP.DEK/GE 1236, 1333)
Width of corpus at distal end of linea m. latissimi dorsi	10 (OCP.DEK/GE 1033)	12.8 (OCP.DEK/GE 1173A, 1210) 13.2 (OCP.DEK/GE 1179) 13.3 (OCP.DEK/GE 1164) 13.4 (OCP.DEK/GE 1289) 13.7 (OCP.DEK/GE 1003) 14* (OCP.DEK/GE 1240) 14.5 (OCP.DEK/GE 1086) 16* (OCP.DEK/GE 1233) 17 (OCP.DEK/GE 1116, 1209, MHNL 20-149229)	20 (OCP.DEK/GE 1072) 21.5 (OCP.DEK/GE 1078) 25* (OCP.DEK/GE 1334)
Width at extremitas distalis	18 (MHNL 20-149225)	23* (MHNL 20-149211, OCP.DEK/GE 1289) 25.5* (OCP.DEK/GE 1075) 27* (MHNL 20-149214) 27 (OCP.DEK/GE 1233) 27.5* (MHNL 20-149216) 28* (OCP.DEK/GE 1240)	34* (OCP.DEK/GE 1109) 47* (OCP.DEK/GE 1236)
Depth at extremitas distalis	8.7 (MHNL 20-149225)	13.5 (OCP.DEK/GE 1195) 14 (MHNL 20-149214) 17 (MHNL 20-149216)	22* (OCP.DEK/GE 1109) 25* (OCP.DEK/GE 1236)
ULNA			
Length	—	350* (MHNL 20-149215)	480* (OCP.DEK/GE 1242)

	D. abdoun	*D. toliapica*	*D. emuinus*
Width at extremitas proximalis	—	16.2 (BMNH A224) 17 (OCP.DEK/GE 1002) 20* (OCP.DEK/GE 1039, MHNL 20-149215) 24.6 (OCP.DEK/GE 1126) 25.3 (BMNH A3692; from Harrison and Walker, 1976)	34.5 (BMNH A94; from Harrison and Walker, 1976)
Depth at extremitas proximalis	—	12.3 (OCP.DEK/GE 1002) 13.2 (BMNH A224) 14.5 (OCP.DEK/GE 1039) 15* (MHNL 20-149215) 18.7 (BMNH A3692; from Harrison and Walker, 1976) 21 (OCP.DEK/GE 1126)	28.2 (BMNH A94; from Harrison and Walker, 1976)
Width of corpus at foramen nutritium	6.5* (OCP.DEK/GE 1022)	9* (OCP.DEK/GE 1013) 9.6 (OCP.DEK/GE 1160) 9.7 (OCP.DEK/GE 1005) 10.5 (OCP.DEK/GE 1149) 11.5 (OCP.DEK/GE 1039, 1148) 11.7 (MHNL 20-149218) 12.7 (OCP.DEK/GE 1135)	—
Width at extremitas distalis	10* (OCP.DEK/GE 1022)	13 (OCP.DEK/GE 1198) 14.4 (MHNL 20-149220) 14.5 (OCP.DEK/GE 1035) 16 (OCP.DEK/GE 1018, MHNL 20-149218) 17.8 (OCP.DEK/GE 1147)	—
Depth at extremitas distalis	7.5* (OCP.DEK/GE 1022)	9.1 (OCP.DEK/GE 1198) 10.4 (OCP.DEK/GE 1035) 11 (MHNL 20-149218) 11.1 (OCP.DEK/GE 1018) 11.2 (MHNL 20-149220)	—
RADIUS			
Width at extremitas proximalis	—	9.4 (OCP.DEK/GE 1212) 10* (OCP.DEK/GE 1298) 11.3 (OCP.DEK/GE 1326)	14.7 (OCP.DEK/GE 1224) 16 (OCP.DEK/GE 1046) 16-17* (OCP.DEK/GE 1242) 18.2 (OCP.DEK/GE 1245)
Width of corpus just distal to extremitas proximalis	—	5 (OCP.DEK/GE 1175, 1212) 6 (OCP.DEK/GE 1326)	7.7 (OCP.DEK/GE 1224) 8 (OCP.DEK/GE 1046)
Width of corpus at foramen nutritium	—	3.3 (OCP.DEK/GE 1175) 4.1 (MHNL 20-149219) 4.3 (MHNL 20-149215)	—
Width of corpus just proximal to extremitas distalis	3.5 (OCP.DEK/GE 1030)	5 (OCP.DEK/GE 1068, 1118, 1199) 6.5* (OCP.DEK/GE 1058)	—
Width at extremitas distalis	8.4 (OCP.DEK/GE 1030)	11.5 (OCP.DEK/GE 1058) 12.2 (OCP.DEK/GE 1118) 12.7 (OCP.DEK/GE 1327)	—

	D. abdoun	*D. toliapica*	*D. emuinus*
CARPOMETACARPUS			
Length	—	138 (OCP.DEK/GE 1241)	—
Width of trochlea carpalis	—	13.7 (OCP.DEK/GE 1012) 15.5 (OCP.DEK/GE 1152)	—
Depth of trochlea carpalis	—	8* (OCP.DEK/GE 1172) 8.2 (OCP.DEK/GE 1139) 9* (OCP.DEK/GE 1012) 11.6 (OCP.DEK/GE 1152)	—
Width of os metacarpale majus in distal half	3.2 (OCP.DEK/GE 1021) 3.2 (OCP.DEK/GE 1158) 3.7 (OCP.DEK/GE 1016)	5.5 (OCP.DEK/GE 1038) 6* (OCP.DEK/GE 1172) 6.3 (OCP.DEK/GE 1101) 6.8 (OCP.DEK/GE 1100) 7 (OCP.DEK/GE 1102) 7.2 (OCP.DEK/GE 1124)	—
Width at extremitas distalis	6.5 (OCP.DEK/GE 1158) 7 (OCP.DEK/GE 1021)	10.5* (OCP.DEK/GE 1038) 12 (OCP.DEK/GE 1101, 1192) 13 (OCP.DEK/GE 1102)	—
Depth at extremitas distalis	5.5 (OCP.DEK/GE 1158) 5.6 (OCP.DEK/GE 1021) 6 (OCP.DEK/GE 1016)	7.4 (OCP.DEK/GE 1192) 8 (OCP.DEK/GE 1101) 9.5 (OCP.DEK/GE 1102)	—
FEMUR			
Width at extremitas proximalis	—	—	33 (OCP.DEK/GE 1059)
Depth at extremitas proximalis	—	—	20 (OCP.DEK/GE 1059)
Width of caput	—	—	14 (OCP.DEK/GE 1059)
Width of corpus at triangular facet	6.8 (OCP.DEK/GE 1096)	10.7 (OCP.DEK/GE 1217)	—
TIBIOTARSUS			
Length	—	139 (MHNL 20-149238)	—
Width at extremitas proximalis	—	15.1 (MHNL 20-149238)	—
Width of corpus in distal half	6.5 (OCP.DEK/GE 1191)	8.4 (OCP.DEK/GE 1227) 9.4 (OCP.DEK/GE 1171) 10 (MHNL 20-149238) 11.9 (OCP.DEK/GE 534B)	14 (OCP.DEK/GE 534A, 1123)
Width at extremitas distalis	—	13.6 (OCP.DEK/GE 1013) 15 (OCP.DEK/GE 1040) 17.3 (MHNL 20-149238) 20 (OCP.DEK/GE 534B)	27.4 (OCP.DEK/GE 534A)
Depth at extremitas distalis	—	12.2 (OCP.DEK/GE 1011) 12.3 (OCP.DEK/GE 1040) 13.4 (OCP.DEK/GE 1013) 15 (MHNL 20-149238) 17 (OCP.DEK/GE 534B)	28.3 (OCP.DEK/GE 534A)

	D. abdoun	*D. toliapica*	*D. emuinus*
Depth of condylus medialis	—	14 (OCP.DEK/GE 1113) 15.8 (MHNL 20-149231) 20 (OCP.DEK/GE 534B)	27.7 (OCP.DEK/GE 1123) 28.7 (OCP.DEK/GE 534A)
TARSOMETATARSUS			
Length	—	78* (based on OCP.DEK/GE 1146 and 1176) 85* (based on OCP.DEK/GE 1146 and MHNL 20-149231)	118 (OCP.DEK/GE 1106)
Width at extremitas proximalis	—	14.7 (BMNH A134; from Harrison and Walker, 1977) 15 (OCP.DEK/GE 1176)	25.6 (OCP.DEK/GE 1106) 26.8 (BMNH A3682; from Harrison and Walker, 1977)
Depth at extremitas proximalis	—	11.3 (BMNH A134; from Harrison and Walker, 1977) 13 (OCP.DEK/GE 1176)	21* (OCP.DEK/GE 1106) 24 (BMNH A3682; from Harrison and Walker, 1977)
Greatest width at extremitas distalis	—	15.7 (OCP.DEK/GE 1146) 17.5* (OCP.DEK/GE 1235)	21.3 (OCP.DEK/GE 1252) 25.3 (OCP.DEK/GE 1106) 27.1 (BMNH A894; from Harrison and Walker, 1977)

pletely obliterated sutura frontoparietalis (see also Elzanowski and Galton, 1991). Rostral to this groove, the surface of the os frontale is transversely striated.

Temporal Region (figs. 4, 5): The processus postorbitalis projects rostrally and is rounded at the tip. It is continuous with the straight lateral border of the temporal region. The area of origin of musculus depressor mandibulae (fossa subtemporalis) is large, well defined, and continues onto the laterodorsal border of the processus paroccipitalis. Rostral to this structure is a shallow depression interpreted here as the area of origin of musculus adductor mandibulae externus, pars articularis (Zusi and Livezey, 2000). Both fossae extend halfway up to the occiput. There is no distinct processus zygomaticus. The area that supports the aponeurosis zygomatica (Elzanowski, 1987; Weber, 1996; Zusi and Livezey, 2000) is a low convexity.

Occipital Region (figs. 3, 5) and Basis Cranii Externa (figs. 3, 6): The sharp crista nuchalis transversa forms a double arch curving ventrally at the midline. The lateroventral part of this structure extends to the tip of the processus paroccipitalis. The prominentia cerebellaris is strongly convex in lateral aspect, and forms a sharp crista nuchalis sagittalis extending from the crista nuchalis transversa down to the foramen magnum. The os supraoccipitale dorsomedially forms a swollen zone with an oblique medial border.

The processus paroccipitalis is strongly developed and projects caudolateroventrally. The tip is vertical, rounded and forms a semilunar-shaped surface in lateral aspect. A slender processus lateralis parasphenoidalis connects the ventral border of the processus paroccipitalis with the lateral border of the lamina parasphenoidalis. The medial part of the processus paroccipitalis forms

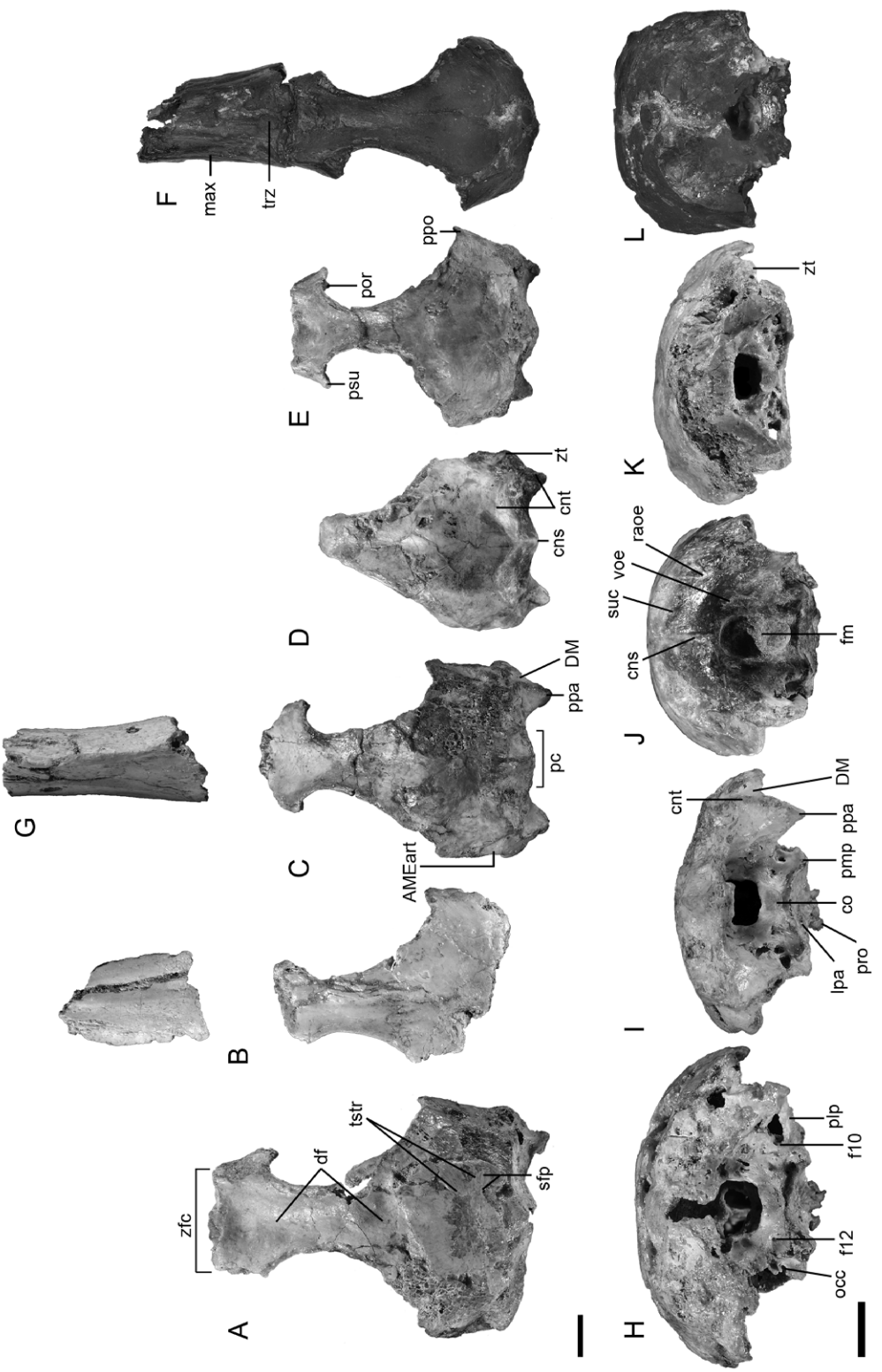

FIGURE 3. *Dasornis toliapica*, skull. **A–F.** Crania in dorsal view: **A.** OCP.DEK/GE 1044; **B.** D1-0027C; **C.** OCP.DEK/GE 1076; **D.** OCP.DEK/GE 1042; **E.** OCP.DEK/GE 1043; **F.** BMNH 44096. **G.** OCP.DEK/GE 1185, fragment of proximal part of maxilla, dorsal view. **H–L.** Crania in caudal view: **H.** OCP.DEK/GE 1044; **I.** OCP.DEK/GE 1076; **J.** OCP.DEK/GE 1042; **K.** OCP.DEK/GE 1043; **L.** BMNH 44096. Scale bars equal 10 mm.

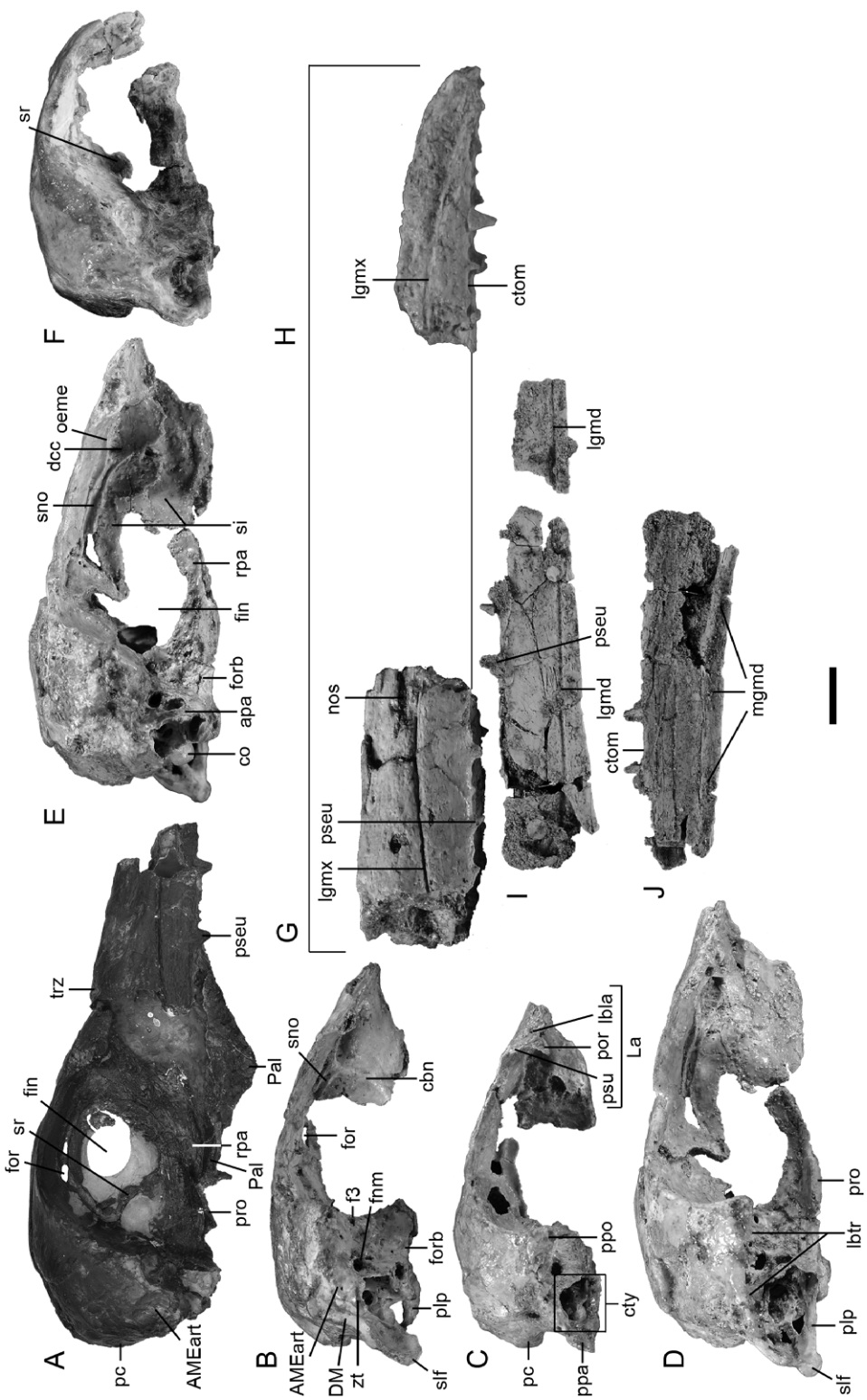

FIGURE 4. *Dasornis toliapica*, skull. **A.–F.** Crania in right lateral view: **A.** BMNH 44096; **B.** OCP.DEK/GE 1076; **C.** OCP.DEK/GE 1043; **D.** OCP.DEK/GE 1044; **E.** reversed OCP.DEK/GE 1044; **F.** reversed OCP.DEK/GE 1042. **G.** OCP.DEK/GE 1185, fragment of proximal part of maxilla, right lateral view. **H.** D1-0027E, distal end of maxilla, right lateral view. **I–J.** OCP.DEK/GE 1166, fragment of right mandibula: **I.** lateral view, **J.** medial view. Scale bar equals 10 mm.

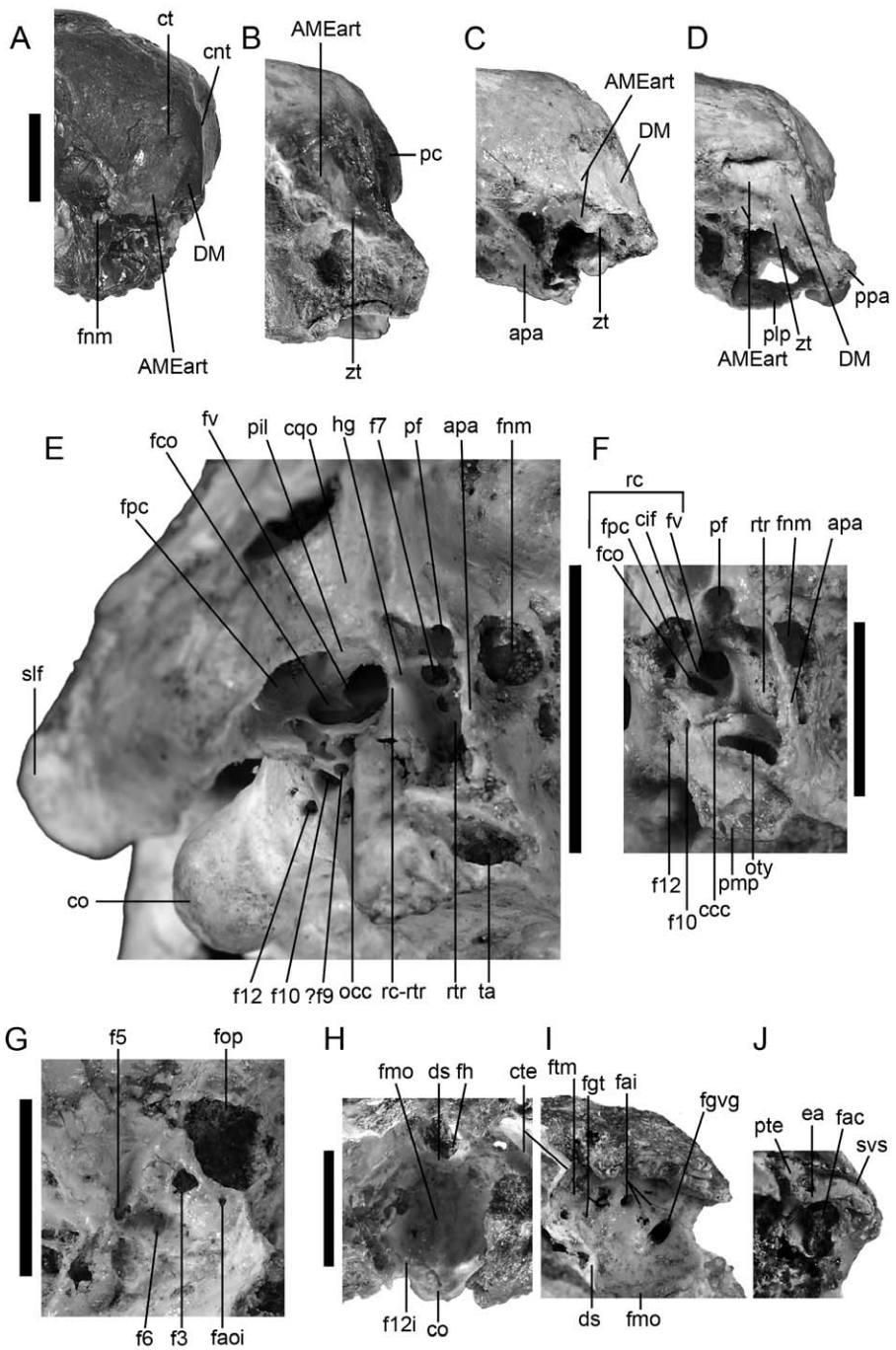

FIGURE 5. *Dasornis toliapica*, skull. **A–D.** Temporal regions in left lateral view: **A.** BMNH 44096; **B.** reversed OCP.DEK/GE 1042; **C.** reversed D1-0027B; **D.** OCP.DEK/GE 1076. **E–F.** Right middle ear regions: **E.** OCP.DEK/GE 1076; **F.** reversed OCP.DEK/GE 1044. **G.** OCP.DEK/GE 1076, region of the foramen opticum. **H.** D1-0027D, cavitas cranialis, dorsal view. **I.** D1-0027D, right wall of cavitas cranialis. **J.** D1-0027B, right osseous labyrinth. Scale bars equal 10 mm.

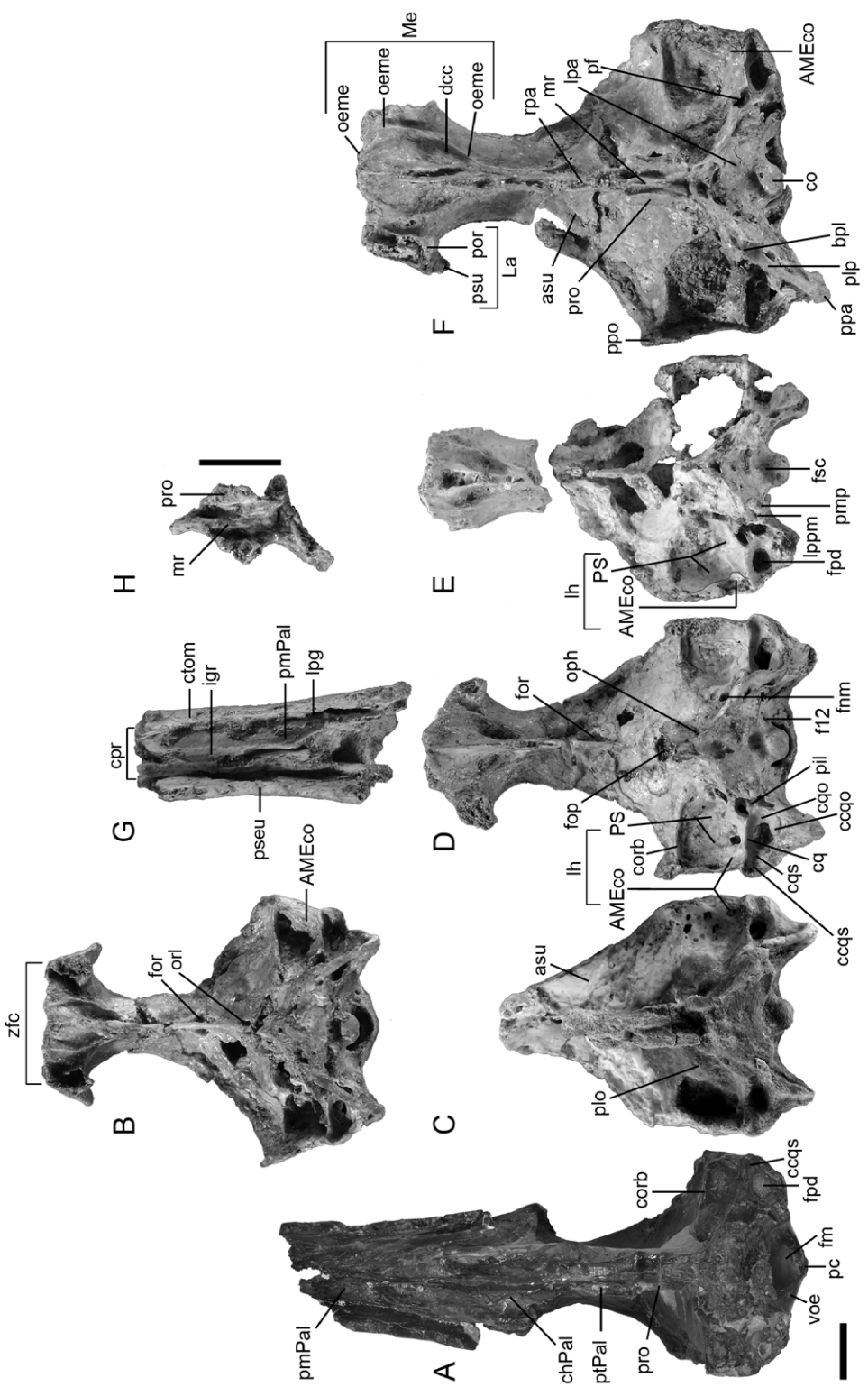

FIGURE 6. *Dasornis toliapica*, skull. **A–F.** Crania in ventral view: **A.** BMNH 44096; **B.** OCP.DEK/GE 1043; **C.** OCP.DEK/GE 1042; **D.** OCP.DEK/GE 1076; **E.** D1-0027B; **F.** OCP.DEK/GE 1044. **G.** OCP.DEK/GE 1185, fragment of proximal part of maxilla, ventral view. **H.** D1-0027C, fragment of rostrum parasphenoidale, ventral view. Scale bars equal 10 mm.

a smooth transition with the occipital plate and with the ventral corner of the prominentia cerebellaris; it shows a short crest and a tubercle close to the tip. The ventral side of the processus paroccipitalis is concave, with a lateral inclination in the medial part. In the London Clay specimens, the processus paroccipitalis is preserved only at the base (Harrison and Walker, 1976: pl. 1C).

A foramen venae occipitalis externae is found on either side at the ventral corner of the prominentia cerebellaris, at the level of the dorsal border of the foramen magnum and just medial to the inner border of the processus paroccipitalis. A short groove continues this foramen ventrally. A foramen rami occipitalis arteriae ophthalmicae externae that is continued dorsally by a long groove is located about two thirds of the way from the crista nuchalis sagittalis to the crista nuchalis transversa. The main groove branches into several smaller grooves.

The foramen magnum is higher than it is broad, with straight lateral borders (fig. 3J). Its plane is nearly perpendicular to that of the lamina parasphenoidalis, i.e., it is oriented downward only slightly. A small, depressed area is present on either side of the foramen magnum and ventral to the foramen venae occipitalis externae. The condylus occipitalis is very large, its width nearly equalling that of the foramen magnum. It is stemmed and slightly kidney shaped, with the dorsal facet showing deep triangular depression. The fossa subcondylaris is large and deep.

The medialmost foramen nervi hypoglossi is located in the stem of the condylus occipitalis. The tiny lateral foramen is far ventral and only slightly lateral to the medial one. The foramen nervi vagi is laterally oriented and its medial border is well defined, curving evenly to join the ventral border of the processus paroccipitalis and the base of the processus medialis parasphenoidalis. This crest is homologous to the crista fossae parabasalis. Milner and Walsh (2009) stated that the divergence of the nervus glossopharyngeus and nervus vagus is close to the exit of the latter, and that the nervus glossopharyngeus exits within the recessus scalae tympani. In one of the braincases, we found a small foramen in extreme marginal position, immediately lateral to the foramen nervi vagi, which may correspond to a foramen nervi glossopharyngealis (fig. 5E). It is not certain whether this is an artefact of preservation, however. There is no ostium canalis ophthalmici externi. A deep notch for the arteria carotis cerebralis lies just above the medial corner of the processus lateralis parasphenoidalis.

The lamina parasphenoidalis is triangular in shape, longitudinally narrow, and slightly concave. It has very sharp lateral borders and slants abruptly at the caudal edge, which is evenly curved. The prominent processus medialis parasphenoidalis occupies the lateral corner of the lamina parasphenoidalis and its lateral side shows a slit-shaped groove. The base of the processus lateralis parasphenoidalis forms a distinct horizontal platform lateral to the lamina parasphenoidalis. The tuba auditiva is completely closed. The ostium pharyngeale is located at the rostral corner of the lamina parasphenoidalis and continued rostrally by a shallow groove. The well-developed ala parasphenoidalis is continuous with the lateral border of the lamina parasphenoidalis and with the processus lateralis parasphenoidalis.

The foramen orbitale for the exit of arteria sphenoidea and nervus palatinus lies in the rostroventral part of the ala parasphenoidalis, close to the sharp ventral border of the basis rostri parasphenoidale (fig. 4). It is continued rostrally by a short, descending groove.

Rostrum Parasphenoidale (figs. 4, 6): The rostrum parasphenoidale exhibits in its ventral corners a pair of elongated processus rostropterygoideus (Weber, 1996). These structures

are roughly parallel to each other and have some lateral and rostral inclination. In the region of the processus rostropterygoideus, the rostrum parasphenoidale tapers upward to the lower edge of the septum interorbitale, and has concave lateral borders. A ridge continues medially the groove for the tuba auditiva and delimits a median surface. The latter structure evenly tapers rostrally and gradually rises to become a high crest at the level of the rostral half of the processus rostropterygoideus. Rostral to these structures, the section of the rostrum parasphenoidale gradually changes from triangular to round. In lateral aspect, a short straight ridge continues the processus rostropterygoideus rostrally.

Middle Ear Region (figs. 4, 5, 6): The arteria carotis cerebralis enters the middle ear region into a deep groove or partly closed canalis caroticus cranialis, deep to the ala parasphenoidalis and dorsal to the large ostium tympanicum (fig. 5). In BMNH 44096, the caudal part of a groove for the arteria carotis cerebralis is preserved on the left hand side. Our interpretation is congruent with that of Milner and Walsh (2009), which state that the arteria carotis cerebralis is enclosed in a bony tunnel. There is no canalis ophthalmicus externus, i.e., the arteria and vena ophthalmicae externae are neither encased in a bony canal in the medial wall of the tympanic cavity, nor is there a groove in which they rest.

The entrance of the recessus tympanicus rostralis is narrow and high (fig. 5). A strongly curved thin ridge separates the recessus tympanicus rostralis from the recessus columellae. A foramen nervi facialis is situated in the medial wall of the recessus tympanicus rostralis. This foramen is continued caudally by a groove that accommodates the nervus hyomandibularis. A shallow groove that continues this foramen rostroventrally accommodates the nervus palatinus. In the dorsal wall of the recessus tympanicus rostralis, an oval foramen that is probably pneumatic lies medial to the ala parasphenoidalis.

The recessus columellae is relatively deep (fig. 5). The fenestra vestibuli is rounded in shape. The oval fenestra cochleae is caudoventral to the fenestra vestibuli. The crista interfenestralis is narrow and oblique. The foramen pneumaticum caudale is very large and faces ventrally. The recessus tympanicus caudalis is well developed and probably communicates with the recessus tympanicus dorsalis. The pila otica is a flat surface facing ventrally.

The cotylae quadratica squamosi and otici cannot be distinguished from one another, because they merge rostrally with a smooth and evenly concave vertical surface (fig. 6). A prominent ridge that is roughly perpendicular to the median axis of the cranium delimits this structure rostrally. The cotyla quadratica squamosi and its lateral extension face ventrally. The lateral border of this extension is visible as a notch in lateral aspect, and continues caudomedially as a sharp ridge. The cotyla quadratica otici is sessile and faces lateroventrally. It is continuous with a flat surface that extends and widens onto the base of the processus paroccipitalis. This surface faces rostrally and has a rounded caudal border. A large foramen pneumaticum dorsale is situated between the cotylae quadratica and caudal to their rostral extension. A concave zone delimits this structure caudolaterally. The extensions of the cotylae quadratica are interpreted as such in *Dasornis toliapica* because these structures do not articulate with the processus oticus ossis quadrati in BMNH 44096. In the latter, the capitulum oticum and capitulum squamosum ossis quadrati merge rostrally with a narrow ridge that articulates with the rostral continuation of the cotylae quadratica (Harrison and Walker, 1976: pl. 2, fig. I). The processus oticus ossis quadrati is thus devoid of

incisura intercapitularis, in contrast to most neornithine birds.

Orbita (figs. 4, 5, 6): The lateral edge of the os frontale is sharp in the region where it widens toward the os lacrimale. The paries caudalis orbitae has only slight caudolateral slant and is not pierced by any fonticulus orbitocranialis. A groove that begins lateral to the fenestra associated with the fossa bulbi olfactorii curves toward the interorbital border of os frontale and turns caudally, roughly paralleling the septum interorbitale (fig. 6). This groove probably accommodates the arteria supraorbitalis.

A deep square concavity is present in the region of the os laterosphenoidale, extending from the ala parasphenoidalis to the lateral border of the temporal region (fig. 6). A conspicuous prominentia lobi optici (Weber, 1996), which houses the globelike tectum mesencephali (see Milner and Walsh, 2009), forms most of its medial border. In the caudolateral part of the hollow is a drop-shaped depression interpreted here as the area of origin of musculus adductor mandibulae externus, pars coronoidea (Weber, 1996; Zusi and Livezey, 2000). The remainder of the hollow probably corresponds to the area of origin of musculus pseudotemporalis superficialis. The sharp crista orbitalis extends from the prominentia lobi optici to the tip of processus postorbitalis.

The foramen nervi maxillomandibularis is rostral to the ala parasphenoidalis. Just caudodorsally to the foramen nervi maxillomandibularis is a tiny recess that represents a remnant of the foramen for the vena cerebralis media (Elzanowski, 1987). The foramen opticum is small and rounded to oval in shape (fig. 5). There is a separate foramen nervi oculomotorii. It is not certain whether the nervus trochlearis is confluent with the nervus opticus. The foramen nervi opthalmici and the groove that continues the latter dorsally are located lateroventrally to the foramen opticum. The foramen nervi abducentis and its continuation are situated in a deep, rounded depression that is far ventral to the foramen opticum. A foramen arteriae ophthalmicae internae is present. At the angulus orbitae (Elzanowski, 1987), just above the foramen opticum, is a paired concavity from which the musculus rectus lateralis probably originates.

The fonticulus interorbitalis is evenly curved rostrodorsally and bounded dorsally by a narrow portion of septum interorbitale that shows a constant width (fig. 4). Its original aspect is not preserved in the Moroccan specimens. In OCP.DEK/GE 1042, the dorsal part of a bridge that probably separated the fonticulus interorbitalis from the foramen opticum is preserved (fig. 4F). Such a bridge is found in BMNH 44096. A small fonticulus orbitocranialis communicates with the fossa bulbi olfactorii and merges with the sulcus nervi olfactorii rostrally. The sulcus nervi olfactorii is wide, shallow, slightly curved, and of constant width. It bifurcates and widens slightly at its rostral extremity. The laterodorsal groove probably conducted the lateral ramus of nervus olfactorius, and the medioventral one conducted the medial ramus. The caudal border of the nasal cavity is a low and blunt crest, and the os ectethmoidale is absent. The lamina dorsalis is strongly developed with a rounded rostral end. It has a sharply defined outer edge, a deep depression for the concha caudalis in the caudal half and a conspicuous oblique column bordering this depression rostroventrally (fig. 6).

Os Lacrimale (figs. 3, 4, 6): The os lacrimale is fused with the os frontale and possibly with a part of the os nasale, immediately caudal to the straight zona flexoria craniofacialis. The lateral border of the os lacrimale above the processus orbitalis is a slightly concave facet that is roughly parallel to the long axis of the cranium. The well-developed processus supraorbitalis

is rounded at the tip and projects caudolaterally. This structure is damaged in the London Clay specimens (Harrison and Walker, 1976). The processus orbitalis is preserved only at the base in the Moroccan specimens.

Cavitas Cranialis (fig. 5): The fossa cranii rostralis is wide, and houses the laterally expanded telencephalon (see Milner and Walsh, 2009). The fossa hypophysialis is small, rounded, and bounded caudally by a high dorsum sellae. Its shape agrees with the hypophysis morphology found in the virtual endocast of *Dasornis toliapica* (Milner and Walsh, 2009). The estimated angle between the plane of the lamina parasphenoidalis and a straight line connecting the dorsum sellae with the dorsalmost point of the condylus occipitalis is 20°. The fossa medullae oblongatae is strongly concave, rounded, devoid of median ridge, and fits well with the globe-shaped rhombencephalon of BMNH 44096 (Milner and Walsh, 2009). The foramen nervi abducentis is in medial position, and opens far ventral to the apex of dorsum sellae.

Milner and Walsh (2009) stated that the nervus trigeminus exits from the rhombencephalon and is contiguous with the ventral margin of the tectum mesencephali. In accordance with this, we found that the fossa ganglii trigemini opens exclusively to the fossa medullae oblongatae and is separated from the fossa tecti mesencephali by a thin ridge. The partial or complete separation of the fossa ganglii trigemini from the fossa tecti mesencephali occurs only in a few groups of neognathous birds among Neornithes (Elzanowski and Galton, 1991).

The bony labyrinth is widely separated from the fossa cranii rostralis by the protuberantia tentorialis (Elzanowski and Galton, 1991; Milner and Walsh, 2009). The eminentia arcuata canalis semicircularis rostralis (see Butendieck and Wissdorf, 1982) is of even width, oval, vertical, and smooth in the rostroventral corner. The rostral group of foramina of the fossa acustica interna is located in a deep well-defined concavity that is oval and higher than wide. There is no depression accommodating the caudal group of foramina. The fovea ganglii vagoglossopharyngealis is caudoventral to this caudal group. The canales nervorum hypoglossi opens slightly medial to the lateral border of the condylus occipitalis.

The fossa cerebelli is partly preserved. It is devoid of interfoliar ridges and sulcus medianus (Elzanowski and Galton, 1991), which correspond to the morphology of the cerebellum of BMNH 44096 (Milner and Walsh, 2009). The canalis semicircularis posterior projects very little into the fossa auriculae cerebelli, which occupies almost the entire area enclosed by the eminentia arcuata. The crista marginalis is prominent and sharp. A sulcus venae semicircularis running along the dorsal margin of the eminentia arcuata canalis semicircularis rostralis is clearly visible in one of the specimens (fig. 5J). This is not congruent with the work of Milner and Walsh (2009), who interpret the vena semicircularis rostralis as fully enclosed within an osseous tunnel.

Maxilla (figs. 3, 4, 6)

A portion that roughly corresponds to the caudal third of the maxilla is preserved. It is heavily distorted and mediolaterally compressed. It lacks the caudalmost part and is broken just anterior to the apertura nasi ossea. Its structure is exceedingly similar to that of BMNH 44096 (Harrison and Walker, 1976). The distal end that corresponds to the rostral third of the maxilla is damaged at the tip and strongly crushed mediolaterally (fig. 4).

The maxilla is elongated, mediolaterally narrow, and dorsoventrally deep. In dorsal aspect, the culmen is broken at the zone where it begins to widen caudally toward the flat triangular region just rostral to the zona flexoria craniofacialis. This triangular structure is well preserved in BMNH 44096 (fig. 3) and BMNH A1 (see Harrison and Walker 1976: pl. 1, fig. B; pl. 4, fig. A). The maxilla has a deep lateral longitudinal groove ascending to the apertura nasi ossea and then paralleling the culmen before descending gradually to a point just behind the rostral tip, which does not seem to turn down strongly. The tiny apertura nasi ossea is longer than it is high (table 1) and situated 2 mm above the lateral groove, at approximately one third the distance from the zona flexoria craniofacialis to the tip of the maxilla. The crista tomialis is straight and thick, and bears numerous toothlike processes. These structures vary in size from mere spines to pointed, conical pseudoteeth. The large pseudoteeth are approximately evenly spaced (around 12 mm apart) on each ramus, and their heights are comparable to those of BMNH 44096. Between each large projection is a small pseudotooth, sometimes flanked rostrally by a still smaller process. Most of the large projections are broken, showing a central hollow within. The large projections of the proximal region slant forward, as in BMNH 44096 (Harrison and Walker, 1976). In the rostral end of the maxilla, however, they arise vertically from the crista tomialis. The lateral surface of the maxilla and the cristae tomiales including the toothlike projections bear numerous canaliculi neurovasculares that open into foveae corpusculorum nervosorum, which consist of shallow, irregular furrows.

The ventral aspect of the proximal maxilla is very similar to that of BMNH 44096 (fig. 6). The straight, wide processus maxillaris of os palatinum curves ventrally from front to back and is separated from its counterpart by a narrow median furrow, which is the rostral continuation of the fossa choanalis. Rostral to this groove, the processus maxillaris of os palatinum merges with the processus palatinus of os premaxillare and possibly with the processus maxillopalatinus of os maxillare, which fuse with their counterpart to form a unique structure, the "central palatal region" (Harrison and Walker, 1976). The latter structure shows a median groove, the "interpalatal groove" (Harrison and Walker, 1976). On either side of the central palatal ridge is a deep longitudinal "lateral palatal groove" that accommodated the crista tomialis and toothlike projections of the mandibula when the jaws were closed (see Harrison and Walker, 1976). The central palatal ridge appears to decrease in depth and width toward the rostral end of the maxilla, which is deeply hollowed.

Mandibula (fig. 4)

A lateromedially crushed portion of pars intermedia is preserved (OCP.DEK/GE 1166). It tapers gradually toward the distal end. The crista tomialis and toothlike processes are similar to those of the maxilla. Only two large toothlike projections are preserved. They slant forward and their heights are comparable to those of the large maxillar projections. The lateral surface of the mandibula, crista tomialis, and pseudoteeth bear canaliculi neurovasculares and foveae corpusculorum nervosorum that are similar to those found in the maxilla. In lateral aspect, a deep straight longitudinal groove gradually gets closer to the ventral margin: in the proximal part, it is located at about one third of the depth of the mandibula above ventral margin; in the distal one, it is located at about one fifth of the depth of the mandibula. The lateral side of the

jaw is nearly flat. The medial one is smooth, slightly convex, and a shallow longitudinal hollow occupies the lower third of it.

Coracoideum (fig. 7)

The processus acrocoracoideus is lateromedially narrow and noticeably elongated dorsoventrally. The facies articularis clavicularis is proximodistally high with a bent, sharp sternal border, and faces medioventrally. The impressio ligamenti acrocoracohumeralis is probably shallow or indistinct. Two parallel crests are located in the caudal part of the apex of processus acrocoracoideus. The medial side of the long collum acrocoracoidei (Ballmann, 1969) is devoid of pneumatic foramina and bears a shallow groove in its dorsal half. This groove is most probably an artifact of preservation, because it is not found in a coracoideum from the Middle Eocene of Belgium tentatively assigned to *Macrodontopteryx oweni* (Mayr and Smith, 2010). The processus acrocoracoideus and its neck project cranially, so that the whole structure makes an angle with the long axis of the corpus.

The facies articularis humeralis is not preserved. The cotyla scapularis is deep and cup shaped. The well-developed processus procoracoideus is proximodistally thick and strongly projects ventrally. Its base is noticeably convex just medial to the cotyla scapularis. A short, sharp crest continues the processus procoracoideus sternally. A pneumatic foramen is just sternal to the cotyla scapularis. Its ventral opening lies in a round concavity. The corpus coracoidei has a strongly curved margo medialis. The lateral extremity of the extremitas sternalis is blunt, with a low facies interna that is nearly perpendicular to the facies dorsalis. The facies externa is a thick convexity in this region. The fragmentary coracoidea described here match well with the complete coracoideum putatively assigned to *M. oweni* (a junior synonym of *Dasornis toliapica*) by Mayr and Smith (2010: fig. 3).

Humerus (figs. 7–10)

The caput humeri is craniocaudally narrow (fig. 8). It shows a distinct dorsal prominence on its cranial facies and tapers ventrally to the wide incisura capitis. An oblique groove is present on its dorsal slope. Its caudal border is well defined. The tuberculum dorsale is well separated from and slightly distal to the caput; it consists of a smooth, indistinct facet that faces proximally. An even convexity continues this structure far distally. The well-developed crista deltopectoralis extends far distally on the shaft and has an evenly curved dorsal border. The low impressio musculi pectoralis is in proximal position on the crista deltopectoralis (fig. 9). It is dorsally indistinct and has an evenly curved distoventral border. The tuberculum ventrale is not completely preserved, but appears well developed (fig. 8). It is oriented somewhat proximally and dorsally, with an oblique concave ventral facet. Its proximal facet is slightly concave with a distinct pit in its dorsal corner. The crista bicipitalis is low and oblique.

The fossa pneumotricipitalis is very large and faces caudally (fig. 8). The crus dorsale fossae is distally continuous with the margo caudalis. The thick crus ventrale fossae is convex in its distal part and forms a flat surface just distal to the tuberculum ventrale. This flat surface

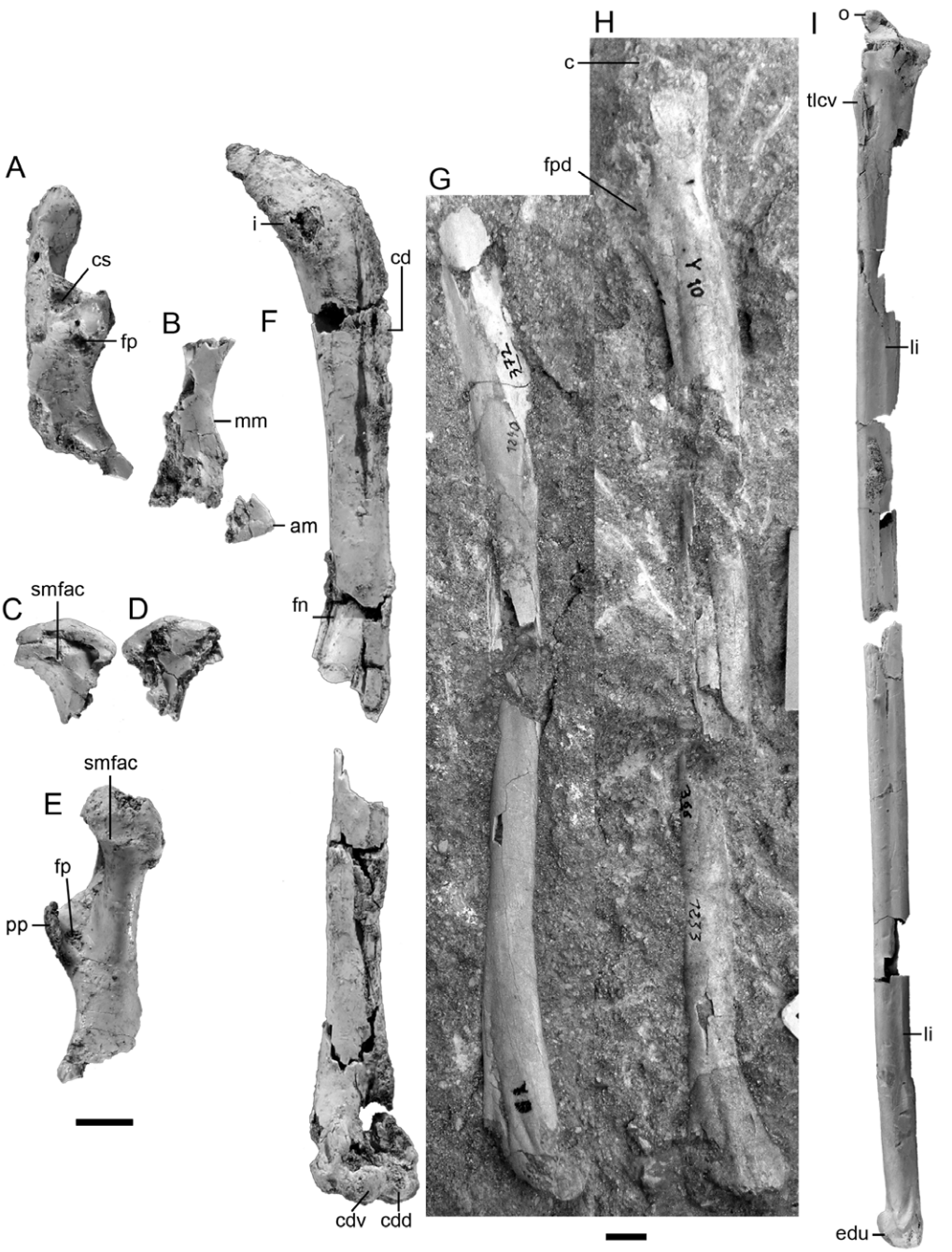

FIGURE 7. *Dasornis toliapica*. **A–E.** Left ossa coracoidei: **A.** OCP.DEK/GE 1195, dorsal view; **B.** reversed OCP.DEK/GE 1088, corpus, dorsal view; **C.** reversed OCP.DEK/GE 1088, processus acrocoracoideus, medial view; **D.** reversed OCP.DEK/GE 1088, processus acrocoracoideus, lateral view; **E.** OCP.DEK/GE 1195, ventral view. **F.** Reversed OCP.DEK/GE 1070, right humerus, cranial view. **G.** OCP.DEK/GE 1240, right humerus, caudal view. **H.** OCP.DEK/GE 1233, right humerus, caudal view. **I.** MHNL 20-149215, left ulna, cranial view. Scale bars equal 10 mm.

exhibits a distinct scar for the insertion of musculus scapulohumeralis caudalis. Two pneumatic foramina are widely separated from each other by a thick ridge. The proximal foramen pneumaticum is roughly oval in shape. The distal one is narrow, proximodistally elongated with tapering extremities.

The short, deep sulcus transversus ends dorsally at the level of the incisura capitis (fig. 9). It is perpendicular to the long axis of the corpus, sharply defined, with tapering ventral extremity. The planum intertuberculare is nearly flat. The low intumescentia humeri is poorly developed dorsally, proximodistally elongated, and shows two prominences that are loosely separated from each other. The proximal one is just distal to the sulcus transversus. The roughly rounded distal one is the higher. The impressio coracobrachialis is very shallow. Its dorsal border is visible as a low, blunt crest. Tiny vascular foramina are present in the distal part of planum intertuberculare, at the level of the impressio coracobrachialis and the distal prominence of the intumescentia.

The corpus humeri is straight (fig. 7) and oval in transverse section. Close to the extremitas proximalis, the margo caudalis is prominent, so that the transverse section of the humerus is triangular (fig. 8). The linea musculi latissimi dorsi is dorsal to the margo caudalis and divided into two widely separated parts. The distal part of the linea is thick, well defined, and continues far distally to the crista deltopectoralis. The section of linea distal to the crista deltopectoralis is close to the margo dorsalis. The proximal part of the linea musculi latissimi dorsi is an almond-shaped facet that is ventral to the distal part. It faces caudally and is parallel to the margo caudalis. The slitlike, proximodistally elongated foramen nutritium (Ballman, 1969) is in distal position on facies cranialis and close to the margo ventralis (figs. 7, 9). The margo dorsalis sharpens close to the distal extremity (fig. 10).

The condylus dorsalis is long, straight, blunt at the tip, and distally prominent (fig. 10). The condylus ventralis is roughly rounded with a low, oblique crest on its ventral side. It is distally prominent and has an abrupt caudal border. It does not extend distally to the condylus dorsalis. The incisura intercondylaris is wide. The fossa musculi brachialis is shallow and roughly oval in shape. The epicondylus dorsalis is a very prominent, proximodistally short convexity. The tuberculum supracondylare dorsale is a small pit just proximal to this structure. The origin of musculus extensor carpi ulnaris is caudodistal to the epicondylus dorsalis and it consists of two deep concavities that are bounded caudally, cranially, and distally by a thick and smooth prominent ridge. There is a distinct separation between this ridge and the condylus dorsalis. The proximal concavity is slightly cranial to the distal one. The epicondylus ventralis is a blunt ridge that is perpendicular to the long axis of the corpus. The facies ventralis just proximal to the former is markedly concave. The large surface of attachment of the ligamentum collaterale ventrale faces cranially, is oval in shape and higher than it is wide. The surface of origin of musculus pronator superficialis is a small pit proximal and slightly caudal to the latter. The processus flexorius is poorly developed and distinctly proximal to the condylus ventralis. The origin of musculus flexor carpi ulnaris consists of two scars that face slightly cranially, the more cranial one the larger and the deeper. The fossa olecrani is fairly shallow. The sulci humerotricipitalis and scapulotricipitalis are shallow. The latter is wide, without prominent borders.

The partial humeri tentatively assigned to *Macrodontopteryx oweni* (a junior synonym of

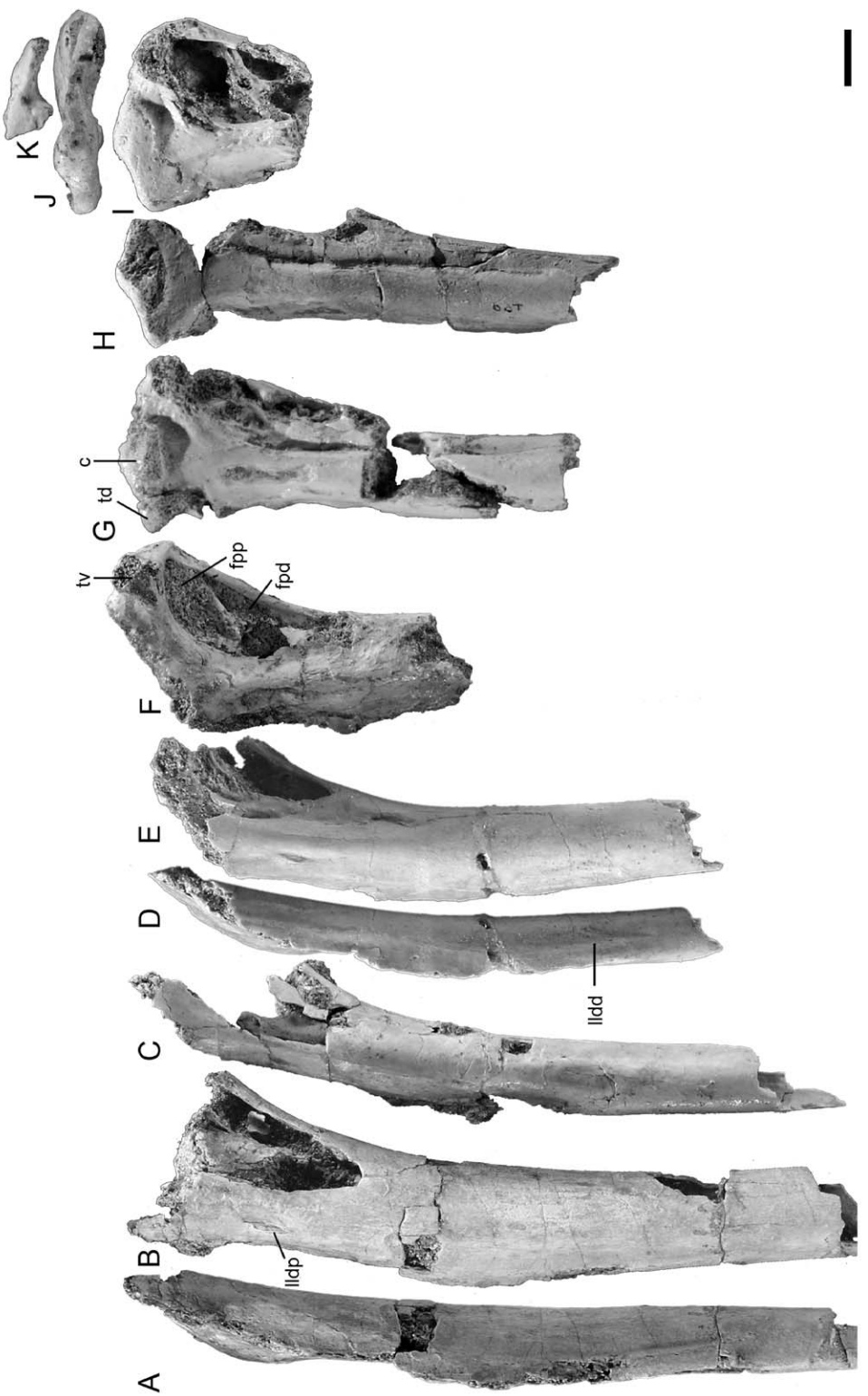

FIGURE 8. *Dasornis toliapica*, proximal part of left humeri. **A, D.** Dorsal view: **A.** MHNL 20-149229; **D.** OCP.DEK/GE 1003. **B, C, E–I.** Caudal view: **B.** MHNL 20-149229; **C.** reversed OCP.DEK/GE 1164; **E.** OCP.DEK/GE 1003; **F.** reversed OCP.DEK/GE 1194; **G.** OCP.DEK/GE 1216; **H.** reversed OCP.DEK/GE 1128; **I.** OCP.DEK/GE 1229. **J, K.** Proximal view: **J.** OCP.DEK/GE 1229; **K.** reversed OCP.DEK/GE 1164. Scale bar equals 10 mm.

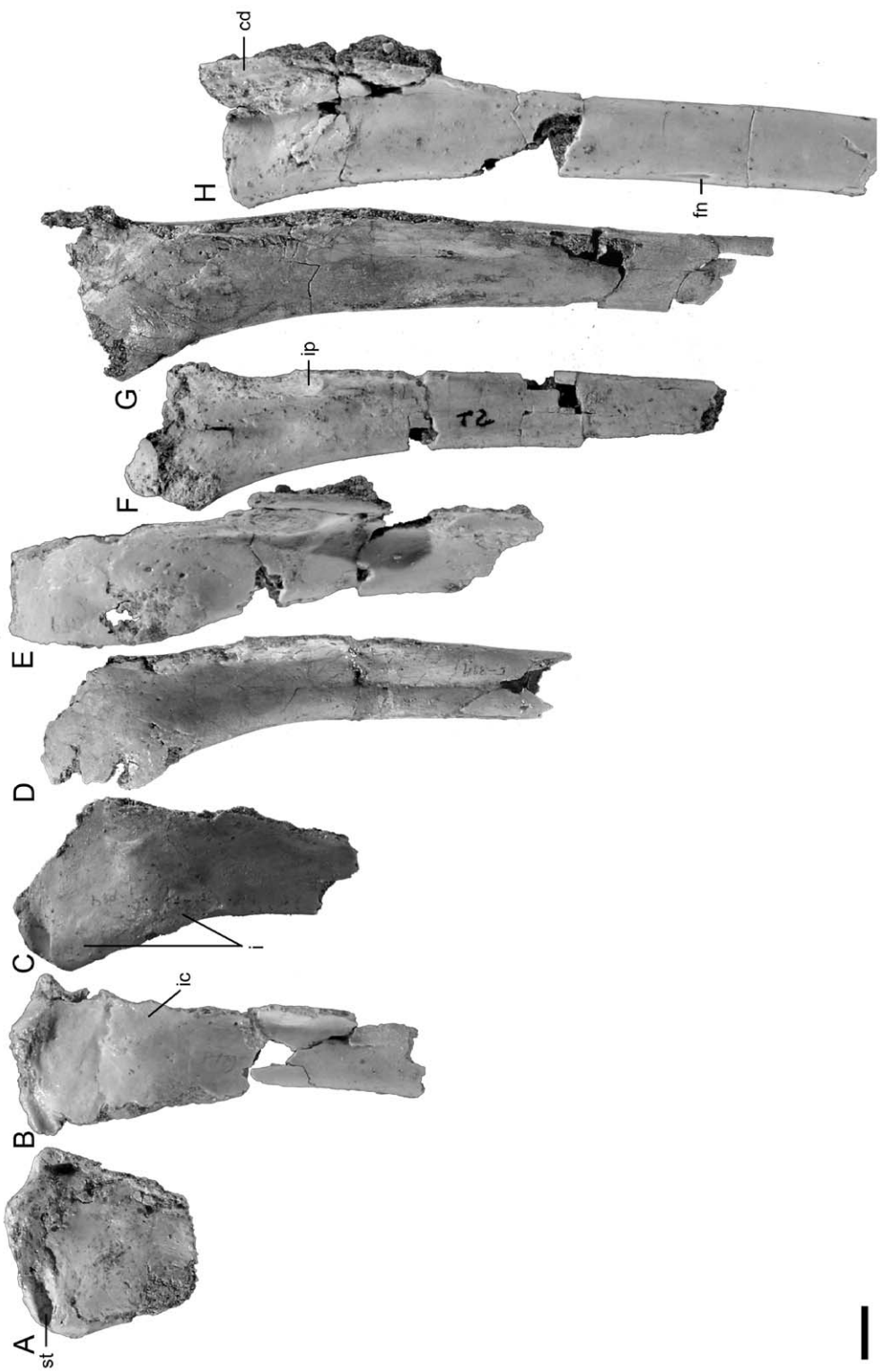

FIGURE 9. *Dasornis toliapica*, proximal part of left humeri in cranial view. **A.** OCP.DEK/GE 1229; **B.** OCP.DEK/GE 1216; **C.** reversed OCP.DEK/GE 1194; **D.** OCP.DEK/GE 1003; **E.** reversed OCP.DEK/GE 1183; **F.** OCP.DEK/GE 1086; **G.** MHNL 20-149229; **H.** OCP.DEK/GE 1116. Scale bar equals 10 mm.

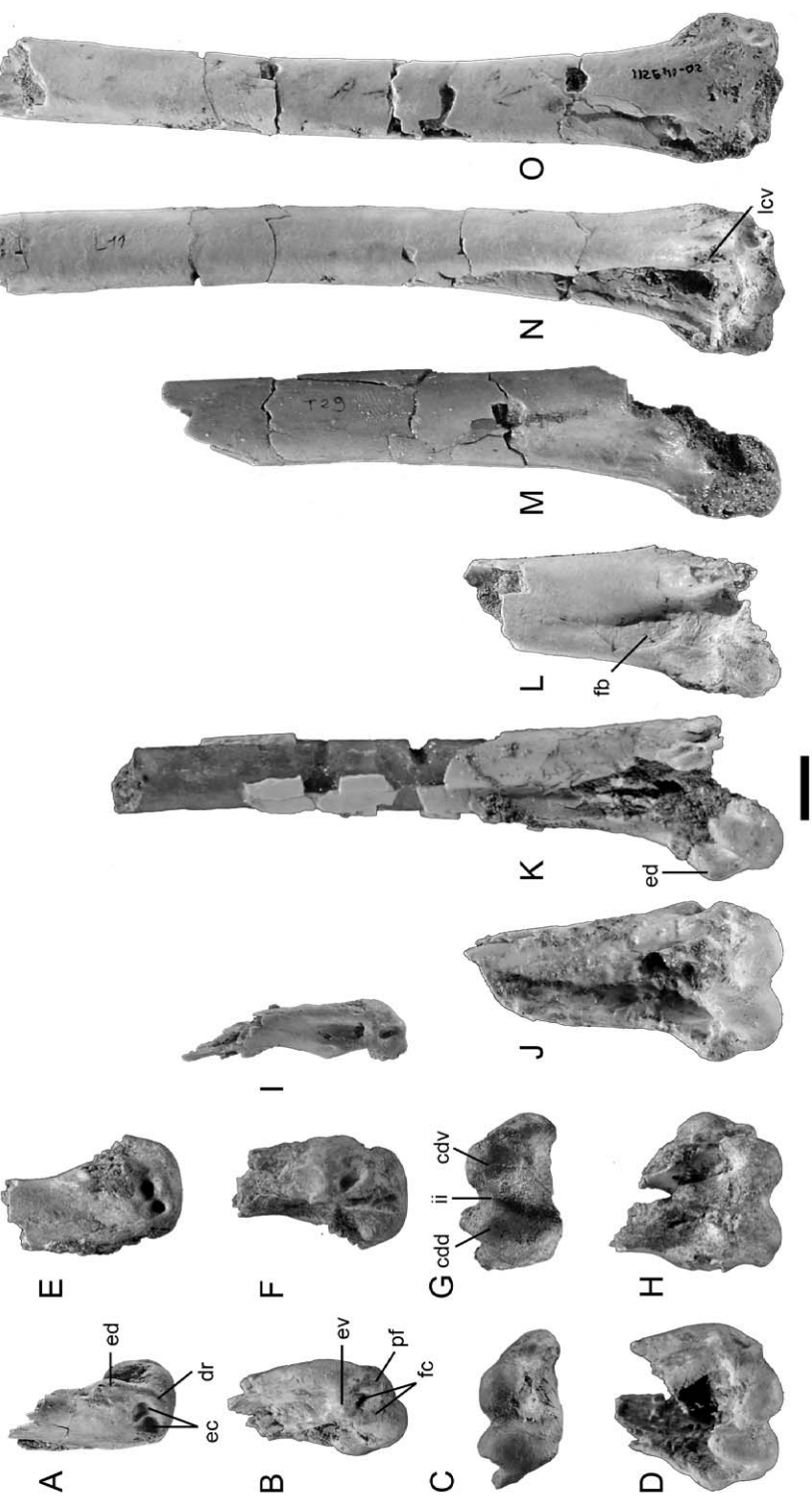

FIGURE 10. *Dasornis toliapica,* distal part of right humeri. **A–D.** MHNL 20-149214, extremitas distalis: **A.** dorsal view; **B.** ventral view; **C.** distal view; **D.** cranial view. **E–H.** Reversed MHNL 20-149216, extremitas distalis: **A.** dorsal view; **B.** ventral view; **C.** distal view; **D.** cranial view. **I.** Reversed OCP.DEK/GE 1164, extremitas distalis, ventral view. **J–N.** Cranial view: **J.** OCP.DEK/GE 1075; **K.** reversed OCP.DEK/GE 1218; **L.** reversed OCP.DEK/GE 1203; **M.** OCP.DEK/GE 1107; **N.** MHNL 20-149211. **O.** MHNL 20-149211, caudal view. Scale bar equals 10 mm.

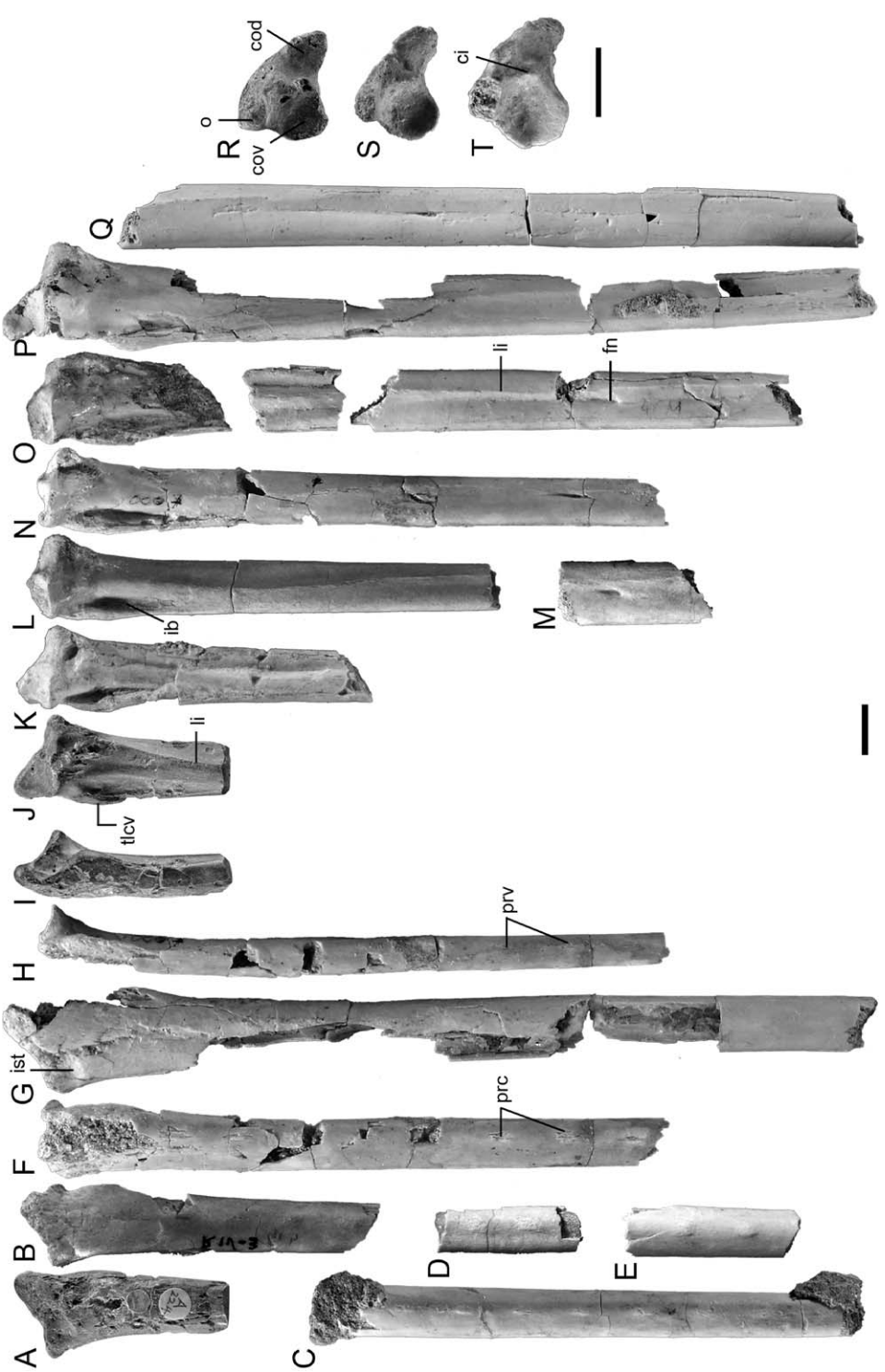

FIGURE 11. *Dasornis toliapica*, proximal part of left ulnae. **A, B, F, G.** Caudal view: **A.** BMNH A224; **B.** reversed OCP.DEK/GE 1002; **F.** OCP.DEK/GE 1005; **G.** MHNL 20-149215. **C–E.** Fragments of corpus in caudal view: **C.** OCP.DEK/GE 1257; **D.** reversed OCP.DEK/GE 1207; **E.** reversed OCP.DEK/GE 1160. **H, I.** Ventral view: **H.** OCP.DEK/GE 1005; **I.** BMNH A224. **J–Q.** Cranial view: **J.** BMNH A224; **K.** reversed OCP.DEK/GE 1002; **L.** OCP.DEK/GE 1283; **M.** OCP.DEK/GE 1135; **N.** OCP.DEK/GE 1005; **O.** OCP.DEK/GE 1039; **P.** MHNL 20-149215; **Q.** reversed MHNL 20-149218. **R–T.** Proximal view: **R.** BMNH A224; **S.** reversed OCP.DEK/GE 1002; **T.** OCP.DEK/GE 1039. Scale bars equal 10 mm.

Dasornis toliapica) by Mayr and Smith (2010: fig. 5) match fairly well with the Moroccan specimens except for three features: the caput humeri protrudes more proximally and there is a conspicuous muscle attachment scar on the dorsal edge and at mid height of the fossa pneumotricipitalis, which is smaller than in *D. toliapica*. These elements indicate that the Belgian specimens belong to a different species, and might be assigned to a different genus.

Ulna (figs. 7, 11, 12)

The extremitas proximalis ulnae and the proximal part of the corpus are exceedingly similar to those of BMNH A224, but more or less caudocranially crushed. Most probably, the original aspect of the ulna is preserved in BMNH A224 (fig. 11R). The impressio musculi brachialis is small, indistinct, and distally tapering (fig. 11). The facies caudodorsalis is strongly convex. The impressio musculi scapulotricipitalis is in distodorsal position and roughly parallel to cotyla dorsalis. The cotyla dorsalis is flat with a straight cranial border and a pointed extremity without any dorsal projection. The cotyla ventralis is round. The crista intercotylaris is well developed, wide, and blunt. The depression for attachment of meniscus radioulnaris is poorly developed. The incisura radialis is rather shallow, with a rounded dorsal edge. The olecranon is prominent, caudocranially narrow, with a bluntly rounded tip that is slightly deflected ventrally. The tuberculum ligamenti collateralis ventralis is prominent, proximodistally elongated, and in distal position.

The corpus is straight (fig. 7), without marked cranial curvature at the proximal end (fig. 11). It is wider than deep, with a well-marked, smooth margo caudalis. Its proximal part shows a low margo interosseus. The sharp linea intermuscularis of facies cranialis extends from the dorsal border of the cotyla dorsalis to the tuberculum carpale (fig. 7I). It is evenly curved in the proximal part and parallel to the margo dorsalis distal to the foramen nutritium (Ballmann, 1969). The papillae remigales are low and longitudinally striated tubercles (figs. 11, 12). A slight caudocranial flattening of the corpus occurs not far from the extremitas distalis (fig. 12).

The extremitas distalis ulnae is somewhat flattened caudocranially and roughly corresponds to an isosceles triangle (fig. 12). The condylus dorsalis, condylus ventralis, and tuberculum carpale are of same width. The condylus dorsalis extends rather far proximally and protrudes caudoventrally. In its ventral part, the smooth condylus ventralis shows a low prominence in cranial position. It has a bluntly pointed ventral extremity. The sulcus intercondylaris is wide and shallow. Its proximal continuation on facies cranialis is a wide flat surface bounded ventrally by a distinct sinuous ridge that extends far proximally. The apex of this ridge is visible in distal view and gives a truncated aspect to the cranial border of the ulna. The distal edge of the smooth tuberculum carpale is straight to slightly curved and slopes only slightly proximally. The ventral edge of the tuberculum extends far proximally on the corpus. The facies cranialis is not deeply excavated between the tuberculum carpale and the continuation of the sulcus intercondylaris. The depressio radialis is shallow with a well-marked proximal edge. The incisura tendinosa is shallow with a straight caudal edge and a curved cranial one. A low tubercle lies at its proximal corner.

The proximal part of the ulna tentatively referred to *Macrodontopteryx oweni* (BMNH

FIGURE 12. *Dasornis toliapica*, distal part of ulnae. **A, B.** Left ulnae, cranial view: **A.** MHNL 20-149215; **B.** MHNL 20-149217. **C–E.** Right ulnae, dorsal view: **C.** reversed MHNL 20-149237; **D.** MHNL 20-149218; **E.** OCP.DEK/GE 1035. **F–H.** Right ulnae, ventral view: **F.** MHNL 20-149218; **G.** OCP.DEK/GE 1035; **H.** OCP.DEK/GE 1198. **I, J.** Right ulnae, cranial view: **I.** OCP.DEK/GE 1198, **J.** MHNL 20-149218. **K, L.** Fragments of right corpus ulnae, caudal view: **K.** reversed MHNL 20-149220; **L.** reversed OCP.DEK/GE 1153. **M–O.** Right ulnae, distal view: **M.** MHNL 20-149218; **N.** OCP.DEK/GE 1035; **O.** OCP.DEK/GE 1198. Scale bars equal 10 mm.

A3692) by Harrison and Walker (1976) is identical to that of *Dasornis toliapica* and its size corresponds to that of the largest individuals of this species (table 2). This justifies the assignment of BMNH A3692 to *D. toliapica*.

Radius (fig. 13)

The cotyla humeralis is almond shaped, dorsoventrally elongated, and caudocranially flattened. Its cranial edge is distinctly proximal to the caudal one. Its ventral border forms a conspicuous overhang that is continuous with the prominent caudal edge of the tuberculum bicipitale. The caput radii is prominent and well developed dorsoventrally. In dorsal aspect, it is oblique and very sharply defined proximally. A crest on the facies caudalis extends from the top of the latter structure to a point slightly distal to the tuberculum bicipitale. This crest together with the tuberculum bicipitale and the facies articularis ulnaris delimit a slightly concave and triangular plateau.

Several isolated fragments of corpus radii are preserved. The corpus is very straight with only a slight ventral curvature toward the extremitas proximalis. Its facies cranialis shows sharply defined lineae intermusculares in its proximal part. A straight groove (caudodorsal groove) continues the caudal part of sulcus tendinosus through most of the length of the corpus.

The extremitas distalis is wide and has a strong ventral curvature. The ligamental prominence (Howard, 1929) is strongly convex and protrudes ventrally. Its proximal border is well defined and sinuous. The depressio ligamentosa and the region proximal to the cranial part of the ligamental prominence are strongly concave and separated from each other by the smooth and curved distal end of the margo ventralis. The protuberance cranial to the sulcus tendinosus (dorsal convexity) is high and caudocranially wide. The caudal border of facies articularis radiocarpalis evenly curves toward the tuberculum aponeurosis ventralis. A small tubercle (ventral tubercle) is just proximal to the depressio ligamentosa, close to the margo interosseus. The sulcus tendinosus is smooth and shallow.

Carpometacarpus (fig. 14)

The os metacarpale alulare does not show any strongly protruding processus extensorius. It forms a somewhat elongated structure parallel to the long axis of os metacarpale majus. A very elongated processus alularis with an orientation comparable to that of *Dasornis toliapica* is found in Gaviidae. The caudodorsal extremity of the trochlea carpalis forms a thick tubercle. The sharp caudoventral border of the trochlea carpalis extends as far distally as this tubercle. The dorsal margin of the trochlea carpalis shows a small prominence just caudal to the well-defined surface of attachment of ligamentum radiocarpo-metacarpale dorsale. The fossa supratrochlearis exhibits a short furrow that can be referred to the facies ligamenti externa (Ballmann, 1969). The proximoventral corner of the trochlea carpalis is thick and overhangs the deep fossa infratrochlearis. The processus pisiformis is very prominent with an oblique proximal margin that reaches the trochlea carpalis caudally. Its cranial border forms a conspicuous overhang that extends far distally. A sharp crest cranial to the processus pisiformis constitutes the caudal edge of the depressio muscularis interna (Ballmann, 1969).

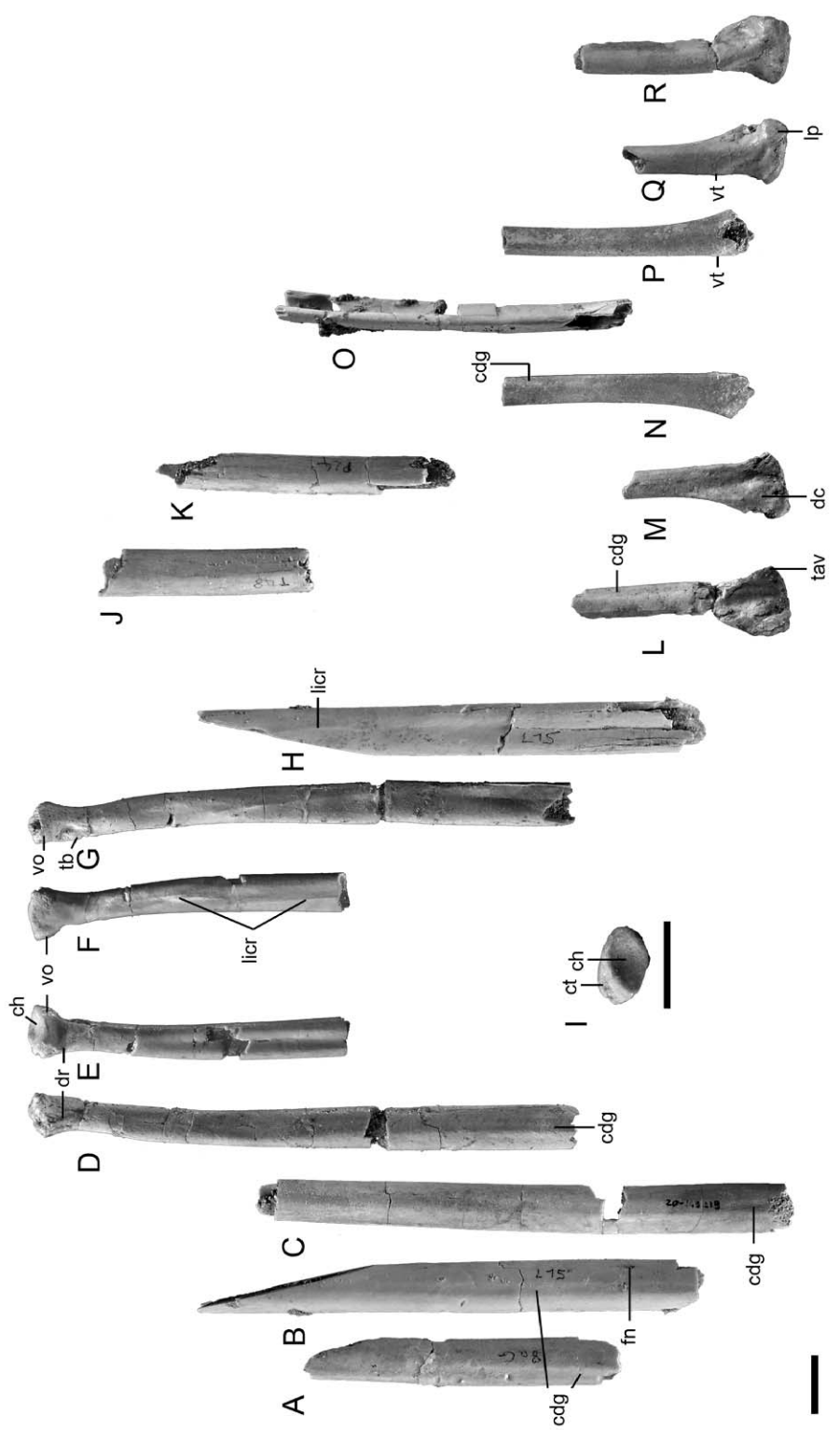

FIGURE 13. *Dasornis toliapica*, radii. **A–E.** Proximal parts of left radii in caudal view: **A.** OCP.DEK/GE 1055; **B.** MHNL 20-149215; **C.** MHNL 20-149219; **D.** OCP.DEK/GE 1175; **E.** OCP.DEK/GE 1212. **F–H.** Proximal parts of left radii in cranial view: **F.** OCP.DEK/GE 1212; **G.** OCP.DEK/GE 1175; **H.** MHNL 20-149215. **I.** OCP.DEK/GE 1212, left radius, proximal view. **J.** OCP.DEK/GE 1121, fragment of corpus radii, dorsal view. **K.** OCP.DEK/GE 1153, fragment of left corpus radii, dorsal view. **L–N.** Distal ends of left radii in dorsal view: **L.** reversed OCP.DEK/GE 1058; **M.** reversed OCP.DEK/GE 1118; **N.** reversed OCP.DEK/GE 1199. **O–R.** Distal ends of left radii in ventral view: **O.** reversed OCP.DEK/GE 1157; **P.** reversed OCP.DEK/GE 1199; **Q.** reversed OCP.DEK/GE 1118; **R.** reversed OCP.DEK/GE 1058. Scale bars equal 10 mm.

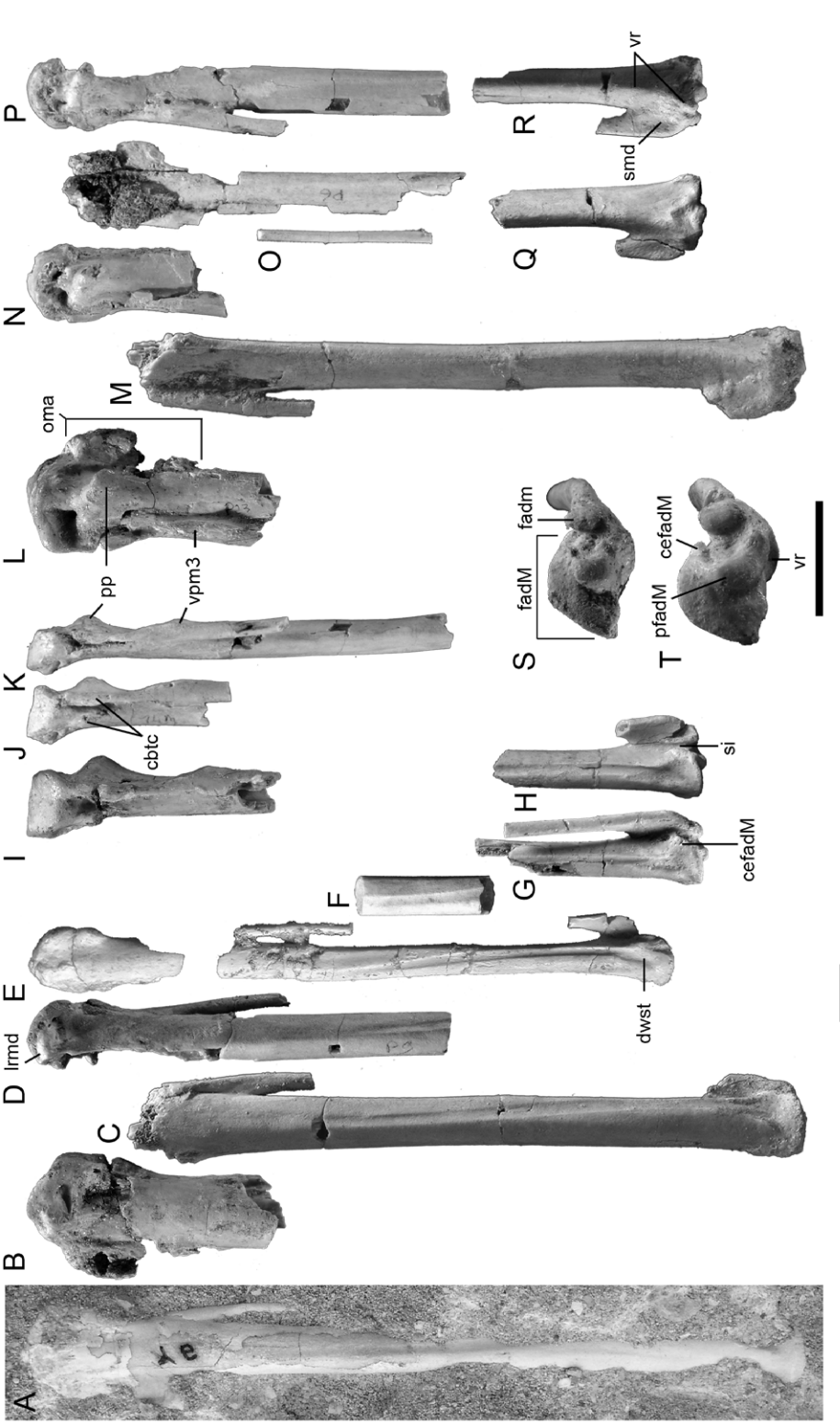

FIGURE 14 *Dasornis toliapica*, left carpometacarpi. **A–H.** Dorsal view: **A.** reversed OCP.DEK/GE 1241; **B.** OCP.DEK/GE 1152; **C.** reversed OCP.DEK/GE 1255; **D.** OCP.DEK/GE 1139; **E.** OCP.DEK/GE 1172; **F.** OCP.DEK/GE 1100; **G.** reversed OCP.DEK/GE 1101; **H.** reversed OCP.DEK/GE 1102. **I–K.** Caudal view: **I.** OCP.DEK/GE 1152; **J.** OCP.DEK/GE 1012; **K.** OCP.DEK/GE 1139. **L–R.** Ventral view: **L.** OCP.DEK/GE 1152; **M.** reversed OCP.DEK/GE 1255; **N.** OCP.DEK/GE 1012; **O.** OCP.DEK/GE 1137; **P.** OCP.DEK/GE 1139); **Q.** reversed OCP.DEK/GE 1101; **R.** reversed OCP.DEK/GE 1102. **S, T.** Distal view: **S.** reversed OCP.DEK/GE 1101; **T.** reversed OCP.DEK/GE 1102. Scale bars equal 10 mm.

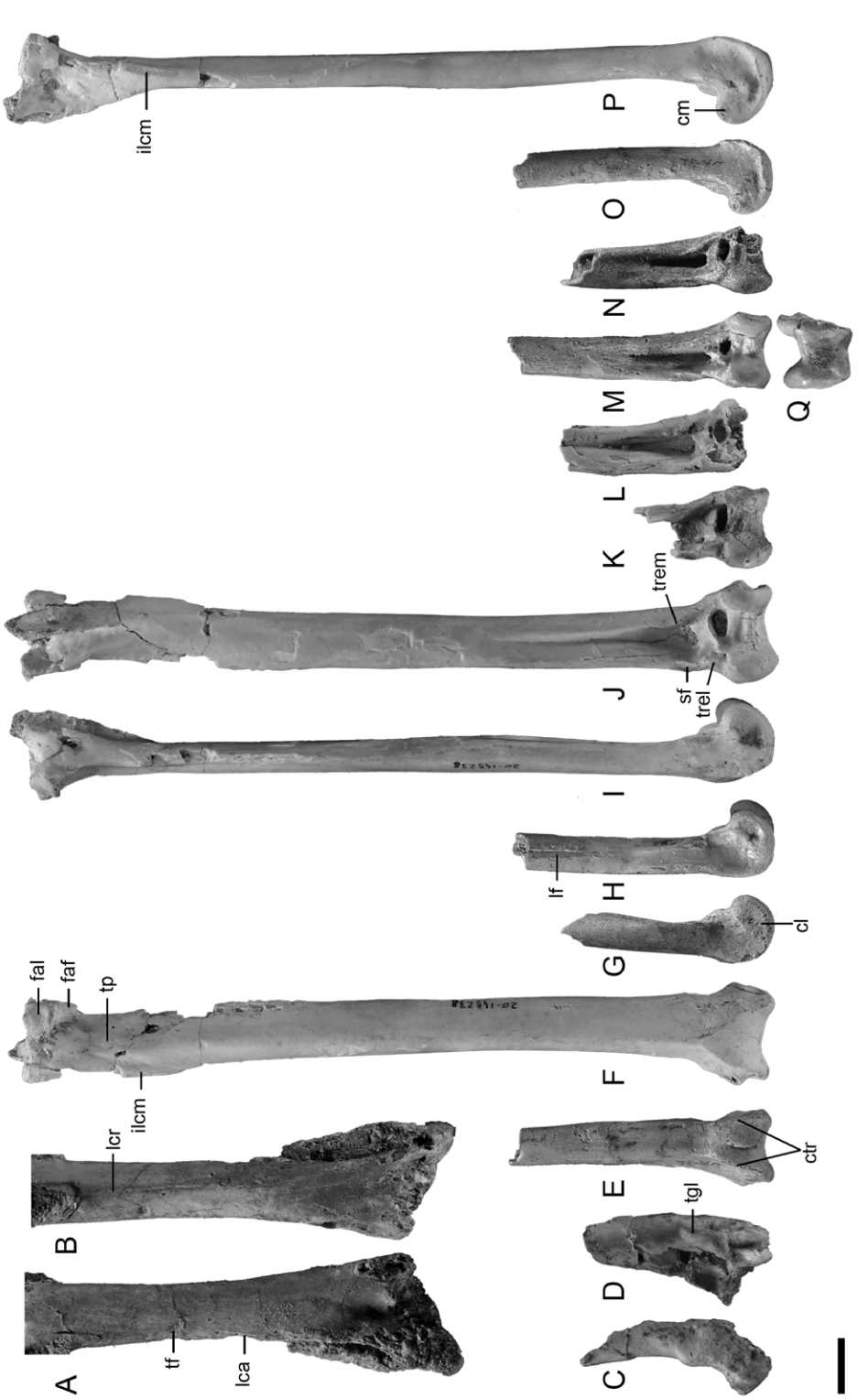

FIGURE 15. *Dasornis toliapica*. **A, B.** OCP.DEK/GE 1045, partial right femur: **A.** caudal view; **B.** cranial view. **C, D.** OCP.DEK/GE 1144, fragment of distal end of right femur: **C.** lateral view; **D.** caudal view. **E, F.** Right tibiotarsi in caudal view: **E.** OCP.DEK/GE 1013; **F.** MHNL 20-149238. **G–I.** Right tibiotarsi in lateral view: **G.** reversed OCP.DEK/GE 1011; **H.** OCP.DEK/GE 1013; **I.** MHNL 20-149238. **J–N.** Right tibiotarsi in cranial view: **J.** MHNL 20-149238; **K.** reversed OCP.DEK/GE 1040; **L.** OCP.DEK/GE 1204; **M.** OCP.DEK/GE 1013; **N.** reversed OCP.DEK/GE 1011. **O–P.** Right tibiotarsi in medial view: **O.** OCP.DEK/GE 1013; **P.** MHNL 20-149238. **Q.** OCP.DEK/GE 1013, right tibiotarsus, distal view. Scale bar equals 10 mm.

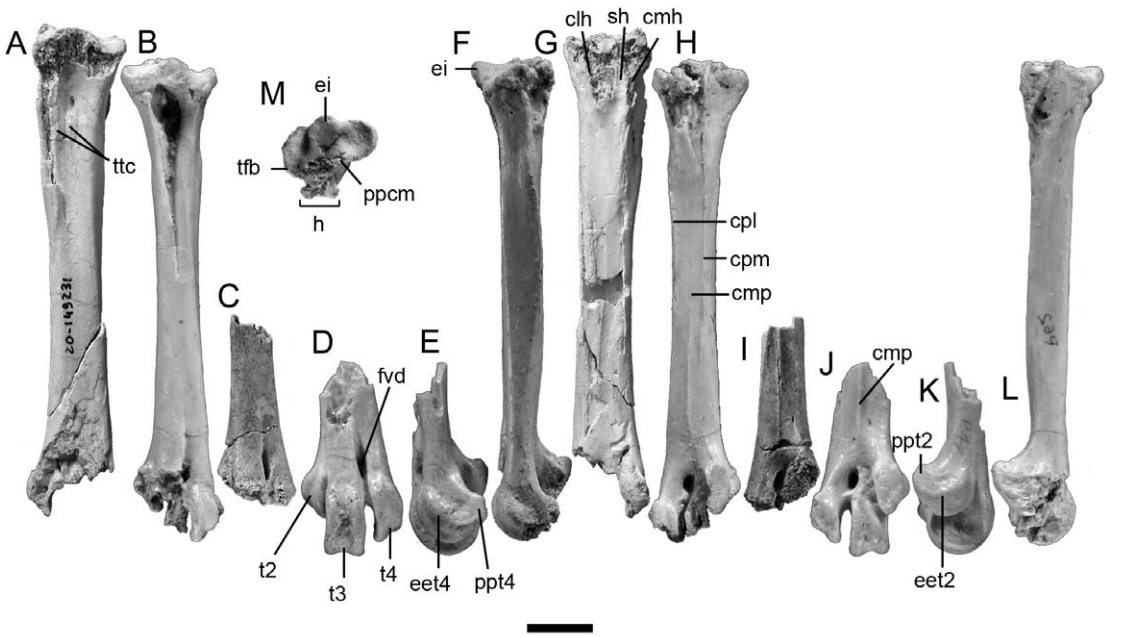

FIGURE 16. *Dasornis toliapica*, left tarsometatarsi. **A–D.** Dorsal view: **A.** MHNL 20-149231; **B.** reversed OCP.DEK/GE 1176; **C.** OCP.DEK/GE 1155; **D.** OCP.DEK/GE 1146. **E, F.** Lateral view: **E.** OCP.DEK/GE 1146; **F.** reversed OCP.DEK/GE 1176. **G–J.** Plantar view: **G.** MHNL 20-149231; **H.** reversed OCP.DEK/GE 1176; **I.** OCP.DEK/GE 1155; **J.** OCP.DEK/GE 1146. **K–L.** Medial view: **K.** OCP.DEK/GE 1146; **L.** reversed OCP.DEK/GE 1176. **M.** Reversed OCP.DEK/GE 1176, proximal view. Scale bar equals 10 mm.

The corpus is long and slender. The straight os metacarpale majus is roughly triangular in shape, because it shows a smooth median ridge on facies ventralis (ventral ridge) that curves caudally close to the facies articularis digitalis major. Just cranial to the distal end of this median crest is a triangular concavity. The sulcus tendinosus distinctly deepens and widens at distal extremity. There is no processus intermetacarpalis. The os metacarpale minus is oval in transverse section and fused proximally to the os metacarpale majus over a long distance. It is nearly straight and parallel to os metacarpale majus, so that the spatium intermetacarpale is narrow. In ventral aspect, it shows a sharp crest and a tubercle just proximal to the spatium intermetacarpale. On the proximal slope of the tubercle is a large surface of attachment of ligamentum ulnocarpo-metacarpale ventrale that can be referred to the facies ligamenti interna (Ballmann, 1969).

The symphysis metacarpalis distalis is long and slightly concave in ventral aspect. The sulcus interosseus is deep and narrow. The facies articularis digitalis major has a regularly curved dorsal margin that extends far caudally. In some specimens, this margin forms a bridge above the sulcus interosseus. The facies articularis digitalis major exhibits a high and well-defined caudal protuberance that is continuous with the distal end of the ventral crest of os metacarpale majus. The facies articularis digitalis minor is oval in shape, dorsally protruding, and distinctly separated from the body of os metacarpale minus.

Femur (fig. 15A–D)

Most of the corpus and a small part of the extremitas distalis are preserved. The corpus is straight and slender. At mid height of the latter is a distinct triangular facet located on facies caudalis and close to the medial edge. The sharp linea intermuscularis caudalis is in extreme medial position and continuous with the crista supracondylaris medialis. It is interrupted proximal to the triangular facet. The linea intermuscularis cranialis is straight and roughly parallel to the lateral border of the corpus.

In caudal aspect, the trochlea fibularis is wide and faces caudally. Just above the condylus fibularis is a distinct notch. The tuberculum musculi gastrocnemialis lateralis is high and conspicuous. The distal impressio ansae musculi iliofibularis is just distal to the latter. The fossa poplitea appears deep. In cranial aspect, the sulcus patellaris and sulcus intercondylaris are deep and wide, and the crista medialis sulci patellaris is narrow and prominent. Proximal to the crista lateralis sulci patellaris is the proximal impressio ansae musculi iliofibularis.

Tibiotarsus (fig. 15E–Q)

The proximal part of the tibiotarsus is preserved only in MHNL 20-149238 (fig. 15F, I, J, P). The partly damaged cristae cnemiales are well developed. The cranial margin of the crista cnemialis cranialis was straight to slightly curved. The facies articularis lateralis protrudes proximally and caudally and is continuous with a very prominent facies articularis fibularis. The fossa flexoria is deep. The caudal incisura between the facies articularis medialis and the facies articularis lateralis is well defined. The impressio ligamenti collateralis medialis is a very prominent and proximodistally elongated tubercle.

The crista fibularis is damaged. The part of the facies caudalis level with the latter structure is convex. The conspicuous tuberositas poplitea consists of three sharp ridges that are parallel to each other. The linea extensoria is well marked. The well-defined lineae musculi fibularis form a wide platform that tapers toward the crista fibularis proximally and toward the sulcus musculi fibularis distally.

The condylus lateralis has a nearly straight caudal margin and projects rather far cranially. The epicondylus lateralis is a blunt oblique ridge that is variably developed. The depressio epicondylaris lateralis is shallow. The condylus medialis is perpendicular to the long axis of the corpus, strongly projects cranially, and has a convex proximal border. It protrudes more cranially and is narrower than the condylus lateralis. The epicondylus medialis is a distinct protuberance that extends beyond the proximal edge of the condylus medialis. A tiny circular pit is present at the extremitas distalis and on the internal side of the condylus medialis. Both condylae are devoid of distal notches. The incisura intercondylaris is very wide with a marked impressio ligamenti intercondylaris. It extends onto the proximal part of the condylus medialis. The deep, sharply defined sulcus musculi fibularis faces craniolaterally. The zone between the latter and the epicondylus lateralis is depressed. The trochlea cartilaginis tibialis is shallow and its proximal end forms a smooth transition with the corpus. The cristae trochleae are poorly developed.

The sulcus extensorius is deep and occupies the median third of the facies cranialis, with the medial border distinctly higher than the lateral one. The lateral tuberositas retinaculi extensori forms a vertical triangular surface that communicates with the lateral margin of the pons supratendineus through a sharp edge. It is located just above the condylus lateralis and separated from the latter by a distinct pit. The medial tuberositas retinaculi extensori is a sharp oblique ridge that is proximodistally elongated. The pons supratendineus is wide and slightly oblique. The distal opening of the canalis extensorius is large, oval, and tapers a little laterally. It is slightly medial to the sulcus extensorius.

Tarsometatarsus (fig. 16)

In the Moroccan fossils, the tarsometatarsus is preserved in its entirety except for the extremitas proximalis and hypotarsus, which are slightly damaged. In contrast, these parts are well preserved in BMNH A134 (Harrison and Walker, 1977: pl. 1), which was initially referred to *Odontopteryx toliapica* by Lydekker (1891) and later assigned to *Neptuniavis minor* by Harrison and Walker (1977). The cotyla medialis is round and its inner plantar corner forms a prominent ridge (plantar prominence) extending to the crista medialis hypotarsi. The cotyla lateralis has a marked dorsodistal slant and its lateroplantar corner shows a prominent tuberculum musculi fibularis brevis. The eminentia intercotylaris is dorsally prominent and laterally deflected with a slight overhang on the lateral side. The hypotarsus is in lateral position, its lateral border in line with the medial edge of the cotyla medialis. It consists of three cristae hypotarsi and two sulci (Harrison and Walker, 1977: pl. 1G). The crista medialis extends further proximally and distally than the two lateralmost cristae. The sulcus medialis is deeper and wider than the sulcus lateralis. The plantar aperture of the lateral foramen vasculare proximale is deeply set at the side of the distal end of the crista lateralis hypotarsi. The plantar aperture of the medial foramen vasculare proximale is proximal and dorsal to the lateral one. The impressio ligamenti collateralis lateralis is a proximodistally elongated scar on facies lateralis, not far beneath the lateral edge of the cotyla lateralis.

The corpus is almost square in transverse section and flares out more widely at the proximal end of the facies subcutanea medialis. The cristae plantares are low and sharply defined. The crista medianoplantaris is straight. The facies medialis shows an evenly curved line ending proximodorsally into a small oval scar that is probably for the origin of musculus extensor hallucis longus. The fossa metatarsi I is very shallow, nearly indistinct.

The fossa infracotylaris dorsalis and the proximal part of the sulcus extensorius are deep. The dorsal opening of the medial foramen vasculare proximale is only a little higher than the lateral one. The tuberositas musculi tibialis cranialis consists of two parts, the lateral one slightly distal to the medial one. The latter is continuous with a sharp ridge extending to the proximal part of the fossa infracotylaris dorsalis and partly hiding the medial foramen vasculare proximale.

The foramen vasculare distale is large and higher than it is wide. In dorsal aspect, it is continued proximally by a deep sulcus musculi extensoris brevis digiti IV (Ballmann, 1969). In plantar aspect, it is recessed and in low position.

All three trochleae are grooved and the external sides of trochleae metatarsi II and IV are

smooth. The trochlea metatarsi II shows a very strong proximal and plantar displacement and is tilted plantarolaterally. Its rounded inner edge extends barely a third of the length of trochlea metatarsi III. The external flange of trochlea metatarsi II is displaced proximally and forms plantarly a proximally pointed projection. The external fovea ligamenti collateralis is very shallow.

The trochlea metatarsi III is dorsally elevated in dorsal aspect, and its base is incised by the foramen vasculare distale. In plantar aspect, the trochlea metatarsi III is proximodistally elongated and slightly oblique, with a pointed extremity. The trochlea metatarsi IV extends about two-thirds the length of the trochlea metatarsi III. Its internal flange is round. Its external flange shows a strong proximoplantar displacement and forms a bluntly rounded plantar projection. The external fovea ligamenti collateralis is a shallow concavity. The incisura intertrochlearis lateralis is wider than the incisura intertrochlearis medialis.

The proximal end of tarsometatarsus tentatively assigned to *Macrodontopteryx oweni* (a junior synonym of *Dasornis toliapica*) by Mayr and Smith (2010: fig. 6) differs from *D. toliapica* and *Dasornis emuinus* in several features: the cotylae are subequal (the cotyla lateralis is distinctly smaller than the cotyla medialis in *Dasornis*), the eminentia intercotylaris is less prominent dorsally, the cristae hypotarsi are more prominent and subequal in height, the corpus is more slender, the crista plantaris lateralis is more sharply defined, and the sulcus extensorius is wider and deeper. These elements indicate that the Belgian specimen belongs to a different species, which might be assigned to a different genus.

Dasornis emuinus (Bowerbank, 1854)

See Mayr (2008) and Mayr and Smith (2010) for a complete list of synonymies.

Referred Material: OCP.DEK/GE 324, incomplete cranium; OCP.DEK/GE 534A, distal part of left tibiotarsus; OCP.DEK/GE 1004, incomplete cranium; OCP.DEK/GE 1046, proximal part of right radius; OCP.DEK/GE 1059, proximal end of right femur; OCP.DEK/GE 1072, proximal part of right humerus in several fragments; OCP.DEK/GE 1078, fragment of shaft of left humerus in proximal half; OCP.DEK/GE 1106, complete left tarsometatarsus; OCP.DEK/GE 1109, distal part of left humerus; OCP.DEK/GE 1123, distal part of right tibiotarsus with incomplete end; OCP.DEK/GE 1130, fragment of shaft of left radius close to proximal end; OCP.DEK/GE 1165, fragment of shaft of left humerus close to proximal end; OCP.DEK/GE 1184, fragment of shaft of right radius; OCP.DEK/GE 1221, fragment of shaft of right radius; OCP.DEK/GE 1224, proximal end of left radius; OCP.DEK/GE 1236, complete right humerus embedded in matrix; OCP.DEK/GE 1237, complete left humerus embedded in matrix; OCP.DEK/GE 1242, distal part of left ulna + proximal part of left radius embedded in matrix; OCP.DEK/GE 1245, proximal end of left radius; OCP.DEK/GE 1252, distal end of left tarsometatarsus; OCP.DEK/GE 1268, fragments of distal end of left tarsometatarsus; OCP.DEK/GE 1269, fragments of cranium; OCP.DEK/GE 1288, incomplete cranium embedded in matrix; OCP.DEK/GE 1300, fragment of cranium; OCP.DEK/GE 1333, incomplete proximal part of right humerus embedded in matrix; OCP.DEK/GE 1334, fragment of shaft of right humerus; D1-0027A, incomplete cranium.

Localities: Ouled Abdoun Basin (Morocco): Sidi Daoui (including Krupp, PH2 and RP13 areas); Recette IV; southern Meraa El Arech (Lahou area).

Stratigraphic Distribution: Bed IIa, Thanetian, Upper Paleocene; intercalary beds II/I, basal Ypresian, lowermost Eocene; bed I, Ypresian, Lower Eocene.

Diagnosis: Gigantic odontopterygiform with a wingspan of 3.5–4.5 m, which differs from *Dasornis toliapica* in the following features: much larger size; cranium, sutura frontoparietalis more pronounced, forming curved groove; lamina parasphenoidalis caudorostrally shorter; caudal extension of cotyla quadratica otici longer and twisted ventrally; foramen pneumaticum dorsale smaller; laterosphenoid hollow triangular owing to the relatively smaller size of the prominentia lobi optici; tibiotarsus with longer sulcus musculi fibularis.

Measurements: See tables 1 and 2.

DESCRIPTION

Cranium (figs. 17–20)

The new skull material referred to *Dasornis emuinus* includes six imperfect crania. The processus paroccipitalis, os lacrimale, and fonticulus interorbitalis are incompletely preserved, but were probably similar to those of the London Clay skulls (Harrison and Walker, 1976; Mayr, 2008). The recessus columellae is not preserved (fig. 20). The foramen nervi trochlearis is at mid height and just lateral to the foramen opticum. It is continued dorsally by a long groove (fig. 20). The structure of the cranium of *D. emuinus* is exceedingly similar to that of *Dasornis toliapica*. Apart from the larger size, the former differs from the latter in a few features: the sutura frontoparietalis is more distinct, and forms a curved groove that marks the caudal edge of the transversely striated zone of the os frontale (fig. 17). The prominentia cerebellaris is narrower with a wide and blunt crista nuchalis sagittalis, but this might be due to preservation (fig. 18). The lamina parasphenoidalis is caudorostrally shorter (fig. 19; see also Mayr, 2008: fig. 3B). The os exoccipitale forms a thick flange extending lateral to the distinct foramen nervi glossopharyngealis, and there is no evidence of notch, groove, or canal for the arteria carotis cerebralis (figs. 18, 20). The caudal extension of the cotyla quadratica otici is longer and twisted ventrally (figs. 19, 20). The foramen pneumaticum dorsale is smaller and occupies the rostralmost third of the surface delimited by the cotylae quadratica plus their extensions (fig. 19). The laterosphenoid hollow (fig. 19) is triangular owing to the relatively smaller size of the prominentia lobi optici (Weber, 1996). The foramen for the exit of the nervus abducens is not situated in a deep pit. The foramen nervi ophthalmici is in more rostral position (fig. 20). The cranial differences between *D. emuinus* and *D. toliapica* must be taken with caution, given the artifacts of preservation and the limited number of available skulls.

Humerus (fig. 21)

The available material covers most of the humerus, and includes two complete humeri embedded in matrix (fig. 21A, B). In these two specimens, the major part of the facies cranialis is visible, but the corpus humeri is crushed (fig. 21A, B). Taking into account all specimens,

visible structures of the extremitas proximalis include the caput, tuberculum dorsale, base of crista deltopectoralis, a part of the dorsal margin of the foramen pneumaticum, and a part of the planum intertuberculare plus impressio coracobrachialis. Most of the corpus is preserved, including the linea musculi latissimi dorsi. Most of the extremitas distalis is conserved, including the shallow oval fossa musculi brachialis and the condylae. Apart from the larger size, the structure of the humerus of *Dasornis emuinus* is exceedingly similar to that of *Dasornis toliapica*. Mayr and Smith (2010) tentatively assigned an incomplete humerus from the Middle Eocene of Belgium to *D. emuinus*. However, two features of the Belgian specimen suggest that it might not belong to *Dasornis*: the caput humeri is caudocranially wider than in the Moroccan fossils and the facies cranialis exhibits a prominent tubercle for the origin of the humeral head of musculus biceps brachii (Mayr and Smith, 2010: fig. 7).

Ulna (fig. 22A)

The specimen OCP.DEK/GE 1242 preserves the distal two thirds of a crushed ulna embedded in matrix, including the partially hidden extremitas distalis. Apart from the larger size, the structure of the ulna of *Dasornis emuinus* is very similar to that of *Dasornis toliapica*.

Radius (fig. 22B–J)

Available material includes the proximal two thirds of a crushed radius embedded in matrix (fig. 22A), the proximal third of the corpus (fig. 22B–E, H–J), plus isolated fragments of corpus (fig. 22G). In dorsal aspect, the distal edge of the caput radii forms a distinct tubercle, but this is uncertain whether this structure is present in *Dasornis toliapica*. The dorsal extremity of the cotyla humeralis joins the caput radii and the oblique crest of the facies caudalis via a smooth ridge. This structure is not preserved in *D. toliapica*. Apart from the larger size, the structure of the radius of *Dasornis emuinus* is very similar to that of *D. toliapica*.

Femur (fig. 23A)

The extremitas proximalis is badly preserved. The caput femoris is distinctly proximal to the plane of the facies articularis antitrochanterica. The proximal part of the crista trochanteris is very feebly developed. The cranial part of the crista trochanteris is low and fairly elongated. A small portion of the corpus is preserved. Its structure is similar to that of the previous species. The linea intermuscularis cranialis is continuous with the distal end of the crista trochanteris.

Tibiotarsus (fig. 23B–G)

The distal half of the tibiotarsus including the extremitas distalis and the facies articularis fibulae is preserved. In *Dasornis emuinus*, the medial tuberositas retinaculi extensori is less sharply defined and the sulcus musculi fibularis extends further proximally than in *Dasornis toliapica*. Apart from this and the larger size, the morphology of the tibiotarsus is identical in the two species.

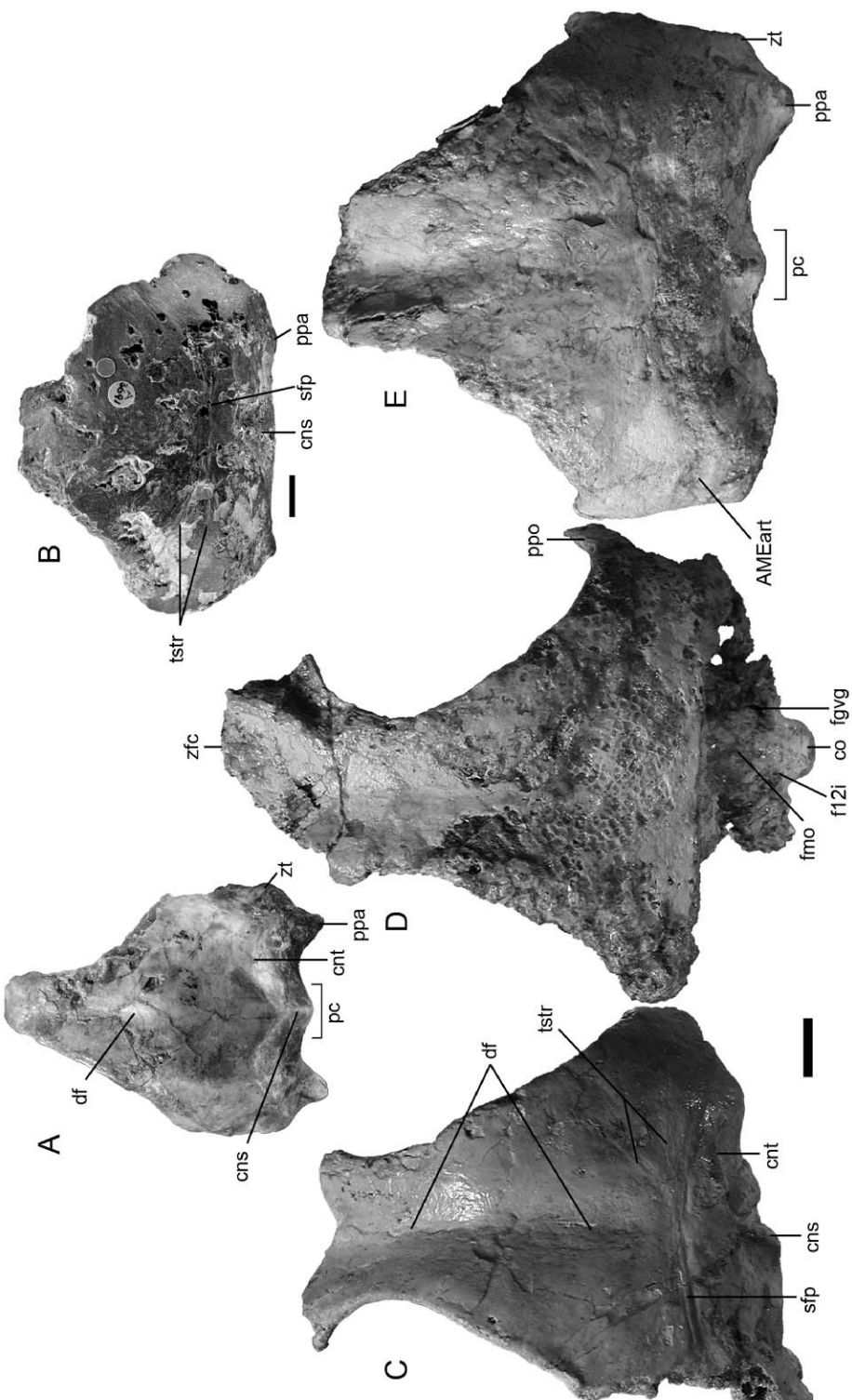

FIGURE 17. **A–E.** Crania in dorsal view: **A.** *Dasornis toliapica* (OCP.DEK/GE 1042); **B.** *Dasornis emuinus* (BMNH A3691); **C.** *D. emuinus* (OCP.DEK/GE 1004); **D.** *D. emuinus* (OCP.DEK/GE 324); **E.** *D. emuinus* (D1-0027A). Scale bars equal 10 mm.

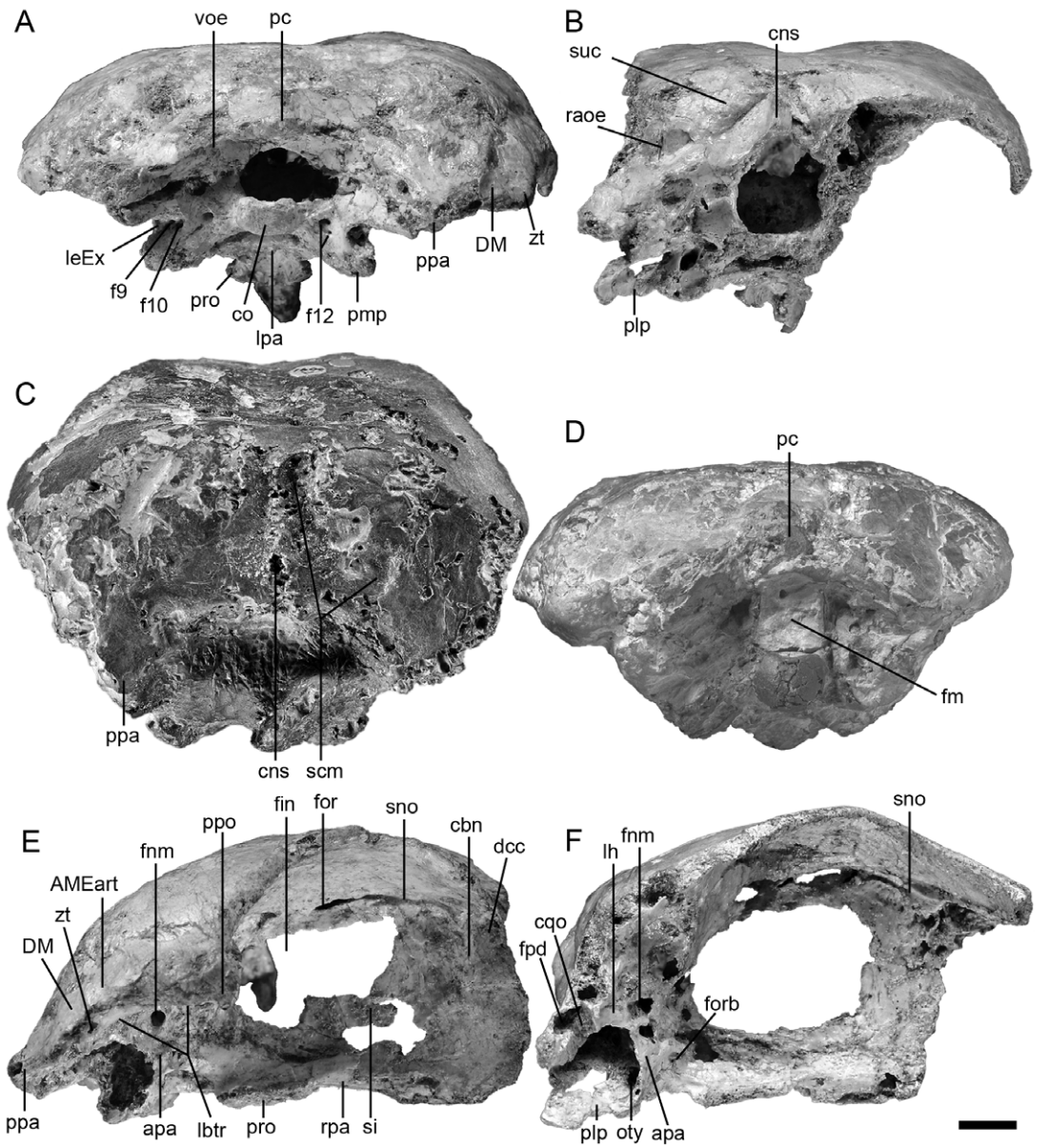

FIGURE 18. *Dasornis emuinus,* skull. **A–D.** Crania in caudal view: **A.** OCP.DEK/GE 1004; **B.** D1-0027A; **C.** BMNH A3691; **D.** BMNH 31929. **E, F.** Crania in right lateral view: **E.** D1-0027A; **F.** reversed OCP.DEK/GE 1004. Scale bar equals 10 mm.

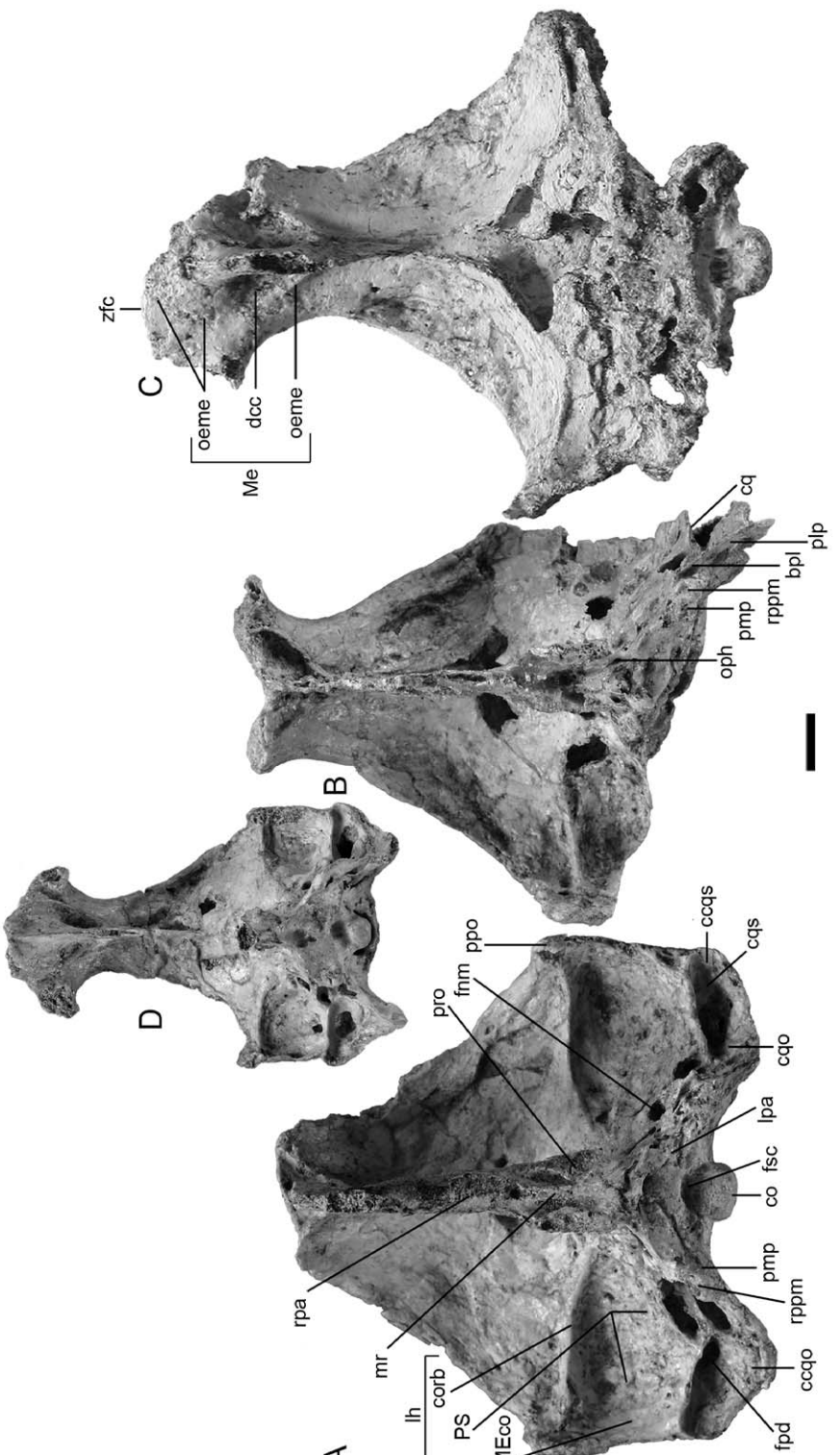

FIGURE 19. Crania in ventral view. **A–C.** *Dasornis emuinus*: **A.** D1-0027A; **B.** OCP.DEK/GE 1004; **C.** OCP.DEK/GE 324. **D.** *Dasornis toliapica*, OCP. DEK/GE 1076. Scale bar equals 10 mm.

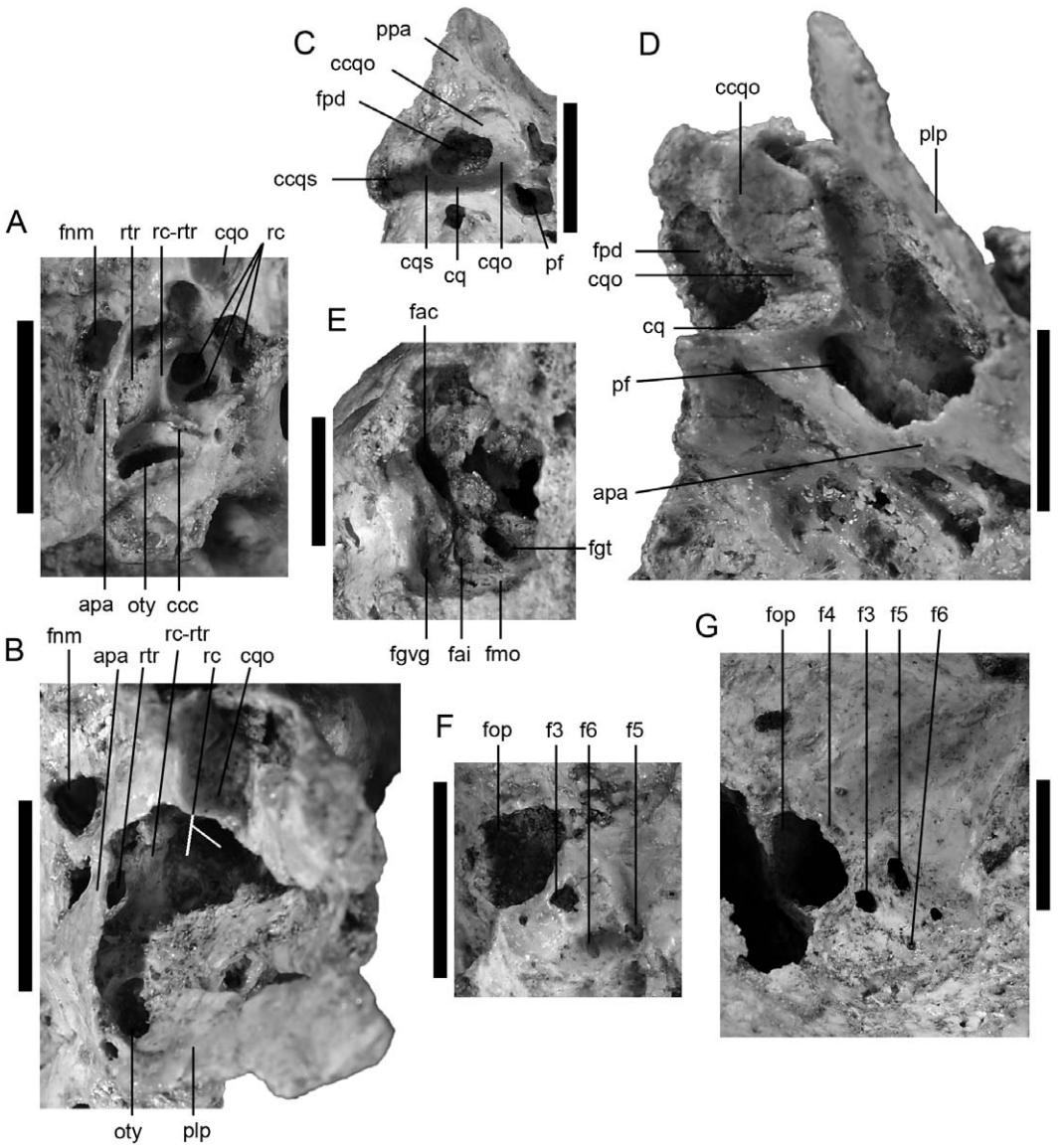

FIGURE 20. **A, B.** Left middle ear regions: **A.** *Dasornis toliapica* (reversed OCP.DEK/GE 1076); **B.** *Dasornis emuinus* (OCP.DEK/GE 1004). **C, D.** Ventral view of left articular surfaces with os quadratum: **C.** *D. toliapica* (OCP.DEK/GE 1044); **D.** *D. emuinus* (OCP.DEK/GE 1004). **E.** *D. emuinus*, caudolateral view of the cavitas cranialis (OCP.DEK/GE 1004). **F, G.** Regions of the foramen opticum: **F.** *D. toliapica* (reversed OCP.DEK/GE 1076); **G.** *D. emuinus* (D1-0027A). Scale bars equal 10 mm.

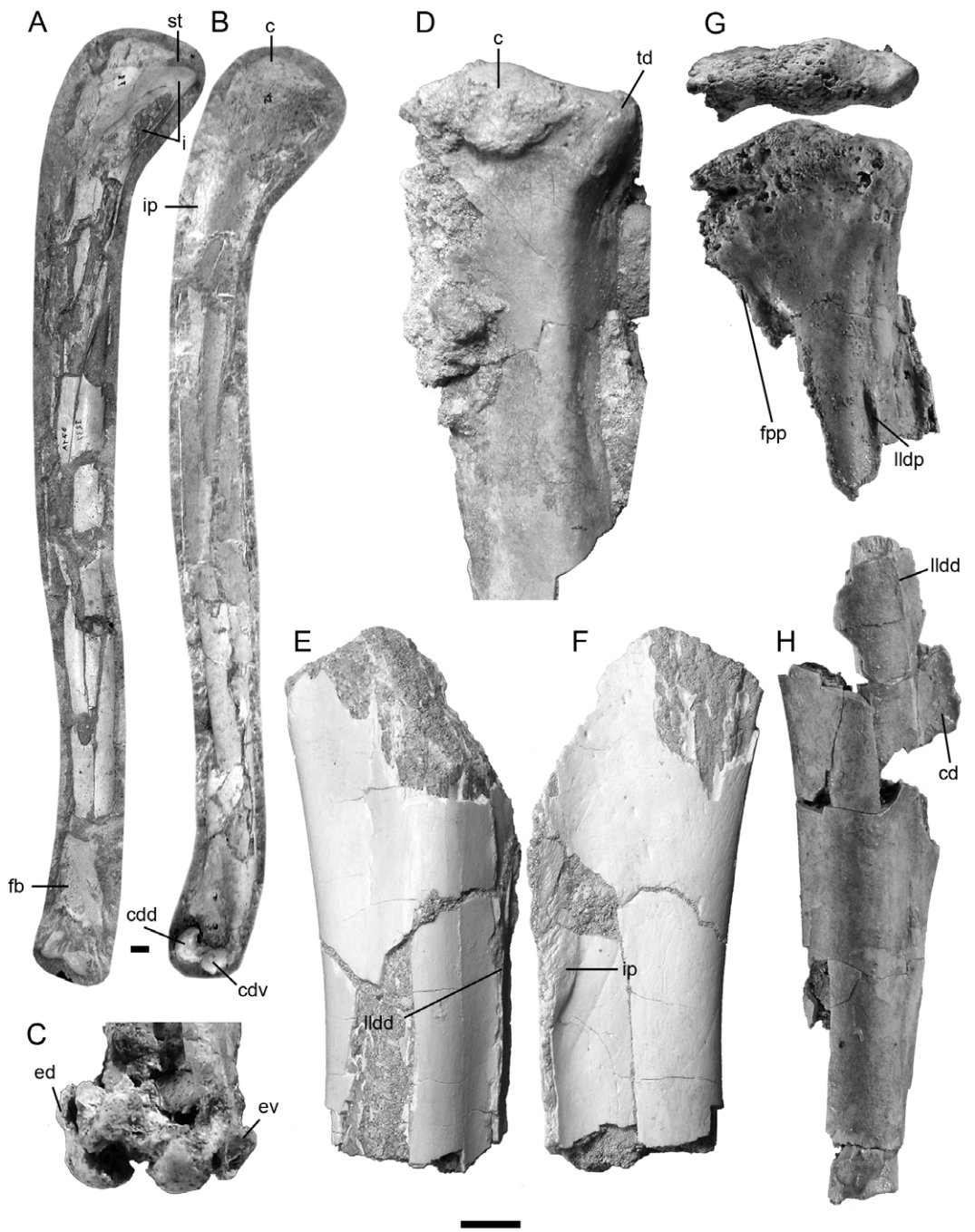

FIGURE 21. **A–H.** *Dasornis emuinus*, right humeri: **A.** reversed OCP.DEK/GE 1237, cranial view; **B.** OCP.DEK/GE 1236, cranial view; **C.** reversed OCP.DEK/GE 1109, cranial view; **D.** OCP.DEK/GE 1333, caudal view; **E.** OCP.DEK/GE 1334, caudal view; **F.** OCP.DEK/GE 1334, cranial view; **G.** OCP.DEK/GE 1072, proximal view; **H.** OCP.DEK/GE 1072, caudal view. Scale bars equal 10 mm.

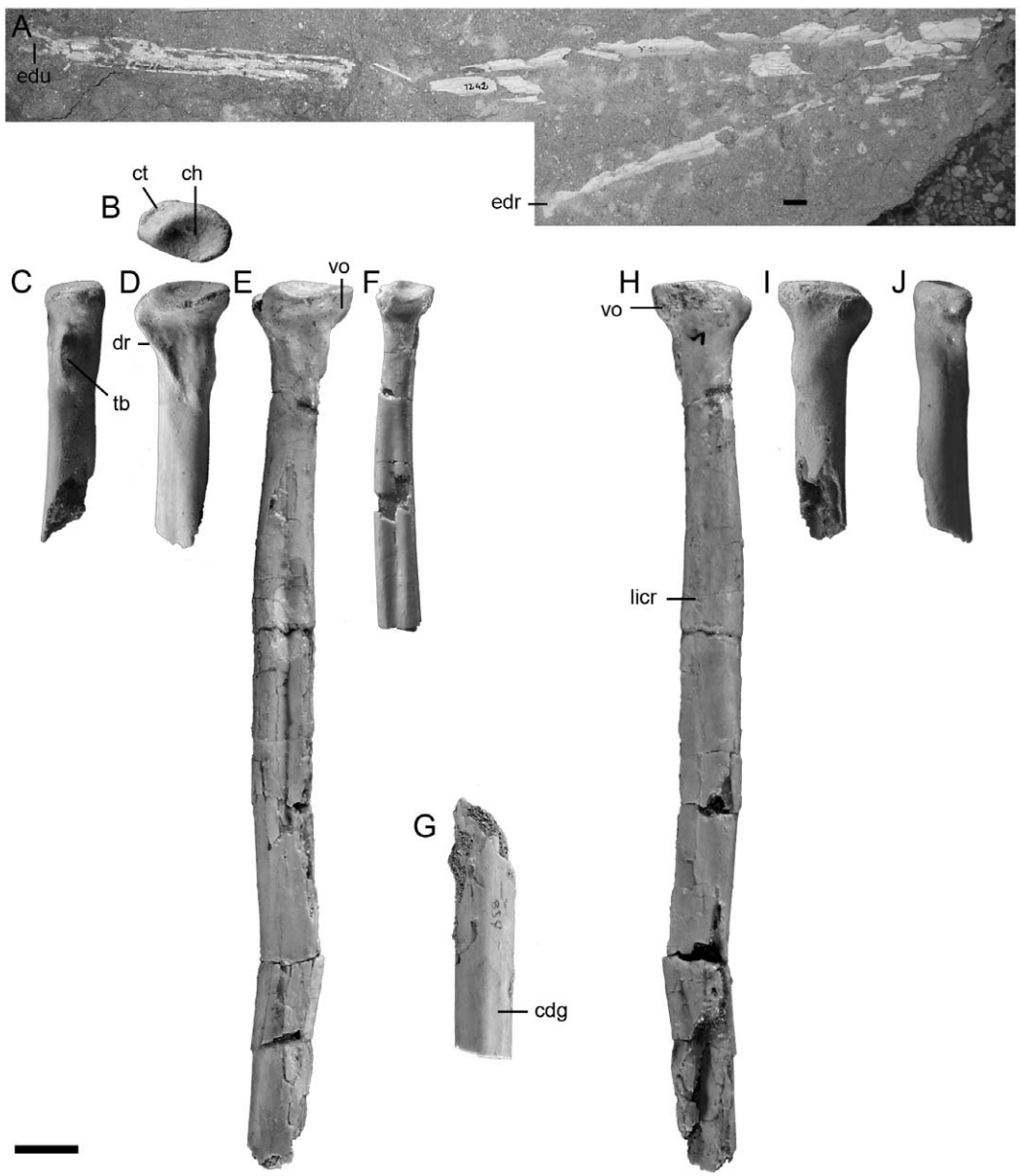

FIGURE 22. **A.** *Dasornis emuinus*, OCP.DEK/GE 1242, ulna and radius embedded in matrix. **B–E.** *D. emuinus*, proximal parts of left radii: **B.** OCP.DEK/GE 1224, proximal view; **C.** OCP.DEK/GE 1224, ventral view; **D.** OCP.DEK/GE 1224, caudal view; **E.** reversed OCP.DEK/GE 1046, caudal view. **F.** *Dasornis toliapica*, OCP.DEK/GE 1212, proximal part of left radius, caudal view. **G.** *D. emuinus*, reversed OCP.DEK/GE 1221, fragment of left corpus radii, caudal view. **H–J.** *D. emuinus*, proximal parts of left radii: **H.** reversed OCP.DEK/GE 1046, cranial view; **I.** OCP.DEK/GE 1224, cranial view; **J.** OCP.DEK/GE 1224, dorsal view. Scale bars equal 10 mm.

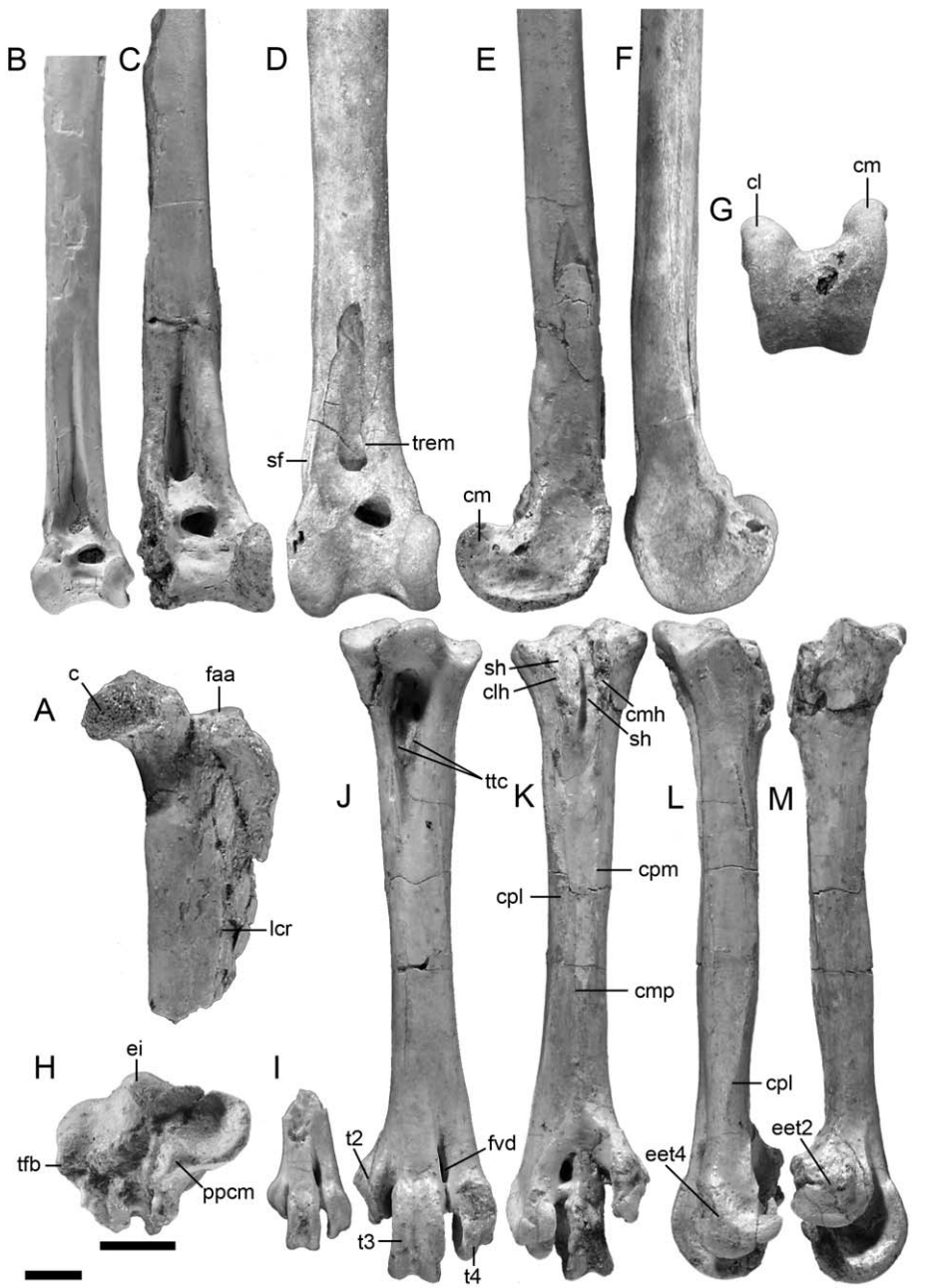

FIGURE 23. **A.** *Dasornis emuinus,* OCP.DEK/GE 1059, proximal end of right femur, cranial view. **B–G.** Distal parts of right tibiotarsi: **B.** *Dasornis toliapica*, MHNL 20-149238, cranial view; **C.** *D. emuinus*, OCP.DEK/GE 1123, cranial view; **D.** *D. emuinus*, reversed OCP.DEK/GE 534A, cranial view; **E.** *D. emuinus*, OCP.DEK/GE 1123, medial view; **F.** *D. emuinus*, reversed OCP. DEK/GE 534A, lateral view; **G.** *D. emuinus*, reversed OCP.DEK/GE 534A, distal view. **H.** *D. emuinus*, OCP.DEK/GE 1106, left tarsometatarsus in proximal view. **I.** *D. toliapica*, OCP.DEK/ GE 1146, distal end of left tarsometatarsus in dorsal view. **J–M.** *D. emuinus*, OCP.DEK/GE 1106, complete left tarsometatarsus: **J.** dorsal view; **K.** plantar view; **L.** lateral view; **M.** medial view. Scale bars equal 10 mm.

Tarsometatarsus (fig. 23H–M)

The extremitas proximalis, hypotarsus, and extremitas distalis agree in morphology and size with those of the material described as *Neptuniavis miranda* by Harrison and Walker (1977: figs. 2, 3) and recently synonymized with *Dasornis emuinus* by Mayr (2008). The curved line and the scar for the origin of musculus extensor hallucis longus on facies medialis are barely distinct in *D. emuinus*, in contrast to *Dasornis toliapica*. Apart from this and the larger size of *D. emuinus*, the structure of the tarsometatarsus is identical in the two species.

Dasornis abdoun, sp. nov., Bourdon

Etymology: Refers to the phosphate basin where the holotype was found.

Holotype: OCP.DEK/GE 1033, incomplete right humerus.

Type Locality: Ouled Abdoun Basin, Sidi Daoui (southeast of TS area, 32°50′87 N and 06°38′48 W: see Gheerbrant et al., 2003).

Type Horizon: Intercalary beds II/I (level 13), basal Ypresian, Lower Eocene (see Gheerbrant et al., 2003).

Referred Material: OCP.DEK/GE 1016, distal part of left carpometacarpus; OCP.DEK/GE 1021, distal part of left carpometacarpus; OCP.DEK/GE 1022, incomplete distal end and fragment of shaft of right ulna; OCP.DEK/GE 1030, distal part of left radius; OCP.DEK/GE 1031, proximal part of left humerus; OCP.DEK/GE 1096, fragment of shaft of right femur; OCP.DEK/GE 1151, fragment of shaft of right tibiotarsus close to proximal end; OCP.DEK/GE 1158, distal part of left carpometacarpus; OCP.DEK/GE 1191, fragment of shaft of right tibiotarsus; MHNL 20-149225, distal end of left humerus.

Localities: Ouled Abdoun Basin, Sidi Daoui (Krupp, RP13 and TS areas).

Horizons: Intercalary beds II/I, basal Ypresian, Lower Eocene.

Diagnosis: Gannet-sized odontopterygiform with a wingspan of 1.5–1.7 m that differs from *D. emuinus* and *D. toliapica* in the following features: much smaller size; humerus, distal almond-shaped foramen pneumaticum absent; intumescentia humeri displaced proximally and more developed; ulna, papillae remigales caudales smooth and narrow; radius, convexity cranial to sulcus tendinosus more prominent with a more strongly curved edge; carpometacarpus, os metacarpale majus caudocranially flattened.

Measurements: See table 2.

DESCRIPTION

Humerus (fig. 24A–I)

The humerus is well preserved, except for the caput, tuberculum dorsale, crista deltopectoralis, and tuberculum ventrale, which are partly damaged. The extremitas distalis is identical to that of *Dasornis toliapica*. The shallow fossa musculi brachialis is better preserved than

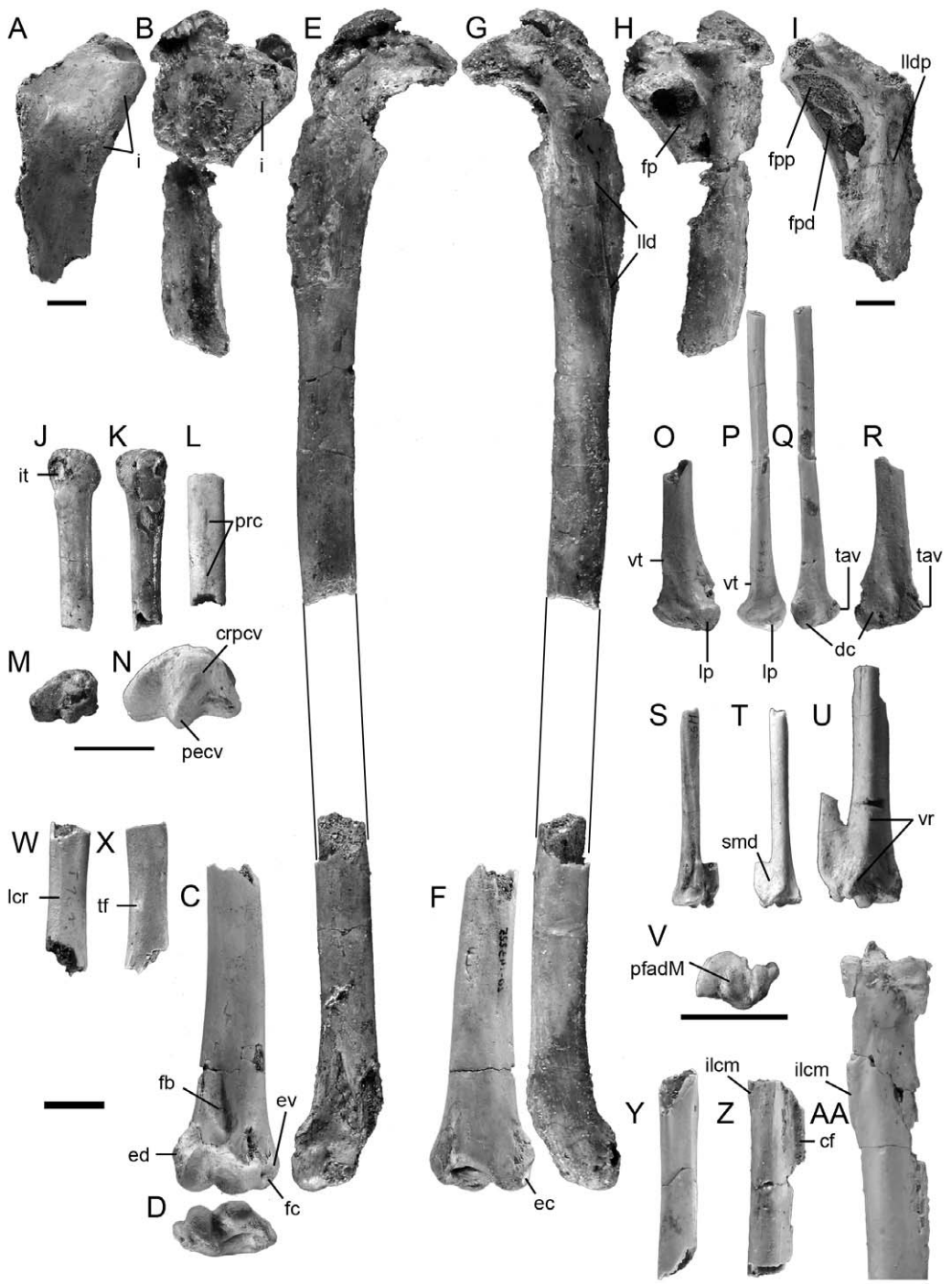

FIGURE 24. **A, I.** *Dasornis toliapica*, OCP.DEK/GE 1194, proximal end of right humerus: **A.** cranial view; **I.** caudal view. **B–H.** *Dasornis abdoun*, sp. nov., right humeri: **B.** reversed OCP.DEK/GE 1031, cranial view; **C.** reversed MHNL 20-149225, cranial view; **D.** reversed MHNL 20-149225, distal view; **E.** OCP.DEK/GE 1033, cranial view; **F.** reversed MHNL 20-149225, caudal view; **G.** OCP.DEK/GE 1033, caudal view; **H.** reversed OCP.DEK/GE 1031, caudal view. **J–L.** *D. abdoun*, sp. nov., OCP.DEK/GE 1022, two fragments of right ulna: **J.** distal end in dorsal view; **K.** distal end in caudal view; **L.** corpus ulnae in caudal view. **M, N.** Right ulnae in distal view: **M.** *D. abdoun*, sp. nov., OCP.DEK/GE 1022; **N.** *D. toliapica*, OCP.DEK/GE 1035. **O–R.** Distal parts of left radii: **O.** *D. toliapica*, reversed OCP.DEK/GE 1118, ventral view; **P.** *D. abdoun*, sp. nov., OCP.DEK/GE 1030, ventral view; **Q.** *D. abdoun*, sp. nov., OCP.DEK/GE 1030, dorsal view; **R.** *D. toliapica*, reversed OCP.DEK/GE 1118, dorsal view. **S–V**. Distal parts of left carpometacarpi: **S.** *D. abdoun*, sp. nov., OCP.DEK/GE 1121, dorsal view; **T.** *D. abdoun*, sp. nov., OCP.DEK/GE 1121, ventral view; **U.** *D. toliapica*, reversed OCP.DEK/GE 1101, ventral view; **V.** *D. abdoun*, sp. nov., OCP.DEK/GE 1121, distal view. **W, X.** *D. abdoun*, sp. nov., OCP.DEK/GE 1096, fragment of right corpus femoris: **W.** cranial view; **X.** caudal view. **Y–AA.** Right tibiotarsi: **Y.** *D. abdoun*, sp. nov., OCP.DEK/GE 1191, fragment of corpus, cranial view; **Z.** *D. abdoun*, sp. nov., OCP.DEK/GE 1151, fragment of corpus, caudal view; **AA.** *D. toliapica*, MHNL 20-149238, proximal end, caudal view. Scale bars equal 10 mm.

in *D. toliapica*: its ventral edge is straight and its dorsal one is curved. The extremitas proximalis and corpus are similar to those of *D. toliapica*, but differ from the latter in several important features: the distal almond-shaped foramen pneumaticum of *D. toliapica* is absent and replaced by a tiny slit. The proximal foramen pneumaticum is larger than in *D. toliapica*. There is no distinct crista bicipitalis. The intumescentia humeri is displaced proximally and much more prominent. The proximal part of the linea musculi latissimi dorsi is a faint ridge that is continuous with the distal part.

Ulna (fig. 24J–N)

Only a short fragment of corpus and the distal end lacking the tuberculum carpale are preserved. The structure is similar to that of *Dasornis toliapica*. However, *Dasornis abdoun* differs from the latter in the more prominent papillae remigales. Furthermore, the papillae remigales caudales are smooth and narrow.

Radius (fig. 24O–R)

The radius consists of a complete distal half. The structure is similar to that of *Dasornis toliapica*, but differs from that of the latter in several important features: the corpus is less flattened dorsoventrally; the extremitas distalis is wider; the convexity cranial to the sulcus tendinosus is more prominent and its ventral border is more strongly curved; the margo interosseus shows a marked convexity at the tuberculum aponeurosis ventralis that is absent in *D. toliapica*; the proximal border of the ligamental prominence (Howard, 1929) is less sinuous; the tubercle above the depressio ligamentosa, close to the margo interosseus, is in more distal and ventral position.

Carpometacarpus (fig. 24S–V)

The extremitas distalis and distal half of os metacarpale majus are preserved. They are similar to those of *Dasornis toliapica*, except that the os metacarpale majus is more flattened caudocranially.

Femur (fig. 24W, X)

A fragment of corpus femoris is preserved. It resembles the corresponding part in *Dasornis toliapica* in the presence of a distinct triangular facet and the position of the lineae intermusculares plus nutrient foramen.

Tibiotarsus (fig. 24Y–AA)

Two caudocranially crushed fragments of corpus are preserved. The proximal one includes a part of the crista fibularis and the distal end of the impressio ligamenti collateralis medialis. The distal one includes the lineae musculi fibularis. The structure is very similar to that of *Dasornis toliapica*. The crista fibularis is better preserved than in *D. toliapica*. It is high with a thick margin that is sharply defined caudally.

Dasornis sp.

Referred Material: OCP.DEK/GE 1000, incomplete right tarsometatarsus; OCP.DEK/GE 1129, fragment of shaft of left humerus close to distal end; OCP.DEK/GE 1136, fragments of shaft of left humerus; OCP.DEK/GE 1154, fragment of ?right coracoideum close to omal end; OCP.DEK/GE 1173B, fragment of shaft of left ulna; OCP.DEK/GE 1259, fragment of shaft of long bone; OCP.DEK/GE 1292, fragment of shaft of long bone, possibly humerus.

Localities: Ouled Abdoun Basin: Sidi Daoui (Krupp and RP13 areas); southern Meraa El Arech (Lahou area); Sidi Chennane (R6–R7 area).

Stratigraphic Distribution: Intercalary beds II/I, basal Ypresian, Lower Eocene; lower bed I, Ypresian, Lower Eocene.

COMPARISON WITH *PELAGORNIS*/*OSTEODONTORNIS* (figs. 25, 26)

Specimens referred to the genera *Pelagornis* Lartet, 1857, and *Osteodontornis* Howard, 1957, were examined for comparison with *Dasornis*. So far, the *Pelagornis*/*Osteodontornis* material is known from the late Eocene to Miocene of North America (Howard, 1957, 1978; Howard and White, 1962; Hopson, 1964; Olson, 1984, 1985; Goedert, 1989; Olson and Rasmussen, 2001; Stidham, 2004), Miocene and Pliocene of South America (Chavez et al., 2007); Miocene of Europe (Lartet, 1857; Mayr et al., 2008), and Pliocene of North Africa (Mourer-Chauviré and Geraads, 2008). Numerous specimens also most probably belong to *Pelagornis*: Miocene

to Pliocene of South America (Cheneval, 1993; Walsh and Hume, 2001; Rincón and Stucchi, 2003; Chavez et al., 2007), including a well-preserved but still undescribed skull from the Miocene of Peru (GoGeometry, 2009), Miocene to Pliocene of Japan (Ono et al., 1985; Ono, 1989), and Miocene of New Zealand (Scarlett, 1972). Most of the comparative material we consulted consists of undescribed specimens deposited in the collections of the LACM and NMNH. We found no differences between *Pelagornis* and *Osteodontornis*. Thus, we regard all the examined specimens as a single taxonomic entity.

Cranium (fig. 25A, B)

The cranium of *Pelagornis*/*Osteodontornis* (see also Olson, 1985: fig. 10; Chavez et al., 2007: fig. 3) differs from that of *Dasornis* in the following features: the sutura frontoparietalis is more sharply defined; the os frontale is wider in the interorbital region, and the rim of this bone is convex just caudal to the os lacrimale; a large deep impressio glandulae nasalis is present in the mediorostral part of the roof of the orbita; the straight sulcus nervi olfactorii is wider and in lower position.

Maxilla and Mandibula

The maxilla and mandibula of *Dasornis* resemble those of other pseudotoothed birds (Spulski, 1910; Lambrecht, 1930; Howard, 1957, 1978; Howard and White, 1962; Hopson, 1964; Howard and Warter, 1969; Harrison and Walker, 1976; Harrison, 1985; Matsuoka et al., 1998; Aslanova and Burchak-Abramovich, 1999; Olson and Rasmussen, 2001; Stidham, 2004; Chavez et al., 2007; Tambussi and Hospitaleche, 2007; Mourer-Chauviré and Geraads, 2008; GoGeometry, 2009). The reconstruction of the maxilla of *Dasornis toliapica* by Harrison and Walker (1976: fig. 15B) does not agree with that proposed here (fig. 4; see also Bourdon, 2005: fig. 1a). Indeed, the distal end of the maxilla of *D. toliapica* is very similar to that of *Osteodontornis orri* (Stidham, 2004) and two less complete and undescribed fragments from the Miocene of Maryland (USNM 237203). *Pelagornis*/*Osteodontornis* shows a transverse groove in the dorsal part of the tip of the maxilla (Olson, 1984; Stidham, 2004), which is absent in *D. toliapica*. In *Osteodontornis* and *Pseudodontornis longirostris*, the longitudinal groove of the maxilla is in more dorsal position than in *Dasornis*, presumably related to the larger toothlike projections and deeper internal grooves (Harrison and Walker, 1976: 39). In *P. longirostris* and *Neodontornis*, the central palatal ridge is strongly convex and more prominent than in *Dasornis* (Harrison and Walker, 1976: figs. 20, 21A), a feature that is also possibly related to the large pseudoteeth and deep internal grooves. An undescribed specimen (USNM 335463) from the Miocene of Oregon that most probably belongs to the *Pelagornis*/*Osteodontornis* assemblage shows the same features (EB, personal obs.). In *D. toliapica*, the caudal end of the longitudinal groove of the mandibula curves dorsally toward the zona flexoria intramandibularis caudalis, whereas this is not the case in *Osteodontornis* (Harrison and Walker, 1976: figs. 15, 32). The pseudoteeth of *D. toliapica* are smaller than in the other odontopterygiform genera, and also exhibit a distinctive forward slant (fig. 4A, G, I). We are not convinced, however, that the pseudotooth arrangement can be a good discriminating feature (e.g.,

FIGURE 25. **A, B.** Crania in left lateral view: **A.** cf. *Pelagornis* (USNM 335463); **B.** *Dasornis toliapica* (OCP.DEK/GE 1194). **C–E.** Proximal parts of left humeri in caudal view: **C.** *Pelagornis* sp. (USNM 425111); **D.** cf. *Pelagornis* (USNM 335794); **E.** *D. toliapica* (reconstructed after OCP.DEK/GE 1229 and MHNL 20-149229). **F–H.** Proximal parts of left humeri in cranial view: **F.** *D. toliapica* (reconstructed after OCP.DEK/GE 1116, OCP.DEK/GE 1229, and MHNL 20-149229); **G.** cf. *Pelagornis* (USNM 335794); **H.** *Pelagornis* sp. (USNM 425111). **I–L.** Distal ends of right humeri: **I.** *Pelagornis miocaenus* (uncataloged holotype, MNHN), dorsal view; **J.** *D. toliapica* (MHNL 20-149214), dorsal view; **K.** *Osteodontornis* (LACM 128423), cranial view; **L.** *D. toliapica* (MHNL 20-149214), cranial view. **M–P.** Proximal extremities of left ulnae: **M.** cf. *Pelagornis* (LACM 128462 [initially referred to *Argillornis*]), cranial view; **N.** *D. toliapica* (BMNH A224), cranial view; **O.** cf. *Pelagornis* (LACM 128462), proximal view; **P.** *D. toliapica* (BMNH A224), proximal view.

Harrison and Walker, 1976: fig. 25). Even the forward orientation of the pseudoteeth in *D. toliapica* must be taken with caution, since these processes seem vertical in the distal end of the maxilla of this species (fig. 4H).

Pterygoideum

The structure found in *Pelagornis* (Olson and Rasmussen, 2001: specimen USNM 425110 figured in pl. 11d; Mourer-Chauviré and Geraads, 2008) is similar to that of *Dasornis toliapica* BMNH 44096 (Harrison and Walker, 1976: pl. 2K–M). *Pelagornis* sp. (Olson and Rasmussen, 2001: specimen USNM 425110 figured in pl. 11d) differs from the latter in the following features: the articulatio pterygopalatina is only slightly concave and bears a pointed process (see also Mourer-Chauviré and Geraads, 2008: 181), whereas it is strongly concave and devoid of a sharp process in *D. toliapica*; the facies articularis parasphenoidalis is large, oval, and sessile, whereas it is pedunculate in *D. toliapica*; the corpus shows a stronger widening toward the processus quadraticus; the dorsal flange of the corpus is more developed than in *D. toliapica*. Except for the articulatio pterygopalatina, the pterygoideum of *Pelagornis mauretanicus* (Mourer-Chauviré and Geraads, 2008) is distinct from that of *Pelagornis* sp. (USNM 425110) and superficially similar to that of *D. toliapica*, because it exhibits a slender corpus and a pedicellate facies articularis parasphenoidalis.

Quadratum

The quadratum of *Dasornis toliapica* (Harrison and Walker, 1976: pl. 1) closely resembles that of *Pelagornis*/*Osteodontornis* (Ono, 1989: fig. 1; Olson and Rasmussen, 2001: pl. 11f; Mourer-Chauviré and Geraads, 2008: figs. 4, 6). The latter differs from the former in having a flatter caudal facies of the corpus, a more prominent condylus pterygoideus, and a more rounded and sharply defined capitula.

Humerus (fig. 25C–L)

The humerus of *Pelagornis*/*Osteodontornis* differs from that of *Dasornis* in many features: the cranial prominence of the caput humeri is wider, protrudes further cranially, and has a straight

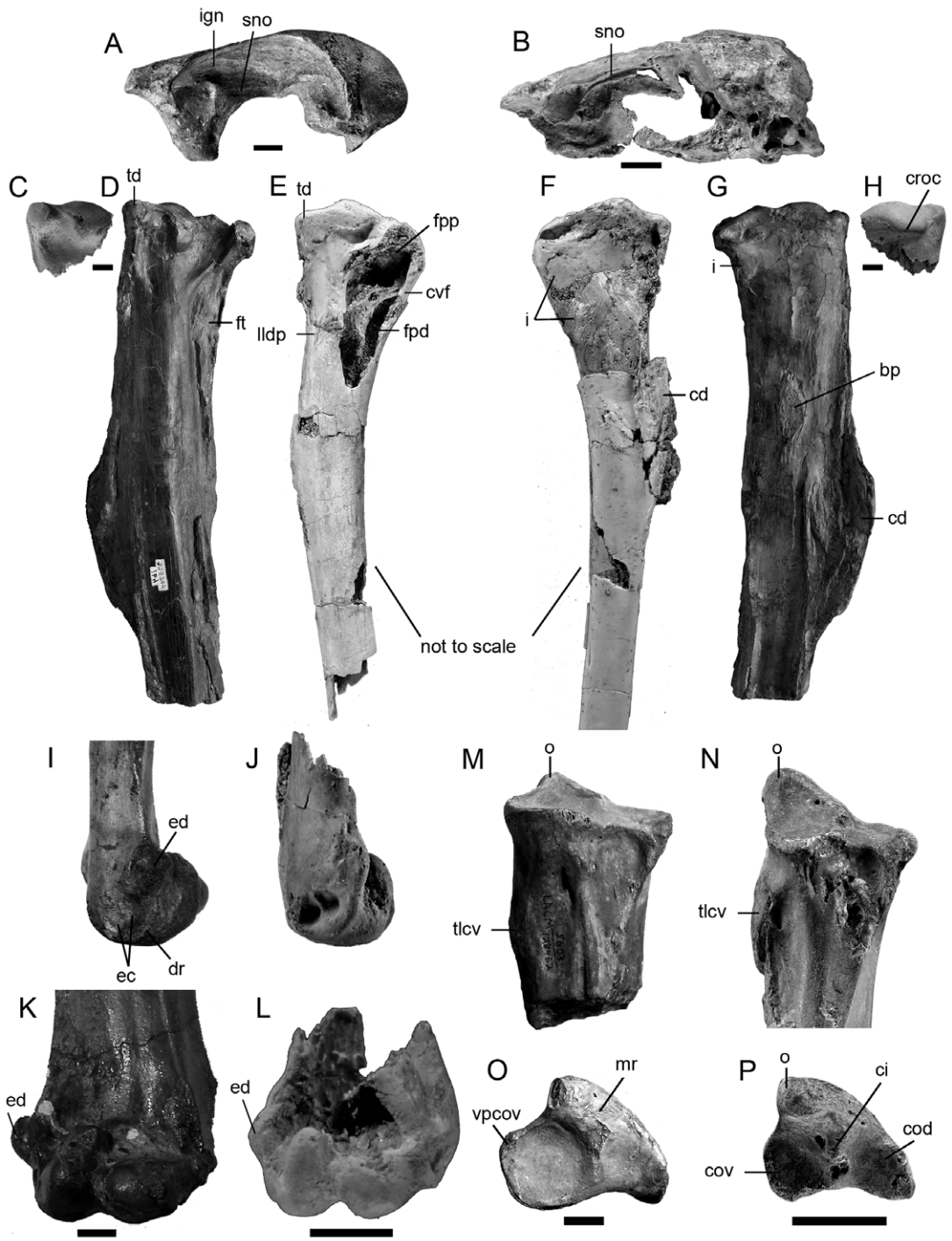

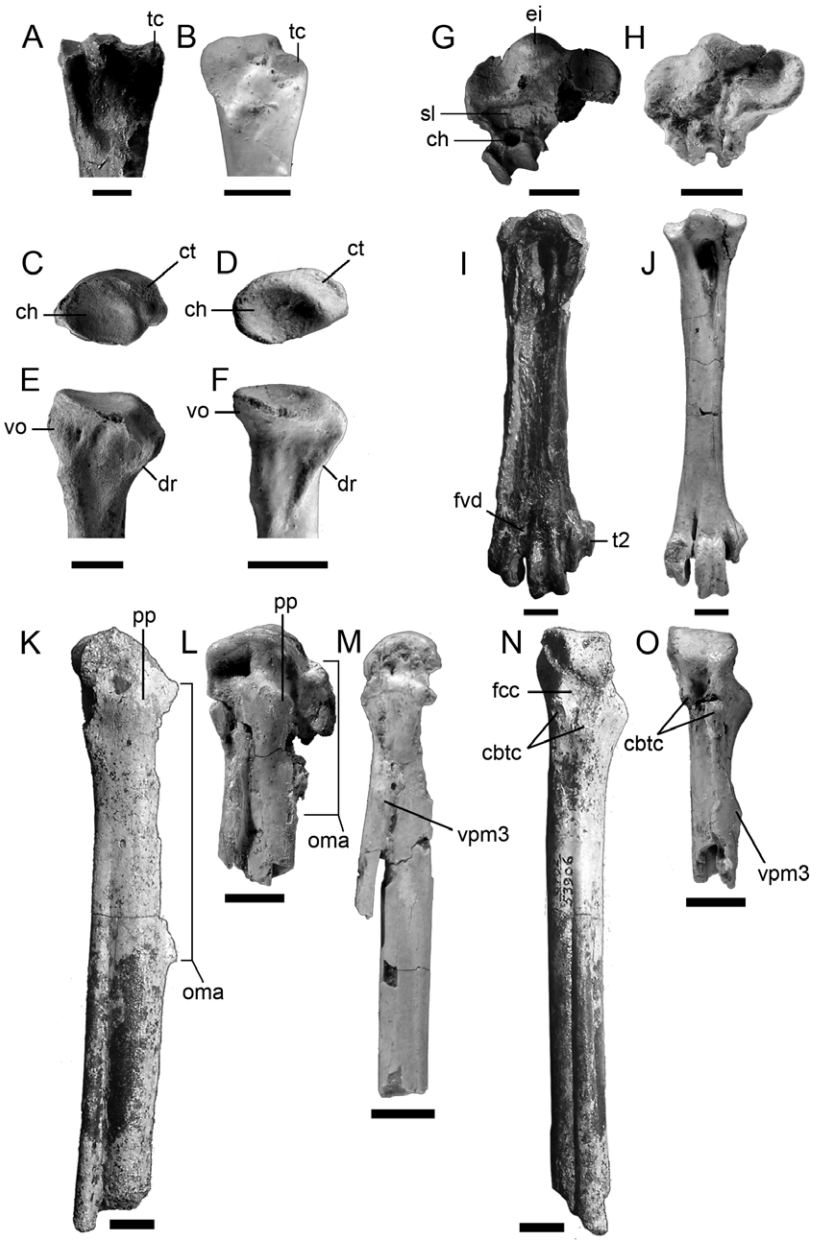

FIGURE 26. **A, B.** Distal ends of right ulnae in ventral view: **A.** cf. *Pelagornis* (USNM 335794); **B.** *Dasornis toliapica* (MHNL 20-149218). **C–F.** Proximal ends of left radii: **C.** *Pelagornis* sp. (USNM 183512), proximal view; **D.** *Dasornis emuinus* (reversed OCP.DEK/GE 1224), proximal view; **E.** *Pelagornis* sp. (USNM 183512), caudal view; **F.** *D. emuinus* (reversed OCP.DEK/GE 1224), caudal view. **G–J.** Right tarsometatarsi: **G.** cf. *Pelagornis* (reversed USNM 237200), proximal view; **H.** *D. emuinus* (reversed OCP.DEK/GE 1106), proximal view; **I.** *Osteodontornis* (LACM 128424), dorsal view; **J.** *D. emuinus* (reversed OCP.DEK/GE 1106), dorsal view. **K–O.** Left carpometacarpi: **K.** *Osteodontornis orri* (LACM 53906), ventral view; **L.** *D. toliapica* (OCP.DEK/GE 1152), ventral view; **M.** *D. toliapica* (OCP.DEK/GE 1139), ventral view; **N.** *O. orri* (LACM 53906), caudal view; **O.** *D. toliapica* (OCP.DEK/GE 1152), caudal view. Scale bars equal 10 mm.

abrupt distal border; the caudal prominence of the caput humeri is higher and tapers far distally; the latter structure is smooth at the distal end and has sharp lateral and medial borders; the incisura capitis is deeper and much wider; the tuberculum dorsale is wide and protrudes proximally to the level of the caput; it forms a distinct surface that faces caudolaterally and that is continued by a tapering ridge; finally, it is separated from the caput by a marked depression; the crista deltopectoralis begins very far distal to the tuberculum dorsale and makes an angle at each extremity; the crista bicipitalis is replaced by a flat prominence located in the medial part of the planum intertuberculare, just proximal to the crista deltopectoralis; the sulcus transversus is wider, shorter, and shallower; there is a sharp process that lies on the proximal border of the sulcus transversus, between the caput humeri and the tuberculum ventrale; the intumescentia humeri is exceedingly small, with no distal and dorsal extension, so that the planum intertuberculare is flat; the fossa pneumotricipitalis is apneumatic and the crus ventrale fossae is nearly straight; the area of insertion of musculus scapulohumeralis caudalis is a flat facet facing ventrally; the margo caudalis is lower in the region of the fossa tricipitalis; the linea musculi latissimi dorsi is straighter and less distinct; the epicondylus dorsalis is oval and more prominent; a furrow delimits the latter proximally and cranially; the distal part of the ridge that delimits the two fossae for origin of musculus extensor carpi ulnaris is not distinctly separated from the condylus dorsalis.

Ulna (fig. 25M–P, 26A, B)

The ulna of *Pelagornis*/*Osteodontornis* (see also Chavez et al., 2007) differs from that of *Dasornis* in many respects: the cotyla ventralis is larger and makes an angle far ventral to the olecranon; the olecranon is not prominent; the tuberculum ligamenti collateralis ventralis does not extend as far distally and forms a flat surface; the corpus ulnae is stouter with a sharper margo cranialis. The extremitas distalis ulnae of an undescribed specimen of *Pelagornis* sp. (USNM 335794) is distinct from that of *Pelagornis mauretanicus* (Mourer-Chauviré and Geraads, 2008: 183), especially concerning the aspect of the tuberculum carpale. The extremitas distalis ulnae of *Pelagornis*, however, differs from that of *Dasornis* in that the condylae end very sharply proximocaudally, and at the same level.

Goedert (1989) tentatively assigned the late Eocene specimen LACM 128462 from Oregon (fig. 25M, O) to the genus *Argillornis*, which is now synonymized with *Dasornis* (Mayr, 2008). However, this ulna matches well with that of *Pelagornis*/*Osteodontornis* in the morphology of the cotyla ventralis, tuberculum ligamenti collateralis ventralis, and corpus. Thus, this specimen is regarded as belonging to *Pelagornis*.

Radius (fig. 26C–F)

In *Pelagornis*/*Osteodontornis*, the extremitas proximalis radii is well preserved in USNM 183512 (fig. 26C, E), and the proximal part is badly preserved in LACM 127875. These specimens differ from *Dasornis* in several features: the cotyla humeralis is oval in shape and less caudocranially flattened; its ventral overhang is less prominent and proximodistally longer;

there is no ridge joining the dorsal extremity of the cotyla humeralis and the caput radii, which is more prominent; the oblique crest that continues the caput radii on the facies caudalis is less prominent in its distal part; the caudal edge of the tuberculum bicipitale is more prominent. The extremitas distalis radii is partially visible in *Pelagornis mauretanicus* (Mourer-Chauviré and Geraads, 2008: 183): it differs from *Dasornis* in the more angular ligamental prominence (Howard, 1929) and in the lower convexity cranial to the sulcus tendinosus.

Carpometacarpus (fig. 26K–O)

The proximal part of carpometacarpus of *Osteodontornis orri* (fig. 26K, N) described by Howard (1978) markedly differs from that of *Dasornis* in several features: the os metacarpale alulare is much longer; the processus pisiformis is larger, blunter, and more rounded in shape; a large pneumatic foramen occupies most of the fossa infratrochlearis; the symphysis of os metacarpale minus and os metacarpale majus is longer (also seen in *Pelagornis mauretanicus*; Mourer-Chauviré and Geraads, 2008); distal to this symphysis, the os metacarpale minus is pressed against the os metacarpale majus, so that the spatium intermetacarpale is absent; the proximal part of the os metacarpale minus does not show any ventral tubercle; the fovea carpalis caudalis is larger and interrupts the caudal extremity of the trochlea carpalis; the facet for ligamentum radiocarpo-metacarpale dorsale is less distinct.

Femur

The femur of *Pelagornis*/*Osteodontornis* differs from that of *Dasornis* in several features: the corpus is shorter and stouter; the triangular facet is smaller; the linea intermuscularis caudalis is indistinct proximal to the triangular facet; the tuberculum musculi gastrocnemialis lateralis is less prominent and in more lateral position; a small depression that is absent in *Dasornis toliapica* delimits the tuberculum musculi gastrocnemialis lateralis caudally; the sulcus patellaris is shallower, and the cristae sulci patellaris are less prominent.

Tibiotarsus

The tibiotarsus of *Pelagornis*/*Osteodontornis* differs from that of *Dasornis* in several features: the condylus medialis is shorter with a more rounded distal margin; the epicondylus medialis is more proximodistally developed; the cristae trochleae are more prominent; the sulcus musculi fibularis faces cranially and has a higher lateral border; the lateral tuberositas retinaculi extensori is oval and medially displaced, and the pons supratendineus is narrower.

Tarsometatarsus (fig. 26G–J)

The tarsometatarsus of *Pelagornis*/*Osteodontornis* differs from that of *Dasornis* in many features: the sulcus ligamentosus is wider and deeper; the eminentia intercotylaris is wider; the hypotarsus shows two canales hypotarsi; the crista lateralis hypotarsi forms a distinct

flat surface facing laterally; an oblique groove extending from the base of the hypotarsus through the cotyla lateralis is present; the corpus tarsometatarsi is shorter, stouter, and dorsoplantarly compressed, so that its transverse section is rectangular; the zone between the crista medianoplantaris and the crista plantaris lateralis forms a longitudinal groove; the fossa metatarsi I is deep (best visible in LACM 128422); the trochlea metatarsi II is less displaced proximally, and is bounded plantaroproximally by a distinct oval depression; the external edges of trochleae metatarsi II and IV are more prominent; the trochlea metatarsi III is not dorsally elevated, so that the surface above the trochleae is flatter; in dorsal aspect, the foramen vasculare distale is smaller and not prolonged proximally by a deep groove; the plantar opening of the foramen vasculare distale is larger.

DISCUSSION

Taxonomic and Nomenclatural Considerations

The abundance of the collected material offers insight into intraspecific size and shape variation of early odontopterygiform species (tables 1, 2; figs. 3–24), especially in *Dasornis toliapica*, which is the most common species found in the Moroccan phosphates. For instance, some cranial structures (e.g., the condylus occipitalis and processus medialis parasphenoidalis) vary in shape and dimension in *D. toliapica*. These structures, however, show some variability within examined species of extant birds (E.B., personal obs.). Thus, we could not provide convincing evidence for more than three species in the Moroccan phosphates, which are distinguished from one another mainly by size. Some cranial structures also differ between the London Clay and Ouled Abdoun specimens of the two larger *Dasornis* species, such as the shape of the foramen magnum, processus rostropterygoideus, and foramina for exit of the cranial nerves (table 1; figs. 3, 4, 6, 18, 19; see also Harrison and Walker, 1976: pl. 1, fig. C; pl. 3, fig. D). However, these features are variable within extant species, and cannot be sufficient to erect two new species for the larger Moroccan fossils.

Most Moroccan specimens are crushed or flattened to varying extent. Compared with the London Clay specimens, the crania show a more or less important degree of dorsoventral flattening (table 1). The undistorted aspect of the braincase of *D. toliapica* may be found in OCP.DEK/GE 1042, which is enclosed in a very hard, silicified nodule (figs. 3–6). In BMNH 44096, the braincase is slightly bent downward, and this results in the following features: the fossa subtemporalis extends less dorsally than the area of origin of musculus adductor mandibulae externus pars articularis (fig. 5), the foramen magnum faces slightly ventrally (fig. 3), and the laterosphenoid hollow faces rostrally (fig. 6). These features are probably due to preservation and thus cannot justify the definition of a new Moroccan species comparable in size to *D. toliapica*.

Taking into account intraspecific variability in size and morphology as well as distortion, we adopt here a conservative taxonomy. A large part of the fossils described herein are assigned to *D. toliapica* (Owen, 1873) and *Dasornis emuinus* (Bowerbank, 1854), which were previously known from the Lower Eocene London Clay of Sheppey (Harrison and Walker, 1976; Mayr, 2008). A few Moroccan remains are assigned to a new, smaller species of *Dasornis*.

Previous taxonomists often proposed new names for very incomplete (e.g. Harrison and Walker, 1976; Harrison, 1985; Averianov et al., 1991) or badly crushed (Aslanova and Burchak-Abramovich, 1982) odontopterygiform specimens. Harrison and Walker (1976) defined no fewer than 11 species, 9 genera, and 4 families inside the Odontopterygiformes, without convincing justification (Olson, 1985; Mayr, 2008). The Ouled Abdoun specimens provide a considerable amount of new morphological information concerning the morphology of early odontopterygiforms. On this basis, we revise the "over split" taxonomy of the London Clay odontopterygiforms proposed by Harrison and Walker (1976) and partly simplified by Mayr (2008). We propose that the two species from the Paleogene of England and Morocco are congeneric, the name *Dasornis* having priority over the name *Odontopteryx*.

Owen (1873) first described *Odontopteryx toliapica* in 1873 on the basis of a single incomplete skull. Lydekker (1891) referred a proximal end of ulna and a proximal end of tarsometatarsus to this species, and these were later figured by Lambrecht (1933). Harrison and Walker (1976) redescribed *O. toliapica* and referred a second incomplete skull to this species. These authors did not retain the tarsometatarsus with the material of *O. toliapica* (Harrison and Walker, 1976, 1977). They referred this specimen to a new species, *Neptuniavis minor*, because "the tarsometarsus is much too large and has procellariiform characters only" (Harrison and Walker, 1977). Both the morphology and size of this proximal tarsometatarsus, however, fit with the new Moroccan specimens referred to *D. toliapica* (table 2). On the basis of these new data, *N. minor* Harrison and Walker, 1977, is synonymized with *D. toliapica* (Owen, 1873). Harrison and Walker (1977) also attributed a distal end of femur to *N. minor*, because this specimen "would appear to be the size and character that might be expected for this species." However, we refrain from assigning it to *D. toliapica* because we were unable to examine this femur, which is neither figured nor precisely described in Harrison and Walker (1977).

The cranium BMNH A1 initially described as *Macrodontopteryx oweni* by Harrison and Walker (1976) matches well with *D. toliapica* and its size corresponds to that of the largest individuals of this species (table 1). BMNH A1 differs from *D. toliapica* in the following features: the groove that continues the foramen orbitale is oriented slightly dorsally (Harrison and Walker, 1976: pl. 4, fig. E); the processus rostropterygoideus is oriented more laterally; the dorsal edge of the fonticulus interorbitalis is straight and makes an angle with the rostral one; the dorsal corner of the foramen opticum is confluent with a large fonticulus orbitocranialis. These small differences are most probably due to individual variation and are not sufficient to justify the placement of BMNH A1 in a separate genus and species. Thus, *M. oweni* Harrison and Walker, 1976, is regarded here as a junior synonym of *D. toliapica* (Owen, 1873).

Most recently, Mayr and Smith (2010) described new odontopterygiform remains from the Middle Eocene of Belgium. The sternum, pectoral girdle bones, and humeri of a single individual were tentatively assigned to *M. oweni*, and an incomplete humerus was tentatively identified as *D. emuinus*. A preliminary comparison with the material described here shows that the two Belgian species are distinct from *D. toliapica* and *D. emuinus* (see above). Because we were unable to examine the Belgian specimens, it is uncertain whether these can be confidently assigned to the genus *Dasornis*.

While comparing other pseudotoothed birds with *Dasornis*, we found that there were no

differences between the genera *Pelagornis* and *Osteodontornis* Howard, 1957, and we regard all the *Pelagornis* and *Osteodontornis* specimens as pertaining to a single taxonomic entity, which corresponds to the *Pelagornis* morphotype. *Osteodontornis* is most probably a junior synonym of *Pelagornis*, but this synonymy cannot be established without a complete revision of the Odontopterygiformes.

As shown above, *Pelagornis* markedly differs from *Dasornis* in skeletal characters of the skull, forelimb, and hind limb. Despite this, we have chosen to place these genera in one single family, Pelagornithidae, rather than maintaining the two families Pelagornithidae and Odontopterygidae. The reason for this is that oversplit taxonomy often complicates the assignment of new specimens to the family level, especially when most species are based on very fragmentary fossils, as is the case for Odontopterygiformes. Indeed, aside from *Dasornis* and *Pelagornis*, odontopterygiform specimens were given a variety of names, such as *Cyphornis magnus* Cope, 1894, *Gigantornis eaglesomei* Andrews, 1916, *Palaeochenoides miocaenus* Shufeldt, 1916, *Tympanonesiotes wetmorei* Hopson, 1964, *Neodontornis stirtoni* (Howard and Warter, 1969), *Caspiodontornis kobystanicus* Aslanova and Burchak-Abramovich, 1982, and no fewer than four species assigned to the genus *Pseudodontornis* Lambrecht, 1930 (Spulski, 1910; Harrison and Walker, 1976; Harrison, 1985; Averianov et al., 1991). Whether some or all of these names are actually synonymous with either *Dasornis* or *Pelagornis* must await a thorough taxonomic revision of the group. At present, the number of species assigned to the Odontopterygiformes remains uncertain, but it is obvious that the number of names proposed in the literature exceeds the number of taxa. However, we maintain the pseudotoothed birds in the Odontopterygiformes, because of their sister-group relationship with Anseriformes (Bourdon, 2005), combined with a highly specialized morphology, which diverges greatly from that of ducks and allies.

Paleoecology and Paleoenvironment of *Dasornis*

The Ouled Abdoun phosphatic deposits correspond to an epicontinental sea that communicated to the West with the Atlantic Ocean (Salvan, 1986; Herbig, 1991; Trappe, 1991). The strong concentration of phosphates in the Moroccan phosphate sea permitted the preservation of an exceptionally rich fauna. Upper Paleocene and Lower Eocene deposits have yielded a huge amount of marine vertebrates (e.g., Arambourg, 1952; Noubhani and Cappetta, 1997; Jalil et al., 2006; Jouve et al., 2008), including seabirds (Bourdon et al., 2008a, 2008b; this study). The strong condensation of the phosphate series in the northeastern margin of the basin indicates the proximity of the shore and is in accordance with the presence of mammals (Gheerbrant et al., 2006; Gheerbrant, 2009; Solé et al., 2009).

The species of *Dasornis*, especially the two larger ones, are very common in the level "Intercalary beds II/I" made of hard phosphatic limestone and dated as lowermost Eocene (fig. 2). This suggests that these seabirds formed large breeding colonies near the shore of the northeastern part of the Ouled Abdoun Sea, some 55 million years ago, as has been hypothesized for the extinct tropicbird *Lithoptila abdounensis* (Bourdon et al., 2008b). Upwellings on the Atlantic margin permitted the formation of Moroccan phosphatic deposits (Lucas and Prévôt-Lucas, 1995). Low-latitude upwelling zones are among the most productives (Ashmole, 1971),

and this may have favored the occurrence of vast seabird breeding colonies.

A large part of the collected specimens are isolated bones, which suggests a postmortem dispersion of bones, with a possible role of marine predators. An important size variation is observed in the postcranial material and skulls referred to *Dasornis toliapica* (tables 1, 2). The smallest Moroccan specimens approximated the size of BMNH 44096 and corresponded to a bird with a 2 m wingspan (that of a small albatross, e.g., *Diomedea nigripes*). The medium-sized specimens, which are the most common, reached a wingspan of around 2.5 m (that of a medium-sized albatross, e.g., *Diomedea cauta*). The largest individuals had a wingspan of about 3 m (that of a large albatross, e.g., *Diomedea epomophora*). The largest specimens are thus approximately 1.5 times larger than the smallest ones. Because these seabirds probably formed large breeding colonies, it is likely that some fragments of long bones pertain to juvenile specimens. Nevertheless, well-preserved specimens belong to adult individuals: epiphyses are fully ossified and sutures are obliterated in available skulls, except for the sutura frontoparietalis (see above).

The presence of several closely related species living in the same environment cannot be excluded given the material at hand. The largest individuals (around 3 m wingspan) could be assigned to *Dasornis oweni* (Harrison and Walker, 1976), initially described as *Macrodontopteryx oweni* by Harrison and Walker (1976) and synonymized here with *D. toliapica*. However, skeletal morphology does not provide evidence for the presence of two species within the *D. toliapica* complex (see above). Secondly, the sizes of braincases and most long bones are continuous between the smallest and the largest specimens, which renders the distinction of two species arbitrary (tables 1, 2). In addition, individual variation and sexual dimorphism can explain size disparity among adults. An important size variation is found, e.g., in *Anseranas semipalmata* (wingspan 125–180 cm, ratio 1.44), *Diomedea exulans* (wingspan 254–351 cm, ratio 1.38) or *Pelecanus onocrotalus* (wingspan 226–360 cm, ratio 1.59) (del Hoyo et al., 1992). Sexual size dimorphism is well known in seabirds, and has been linked to a variety of factors such as sexual selection (Serrano-Meneses and Székely, 2006).

Dasornis emuinus is distinctly larger in size than *D. toliapica* (tables 1, 2). The wingspan of the smallest individuals is approximately 3.5 m, equaling that of a large individual of *D. exulans* (see above). The wingspan of the largest individuals approximates 4.5 m, which is smaller than the estimated winspan for *Osteodontornis orri* (5.5 to 6 m; Olson, 1985). Size variation is less important than in *D. toliapica*, since the largest specimens are approximately 1.3 times larger than the smallest ones. This may be explained by a variety of factors, including sampling bias and relative scarcity of *D. emuinus* with respect to *D. toliapica*. *Dasornis abdoun* is much smaller is size than *D. toliapica*, and constitutes the smallest species of pseudotoothed bird ever discovered. The estimated wingspan is 1.5 to 1.7 m, which is comparable to that of a Northern Gannet (*Sula bassana*).

The morphology of the humerus in *Dasornis* strikingly differs from that of *Pelagornis*/*Osteodontornis* (fig. 25C–L). In *Pelagornis*, the morphological peculiarities of the humerus that are supposedly related to gliding flight are more pronounced than in *Dasornis:* the caput humeri is caudocranially wider; the tuberculum dorsale and tuberculum ventrale are more

prominent and in more proximal position; the crista deltopectoralis is somewhat square in outline and located far distally from the caput. The *Pelagornis* sternum (Mayr et al., 2008) exhibits a more derived morphology than a sternum putatively assigned to *Dasornis* (Mayr and Smith, 2010): it is strongly vaulted and the carina sterni shows a marked cranial projection for the articulation with the furcula. These features probably reduced loadings linked to gigantic size and sustained gliding flight (Mayr et al., 2008). Moreover, *Pelagornis* had relatively shorter and stouter legs than *Dasornis* (especially concerning the tarsometatarsus; fig. 26I, J), and was possibly more clumsy on land. Altogether, these differences suggest that *Dasornis* was less narrowly specialized for soaring flight than *Pelagornis*. Pseudotoothed birds pertaining to the *Dasornis* morphotype were more generalists and could probably use flapping flight, even if limited. In contrast, the *Pelagornis* morphotype included exceedingly specialized gliders which were most likely unable of sustained flapping flight and relied almost entirely on winds to provide lift (Olson, 1985).

Our work provides evidence that *Dasornis* was widespread by the Lower Paleogene, as it is currently known from the Lower Eocene of England (Harrison and Walker, 1976; Mayr, 2008) and Upper Paleocene/Lower Eocene of Morocco (this study). Nessov (1992: fig. 5O, P) described a distal end of ulna from the Upper Paleocene of Kazakhstan. This author suggested anseriform affinities for this ulna, but comparison with our material shows that it belongs to *Dasornis*. The size of the Kazakhstanish ulna matches well with the smallest species described from the Moroccan phosphates, *D. abdoun*, but the latter is represented by too fragmentary material to allow direct comparison. Fragmentary specimens of *Odontopteryx* (a junior synonym of *Dasornis*) have been described from the Lower Eocene of North America (Olson, 1999) and Middle Eocene of Mexico (González-Barba et al., 2002), but these records are tentative. In the current state of knowledge, Middle Eocene remains from Belgium recently described by Mayr and Smith (2010) cannot be assigned confidently to *Dasornis* (see above). *D. toliapica* and *D. emuinus* were present in both the Moroccan phosphates and the London Clay by the Lower Eocene, which is congruent with their paleoecology: both species were pelagic feeders specialized for gliding flight, and could disperse on large territories like extant albatrosses (Diomedeidae). Interestingly, prophaethontid remains have been recorded from exactly the same Lower Paleogene localities as *Dasornis* (Bourdon et al., 2008b).

The Lower Eocene London Clay Formation of southeast England is a succession of marine silty clays and sandy silts that constitute a remnant of a larger depositional area covering much of the North Sea in the early Tertiary (King, 1981; Allison, 1988). Numerous plant remains indicate a subtropical to tropical climate (Reid and Chandler, 1933; Collinson, 1983; Collinson and Hooker, 1987; Poole, 1993). Upper Paleocene deposits from Kazakhstan formed in a shallow bay with a high biological productivity that was connected with upwelling processes (Nessov, 1992). The climate of the Zhylga locality was humid and nearly tropical, with forests and small freshwater or brackish water bays near the shore (Nessov, 1992). Some studies suggest a warm, humid climate and tropical forests near the shore of the Moroccan phosphate sea (Boureau, 1951; Herbig and Gregor, 1990). This is compatible with the discovery of various folivorous mammals such as proboscideans and

hyracoids (Gheerbrant et al., 2003; Gheerbrant, 2009). Moreover, a palynological study of the Moroccan phosphates has shown the uniformity of Moroccan and European floras in the Paleocene and Lower Eocene (Ollivier-Pierre, 1982). In sum, paleoenvironmental studies show that the Ouled Abdoun, London Clay, and Zhylga marine deposits formed in a tropical climate. This is congruent with the fact that avian taxa nowadays restricted to the intertropical zone were found in northern Europe in the Lower Paleogene, as exemplified by the avifaunas from the London Clay and Fur Formation (Dyke, 2001; Kristoffersen, 2001; Dyke and Van Tuinen, 2004; Mayr, 2005, 2009; Lindow and Dyke, 2006; Waterhouse et al., 2008). This could also explain the occurrence of both *Dasornis* and prophaethontids in all three Paleogene localities.

ACKNOWLEDGMENTS

A convention between the MNHN, the OCP, the MEM, the Cadi Ayyad University, and the Chouaîb Doukkali University has permitted the study of the Ouled Abdoun avifauna. We are grateful to the staff of the OCP mining center of Khouribga for their efficient support during field works in the Ouled Abdoun quarries. We thank the MHNL and Rhinopolis Association for permission to study the Ouled Abdoun material deposited in their collections. The AMNH, LACM, MNHN, NHM, and NMNH kindly provided access to their collections. Most of the photographs were taken by D. Serrette and P. Loubry (MNHN). This work has been supported by the Prévost Fund of the MNHN, the NMNH (award for short-term scholars), the Collège de France (Paris) and the AMNH (Chapman Memorial Fund, Department of Ornithology). Cécile Mourer-Chauviré made useful comments on the manuscript.

REFERENCES

Allison, P.A. 1988. Taphonomy of the Eocene London Clay biota. Palaeontology 31: 1079–1100.

Andrews, C.W. 1916. Note on the sternum of a large carinate bird from the (?) Eocene of southern Nigeria. Proceedings of the Zoological Society of London 1916: 519–524.

Arambourg, C. 1952. Les vertébrés fossiles des gisements de phosphates (Maroc, Algérie, Tunisie). Notes et Mémoires du Service Géologique du Maroc 92: 1–372.

Ashmole, N.P. 1971. Sea bird ecology and the marine environment. *In* D.S. Farner and J.R. King (editors), Avian biology. Vol. 1: 223–286. New York: Academic Press.

Aslanova, S.M., and N.I. Burchak-Abramovich. 1982. The first and unique find of the fossil of Perekishkul toothed bird in the territory of USSR and in the Asiatic continent. Izvestiâ Akademii Nauk SSR. Seriâ Biologiceskaâ 8: 406–412.

Aslanova, S.M., and N.I. Burchak-Abramovich. 1999. A detailed description of *Caspiodontornis kobystanicus* from the Oligocene of the Caspian seashore. Acta Zoologica Cracoviensia 42: 423–433.

Averianov, A.O., A.V. Panteleyev, O.R. Potapova, and L.A. Nessov. 1991. Bony-toothed birds (Aves: Pelecaniformes: Odontopterygia) from the Late Paleocene and Eocene of the western margin of ancient Asia. Proceedings of the Zoological Institute, USSR Academy of Sciences 239: 3–12.

Ballmann, P. 1969. Les oiseaux miocènes de la Grive-Saint-Alban (Isère). Geobios 2: 157–204.

Baumel, J.J., A.S. King, J.E. Breazile, H.E. Evans, and J.C. Vanden Berge. 1993. Handbook of avian anatomy: nomina anatomica avium, 2nd ed. Cambridge: Nuttall Ornithological Club, 779 pp.

Bourdon, E. 2005. Osteological evidence for sister group relationship between pseudo-toothed birds (Aves: Odontopterygiformes) and waterfowls (Anseriformes). Naturwissenschaften 92: 586–591.

Bourdon, E. 2006a. A new avifauna from the early Tertiary of the Ouled Abdoun Basin, Morocco: contribution to higher-level phylogenetics of modern birds (Neornithes). Journal of Vertebrate Paleontology 26: 44A.

Bourdon, E. 2006b. L'avifaune du Paléogène des phosphates du Maroc et du Togo: diversité, systématique et apports à la connaissance de la diversification des oiseaux modernes (Neornithes). Unpublished Ph.D. thesis, Muséum National d'Histoire Naturelle, Paris, 330 pp.

Bourdon, E., B. Bouya, and M. Iarochène. 2005. Earliest African Neornithine bird: a new species of Prophaethontidae (Aves) from the Paleocene of Morocco. Journal of Vertebrate Paleontology 25: 157–170.

Bourdon, E., M. Amaghzaz, and B. Bouya. 2008a. A new seabird (Aves, cf. Phaethontidae) from the Lower Eocene phosphates of Morocco. Geobios 41: 455–459.

Bourdon, E., C. Mourer-Chauviré, M. Amaghzaz, and B. Bouya. 2008b. New specimens of *Lithoptila abdounensis* (Aves, Prophaethontidae) from the Lower Paleogene of Morocco. Journal of Vertebrate Paleontology 28: 751–761.

Boureau, E. 1951. Contribution à l'étude paléoxylologique de l'Afrique du Nord (III): *Pterocarpoxylon arambourgii* n. gen., n. sp., bois silicifié de Leguminoseae–Papilioneae découvert dans les phosphates yprésiens de Khouribga (Maroc). Bulletin du Muséum National d'Histoire Naturelle 2e Série 23: 552–557.

Bowerbank, J.S. 1854. On the remains of a gigantic bird (*Lithornis emuinus*) from the London Clay of Sheppey. Annals and Magazine of Natural History 14:263–264.

Butendieck, E., and H. Wissdorf. 1982. Beitrag zur Benennung der Knochen des Kopfes beim Truthuhn (*Meleagris gallopavo*) unter Berücksichtigung der Nomina anatomica Avium (1979). Zoologische Jahrbücher, Abteilung für Anatomie und Ontogenie der Tiere 107: 153–184.

Chavez, M., M. Stucchi, and M. Urbina. 2007. El registro de Pelagornithidae (Aves: Pelecaniformes) y la avifauna neógena del Pacífico sudeste. Bulletin de l'Institut Français d'Études Andines 36: 175–197.

Cheneval, J. 1993. L'Avifaune mio-pliocène de la Formation Pisco (Pérou). Étude Préliminaire. Documents des Laboratoires de Géologie de Lyon 125: 85–95.

Collinson, M.E. 1983. Fossil plants of the London Clay. Palaeontological Association Field Guides to Fossils 1. London: Palaeontological Association, 121 pp.

Collinson, M.E., and J.J. Hooker. 1987. Vegetational and mammalian faunal changes in the early Tertiary of southern England. *In* E.M. Friis, W.G. Chaloner, and P.R. Crane (editors), The origins of angiosperms and their biological consequence: pp. 259–304. Cambridge: Cambridge University Press.

Cope, E.D. 1894. On *Cyphornis*, an extinct genus of birds. Journal of the National Academy of Science of Philadelphia 9: 449–452.

del Hoyo, J., A. Elliott, and J. Sargatal. 1992. Handbook of the birds of the world. Vol. 1: Ostrich to ducks. Barcelona: Lynx Edicions, 696 pp.

Dyke, G.J. 2001. A mousebird (Aves: Coliiformes) from the Eocene of England. Journal für Ornithologie 42: 7–15.

Dyke, G.J., and M. Van Tuinen. 2004. The evolutionary radiation of modern birds (Neornithes): reconciling molecules, morphology and the fossil record. Zoological Journal of the Linnean Society 141: 153–177.

Elzanowski, A. 1987. Cranial and eyelid muscles and ligaments of the tinamous (Aves: Tinamiformes). Zoologische Jahrbücher, Abteilung für Anatomie und Ontogenie der Tiere 116: 63–118.

Elzanowski, A., and P.M. Galton. 1991. Braincase of *Enaliornis*, an early Cretaceous bird from England. Journal of Vertebrate Paleontology 11: 90–107.

Fürbringer, M. 1888. Untersuchungen zur morphologie und systematik der Vögel, zugleich ein Beitrag zur Anatomie der Stütz- und Bewegungsorgane. Amsterdam: Van Holkema, 1751 pp.

Gharbi, A. 1998. Les phosphates marocains. Chroniques de la Recherche Minière 531–532: 127–138.

Gheerbrant, E. 2009. Paleocene emergence of elephant relatives and the rapid radiation of African ungulates. Proceedings of the National Academy of Science of the United States of America 106: 10717–10721.

Gheerbrant, E., et al. 2003. Les localités à mammifères des carrières de Grand Daoui, bassin des Ouled Abdoun, Maroc, Yprésien: premier état des lieux. Bulletin de la Société Géologique de France 174: 279–293.

Gheerbrant, E., M. Iarochène, M. Amaghzaz, and B. Bouya. 2006. Early African hyaenodontid mammals and their bearing on the origin of the Creodonta. Geological Magazine 143: 475–489.

Goedert, J.L. 1989. Giant Late Eocene marine birds (Pelecaniformes: Pelagornithidae) from northwestern Oregon. Journal of Paleontology 63: 939–944.

GoGeometry. 2009. Fossil skull of giant toothy seabird found in Ocucaje, Ica, Peru (http://www.gogeometry.com/incas/peru_fossil_skull_giant_bird.html).

González-Barba, G., J.L. Goedert, and T. Scwennicke. 2004. First record of *Osteodontornis* (Aves: Pelagornithidae) from Mexico. *In* E. Buffetaut and J. Le Leuff (editors), Abstracts of the Sixth International Meeting of the Society of Avian Paleontology and Evolution: p. 26. Quillan.

González-Barba, G., T. Scwennicke, J.L. Goedert, and L.G. Barnes. 2002. Earliest Pacific Basin record of the Pelagornithidae (Aves: Pelecaniformes). Journal of Vertebrate Paleontology 22: 722–725.

Harrison, C.J.O. 1985. A bony-toothed bird (Odontopterygiformes) from the Palaeocene of England. Tertiary Research 7: 23–25.

Harrison, C.J.O., and C.A. Walker. 1976. A review of the bony-toothed birds (Odontopterygiformes): with description of some new species. Tertiary Research Special Paper 2: 1–62.

Harrison, C.J.O., and C.A. Walker. 1977. Birds of the British Lower Eocene. Tertiary Research Special Paper 3: 1–63.

Harrison, C.J.O., and C.A. Walker. 1979. Birds of the British Lower Oligocene. Tertiary Research Special Paper 5: 29–43.

Hasegawa, Y., K. Ono, and Y. Koda. 1986. Odontopterygid bird from the Oligocene Iwaki Group. Abstracts of the Annual Meeting of the Palaeontological Society of Japan: 24.

Herbig, H.-G. 1991. Das marine Paläogen am Südrand des Zentralen Hohen Atlas und im Mittleren Atlas Marokkos. Stratigraphie, Fazies, Paläogeographie und Paleotektonik. Berliner Geowissenschaftliche Abhandlungen, A 135: 1–289.

Herbig, H.G., and H.J. Gregor. 1990. The mangrove-forming palm *Nypa* from the early Paleogene of southern Morocco. Paleoenvironment and paleoclimate. Géologie Méditerranéenne 17: 123–137.

Hopson, J.A. 1964. *Pseudodontornis* and other large marine birds from the Miocene of South Carolina. Postilla 83: 1–19.

Howard, H. 1929. The avifauna of Emeryville Shellmound. University of California Publications in Zoology 32: 301–394.

Howard, H. 1957. A gigantic "toothed" marine bird from the Miocene of California. Bulletin of the Department of Geology of the Santa Barbara Museum of Natural History 1: 1–23.

Howard, H. 1978. Late Miocene marine birds from Orange County, California. Contributions in Science

290: 1–25.
Howard, H., and J.A. White. 1962. A second record of *Osteodontornis*, Miocene "toothed" bird. Los Angeles County Museum Contributions in Science 52: 1–12.
Howard, H., and S.L. Warter. 1969. A new species of bony-toothed bird (Family Pseudodontornithidae) from the Tertiary of New Zealand. Records of the Canterbury Museum 8: 345–357.
Jalil, N.-E., et al. 2006: Les vertébrés fossiles des phosphates du Maroc. Nouvelle convention et état des connaissances. The Second International Conference on the Valorization of Phosphates and Phosphorus Compounds, Marrakech, Morocco.
Jouve, S., B. Bouya, and M. Amaghzaz. 2008. A long-snouted dyrosaurid (Crocodyliformes, Mesoeucrocodylia) from the Paleocene of Morocco: phylogenetic and palaeobiogeographic implications. Palaeontology 51: 281–294.
King, C. 1981. The stratigraphy of the London Clay and associated deposits. Tertiary Research Special Paper 6: 1–158.
Kristoffersen, A.V. 2001. An early Paleogene trogon (Aves: Trogoniformes) from the Fur Formation, Denmark. Journal of Vertebrate Paleontology 22: 661–666.
Lambrecht, K. 1930. Studien über fossile Riesenvögel: I. *Pseudodontornis* n. g. Geologica Hungarica. Series Palaeontologica 7: 1–17.
Lambrecht, K. 1933. Handbuch der Palaeornithologie. Berlin: Gebrüder Borntraeger, 1024 pp.
Lartet, E. 1857. Note sur un humérus fossile d'oiseau, attribué à un très grand palmipède de la section des Longipennes. Compte Rendu Hebdomadaire des Séances de l'Académie des Sciences 44: 736–741.
Lindow, B.E.K., and G.J. Dyke. 2006. Bird evolution in the Eocene: climate change in Europe and a Danish fossil fauna. Biological Reviews 81: 483–499.
Livezey, B.C., and R.L. Zusi. 2006. Higher-order phylogeny of modern birds (Theropoda, Aves: Neornithes) based on comparative anatomy. I. Methods and characters. Bulletin of the Carnegie Museum of Natural History 37: 1–556.
Lucas, J., and L. Prévôt-Lucas. 1995. Tethyan phosphates and bioproductites. *In* A.E.M. Nairn and F.G. Stehli (editors), The ocean basins and margins. Vol. 8: The Tethys Ocean: 367–391. New York: Plenum Press.
Lydekker, R. 1891. Catalogue of the fossil birds in the British Museum (Natural History). London: British Museum (Natural History), 368 pp.
Matsuoka, H., F. Sakakura, and F. Ohe. 1998. A Miocene pseudodontorn (Pelecaniformes: Pelagornithidae) from the Ichishi Group of Misato, Mie Prefecture, central Japan. Paleontological Research 2: 246–252.
Mayr, G. 2005. The Paleogene fossil record of birds in Europe. Biological Reviews 80: 515–542.
Mayr, G. 2008. A skull of the giant bony-toothed bird *Dasornis* (Aves: Pelagornithidae) from the Lower Eocene of the Isle of Sheppey. Palaeontology 51: 1107–1116.
Mayr, G. 2009. Paleogene fossil birds. Berlin: Springer, 262 pp.
Mayr, G., C.J. Hazevoet, P. Dantas, and M. Cachao. 2008. A sternum of a very large bony-toothed bird (Pelagornithidae) from the Miocene of Portugal. Journal of Vertebrate Paleontology 28: 762–769.
Mayr, G., and T. Smith. 2010. Bony-toothed birds (Aves: Pelagornithidae) from the Middle Eocene of Belgium. Palaeontology 53: 365–376.
McKee, J.W.A. 1985. A pseudodontorn (Pelecaniformes: Pelagornithidae) from the Middle Pliocene of Hawera, Taranaki, New Zealand. New Zealand Journal of Zoology 12: 181–184.
Milner, A.C., and S.A. Walsh. 2009. Avian brain evolution: new data from Palaeogene birds (Lower Eocene) from England. Zoological Journal of the Linnean Society 155: 198–219.

Mourer-Chauviré, C., and D. Geraads. 2008. The Struthionidae and Pelagornithidae (Aves: Struthioniformes, Odontopterygiformes) from the late Pliocene of Ahl al Oughlam, Morocco. Oryctos 7: 169–194.

Nessov, L.A. 1992. Mesozoic and Paleogene birds of the USSR and their paleoenvironments. *In* K.E. Campbell (editor), Papers in avian paleontology honoring Pierce Brodkorb. Natural History Museum of Los Angeles County, Science Series 36: 465–478.

Noubhani, A., and H. Cappetta. 1997. Les Orectolobiformes, Carcharhiniformes et Myliobatiformes (Elasmobranchii, Neoselachii) des bassins à phosphate du Maroc (Maastrichtien-Lutétien basal). Systématique, biostratigraphie, évolution et dynamique des faunes. Palaeo Ichthyologica 8: 1–327.

Office Chérifien des Phosphates. 1989. The phosphate basins of Morocco. *In* A.J.G. Notholt, R. P. Sheldon, and D.F. Davidson (editors), Phosphate deposits of the world. Vol. 2: Phosphates rock resources: 301–311. Cambridge: Cambridge University Press.

Okazaki, Y. 1989. An occurence of fossil bony-toothed bird (Odontopterygiformes) from the Ashiya Group (Oligocene), Japan. Bulletin of the Kitakyushu Museum of Natural History 9: 123–126.

Ollivier-Pierre, M.-F. 1982. La microflore du Paléocène et de l'Eocène des séries phosphatées des Ganntour (Maroc). Sciences Géologiques, Bulletin 35: 117–127.

Olson, S.L. 1984. A brief synopsis of the fossil birds from the Pamunkey River and other Tertiary marine deposits in Virginia. *In* L.W. Ward and K. Krafft (editors), Stratigraphy and paleontology of the outcropping Tertiary beds in the Pamunkey River region, central Virginia coastal plain—Guidebook for Atlantic Coastal Plain Geological Association 1984 field trip: 217–223. Norfolk: Atlantic Coastal Plain Geological Association.

Olson, S.L. 1985. The fossil record of birds. *In* D.S. Farner, J.R. King, and K.C. Parkes (editors), Avian biology. Vol. 8: 79–256. New York: Academic Press.

Olson, S.L. 1999. Early Eocene birds from eastern North America: a faunule from the Nanjemoy Formation of Virginia. *In* R.E. Weems and G.J. Grimsley (editors), Early Eocene vertebrates and plants from the Fisher/Sullivan site (Nanjemoy Formation) Stafford County, VA. Virginia Division of Mineral Resources Publication 152: 123–132.

Olson, S.L., and P.C. Rasmussen. 2001. Miocene and Pliocene birds from the Lee Creek Mine, North Carolina. Smithsonian Contributions to Paleobiology 90: 233–365.

Ono, K. 1989. A bony-toothed bird from the Middle Miocene, Chichibu Basin, Japan. Bulletin of the National Science Museum of Tokyo, Series C (Geology) 15: 33–38.

Ono, K., Y. Hasegawa, and T. Kawakami. 1985. Part IV. First record of the Pliocene bony-toothed bird (Odontopterygiformes) from Japan. Bulletin of the Iwate Prefectural Museum 3: 155–157.

Owen, R. 1870. On *Dinornis* (Part XIV), containing contributions to the craniology of the genus, with a description of a fossil cranium of *Dasornis londinensis* Ow., from the London Clay of Sheppey. Transactions of the Zoological Society of London 7: 123–150.

Owen, R. 1873. Description of the skull of a dentigerous bird (*Odontopteryx toliapicus*, Ow.) from the London Clay of Sheppey. Quarterly Journal of the Geological Society of London 29: 511–522.

Poole, I. 1993. A dipterocarpaceous twig from the Eocene London Clay Formation of southeast England. Special Papers in Palaeontology 49: 155–163.

Rasmussen, P.C. 1998. Early Miocene avifauna from the Pollack Farm site, Delaware. *In* R.N. Benson (editor), Geology and paleontology of the Lower Miocene Pollack Farm fossil site, Delaware: 149–151: Delaware Geological Survey Special Publication.

Reid, E.M., and M.E.J. Chandler. 1933. The Flora of the London Clay. London: British Museum (Natural History), 561 pp.

Rincón, A.D., and M. Stucchi. 2003. Primer registro de la familia Pelagornithidae (Aves: Pelecaniformes) para Venezuela. Boletín de la Sociedad Venezolana de Espeleología 37: 27–30.

Salvan, H.M. 1986. Géologie des gîtes minéraux marocains. Vol. 3: Phosphates. Notes et Mémoires du Service Géologique du Maroc 276: 1–392.

Scarlett, R.J. 1972. Bone of a presumed odontopterygian bird from the Miocene of New Zealand. Journal of Geology and Geophysics 15: 269–274.

Serrano-Meneses, M.-A., and T. Székely. 2006. Sexual size dimorphism in seabirds: Sexual selection, fecundity selection and differential niche-utilization. Oikos 113: 385–394.

Shufeldt, R.W. 1916. New extinct bird from South Carolina. Geological Magazine 6: 343–347.

Solé, F., E. Gheerbrant, M. Amaghzaz, and B. Bouya. 2009. Further evidence of the African antiquity of hyaenodontid ('Creodonta', Mammalia) evolution. Zoological Journal of the Linnean Society 156: 827–846.

Spulski, B. 1910. *Odontopteryx longirostris* n. sp. Zeitschrift der Deutschen geologischen Gesellschaft 62: 507–524.

Stidham, T.A. 2004. New skull material of *Osteodontornis orri* (Aves: Pelagornithidae) from the Miocene of California. PaleoBios 24: 7–12.

Stilwell, J.D., C.M. Jones, R.H. Levy, and D.M. Harwood. 1998. First fossil bird from East Antarctica. Antarctic Journal 23: 12–16.

Tambussi, C.P., and C. Acosta Hospitaleche. 2007. Antarctic birds (Neornithes) during the Cretaceous-Eocene times. Revista de la Asociación Geológica Argentina 62: 604–617.

Tonni, E.P. 1980. Un pseudodontornítido (Pelecaniformes, Odontopterygia) de gran tamaño, del Terciario de Antártida. Ameghiniana 17: 273–276.

Tonni, E.P., and C.P. Tambussi. 1985. Nuevos restos de Odontopterygia (Aves: Pelecaniformes) del Terciario temprano de Antártida. Ameghiniana 21: 121–124.

Trappe, J. 1991. Stratigraphy, facies distribution and paleogeography of the marine Paleogene from the Western High Atlas, Morocco. Neues Jahrbuch für Geologie und Paläontologie, Monatshefte 180: 279–321.

Walsh, S.A., and J.P. Hume. 2001. A new Neogene marine avian assemblage from North-Central Chile. Journal of Vertebrate Paleontology 21: 484–491.

Waterhouse, D.W., B.E.K. Lindow, N. Zelenkov, and G.J. Dyke. 2008. Two new fossil parrots (Psittaciformes) from the Lower Eocene Fur Formation of Denmark. Palaeontology 51: 575–582.

Weber, E. 1996. Das Skelet-Muskel-System des Kieferapparates von *Aepypodius arfakianus* (Salvadori, 1877) (Aves, Megapodiidae). Courier Forschungsinstitut Senckenberg 189: 1–132.

Wetmore, A. 1917. The relationships of the fossil bird *Palaeochenoides miocaenus*. Journal of Geology 15: 555–557.

Zusi, R.L., and B.C. Livezey. 2000. Homology and phylogenetic implications of some enigmatic cranial features in galliform and anseriform birds. Annals of the Carnegie Museum 69: 157–193.

APPENDIX

Anatomical Abbreviations

Cranium: **AMEart**, impressio musculi adductoris mandibulae externus pars articularis; **AMEco**, impressio musculi adductoris mandibulae externus pars coronoidea; **apa**, ala parasphenoidalis; **asu**, groove for arteria supraorbitalis; **bpl**, base of processus lateralis parasphenoidalis; **cbn**, caudal border of nasal cavity; **ccc**, canalis caroticus cranialis; **ccqo**, continuation of cotyla quadratica otici; **ccqs**, continuation of cotyla quadratica squamosi; **cif**, crista interfenestralis; **cns**, crista nuchalis sagittalis; **cnt**, crista nuchalis transversa; **co**, condylus occipitalis; **corb**, crista orbitalis; **cq**, rostral continuation of the cotylae quadratica; **cqo**, cotyla quadratica otici; **cqs**, cotyla quadratica squamosi; **ct**, crista temporalis; **cte**, crista tentorialis; **cty**, cavum tympanicum; **dcc**, depression for concha caudalis; **df**, depressio frontalis; **DM**, impressio musculi depressoris mandibulae; **ds**, dorsum sellae; **ea**, eminentia arcuata; **f3**, foramen nervi oculomotorii; **f5**, foramen nervi opthalmici; **f6**, foramen nervi abducentis; **f7**, foramen nervi facialis; **f9**, foramen nervi glossopharyngealis; **f10**, foramen nervi vagi; **f12**, foramen nervi hypoglossi; **f12i**, canalis nervi hypoglossi; **fac**, fossa auriculae cerebelli; **fai**, fossa acustica interna; **faoi**, foramen arteriae ophthalmicae internae; **fco**, fenestra cochleae; **fgt**, fossa ganglii trigemini; **fgvg**, fovea ganglii vagoglossopharyngealis; **fh**, fossa hypophysialis; **fin**, fonticulus interorbitalis; **fm**, foramen magnum; **fmo**, fossa medullae oblongatae; **fnm**, foramen nervi maxillomandibularis; **fop**, foramen opticum; **for**, fonticulus orbitocranialis; **forb**, foramen orbitale; **fpc**, foramen pneumaticum caudale; **fpd**, foramen pneumaticum dorsale; **fsc**, fossa subcondylaris; **ftm**, fossa tecti mesencephali; **fv**, fenestra vestibuli; **hg**, groove for nervus hyomandibularis; **La**, os lacrimale; **lbla**, lateral border of os lacrimale; **lbtr**, lateral border of temporal region; **lh**, laterosphenoid hollow; **lpa**, lamina parasphenoidalis; **lppm**, lateral pit of processus medialis parasphenoidalis; **Me**, os mesethmoidale; **mr**, median ridge of rostrum parasphenoidale; **occ**, ostium canalis carotici; **oeme**, outer edge of os mesethmoidale; **oph**, ostium pharyngeale; **orl**, origin of musculus rectus lateralis; **oty**, ostium tympanicum; **pc**, prominentia cerebellaris; **pf**, pneumatic foramen; **pil**, pila otica; **plo**, prominentia lobi optici; **plp**, processus lateralis parasphenoidalis; **pmp**, processus medialis parasphenoidalis; **por**, processus orbitalis; **ppa**, processus paroccipitalis; **ppo**, processus postorbitalis; **pro**, processus rostropterygoideus; **PS**, impressio musculi pseudotemporalis superficialis; **psu**, processus supraorbitalis; **pte**, protuberantia tentorialis; **raoe**, foramen rami occipitalis arteriae ophthalmicae externae; **rc**, recessus columellae; **rc-rtr**, ridge separating recessus columellae and recessus tympanicus rostralis; **rpa**, rostrum parasphenoidale; **rppm**, rostral pit of processus medialis parasphenoidalis; **rtr**, recessus tympanicus rostralis; **sfp**, sutura frontoparietalis; **si**, septum interorbitale; **slf**, semilunar facet of processus paroccipitalis; **sno**, sulcus nervi olfactorii; **sr**, septal ridge; **suc**, supraoccipital convexity; **svs**, sulcus venae semicircularis; **ta**, tuba auditiva; **trz**, triangular zone at the base of maxilla; **tstr**, transverse striations; **voe**, foramen venae occipitalis externae; **zfc**, zona flexoria craniofacialis; **zt**, zygomatic tubercle.

Maxilla and os palatinum: **chPal**, pars choanalis of os palatinum; **cpr**, central palatal region; ctom, crista tomialis; **igr**, interpalatal groove; **lgmx**, lateral groove of maxilla; **lpg**, lateral palatal groove; **max**, maxilla; **nos**, apertura nasi ossea; **Pal**, os palatinum; **pmPal**, processus maxillaris of os palatinum; **pseu**, pseudotooth; **ptPal**, processus pterygoideus of os palatinum.

Mandibula: **ctom**, crista tomialis; **lgmd**, lateral groove of mandibula; **mgmd**, medial groove of mandibula; **pseu**, pseudotooth.

Coracoideum: **am**, angulus medialis; **cs**, cotyla scapularis; **fp**, pneumatic foramen; **mm**, margo medialis; **pp**, processus procoracoideus; **smfac**, sternal margin of facies articularis clavicularis.

Humerus: **bp**, bicipital prominence; **c**, caput humeri; **cd**, crista deltopectoralis; **cdd**, condylus dorsalis; **cdv**, condylus ventralis; **croc**, cranial overhang of caput humeri; **cvf**, crus ventrale fossae; **dr**, dorsal

ridge surrounding the area of origin of musculus extensor carpi ulnaris; **ec**, origin of musculus extensor carpi ulnaris; **ed**, epicondylus dorsalis; **ev**, epicondylus ventralis; **fb**, fossa musculi brachialis; **fc**, origin of musculus flexor carpi ulnaris; **fn**, foramen nutritium; **fpd**, distal foramen pneumaticum; **fpp**, proximal foramen pneumaticum; **ft**, fossa tricipitalis; **i**, intumescentia humeri; **ic**, impressio coracobrachialis; **ii**, incisura intercondylaris; **ip**, impressio musculi pectoralis; **lcv**, surface of attachment of ligamentum collaterale ventrale; **lldd**, distal part of linea musculi latissimi dorsi; **lldp**, proximal part of linea musculi latissimi dorsi; **pf**, processus flexorius; **st**, sulcus transversus; **td**, tuberculum dorsale; **tv**, tuberculum ventrale.

Ulna: **ccsi**, cranial continuation of sulcus intercondylaris; **cd**, condylus dorsalis; **ci**, crista intercotylaris; **cod**, cotyla dorsalis; **cov**, cotyla ventralis; **crpcv**, cranial prominence of condylus ventralis; **dr**, depressio radialis; **edu**, extremitas distalis ulnae; **fn**, foramen nutritium; **ib**, impressio musculi brachialis; **ist**, impressio musculi scapulotricipitalis; **it**, incisura tendinosa; **li**, linea intermuscularis of facies cranialis; **mr**, depression for attachment of meniscus radioulnaris; **o**, olecranon; **pctc**, proximal continuation of tuberculum carpale; **pecv**, pointed extremity of condylus ventralis; **prc**, papillae remigales caudales; **prv**, papillae remigales ventrales; **si**, sulcus intercondylaris; **tc**, tuberculum carpale; **tlcv**, tuberculum ligamenti collateralis ventralis; **vpcov**, ventral prominence of cotyla ventralis.

Radius: **cdg**, caudodorsal groove; **ch**, cotyla humeralis; **ct**, caput radii; **dc**, dorsal convexity; **dr**, dorsal ridge; **edr**, extremitas distalis radii; **fn**, foramen nutritium; **licr**, linea intermuscularis of facies cranialis; **lp**, ligamental prominence; **tav**, tuberculum aponeurosis ventralis; **tb**, tuberculum bicipitale; **vo**, ventral overhang; **vt**, ventral tubercle.

Carpometacarpus: **cbtc**, caudal border of trochlea carpalis; **cefadM**, caudal extremity of facies articularis digitalis major; **dwst**, distal widening of sulcus tendinosus; **fadM**, facies articularis digitalis major; **fadm**, facies articularis digitalis minor; **fcc**, fovea carpalis caudalis; **lrmd**, surface of attachment of ligamentum radiocarpo-metacarpale dorsale; **oma**, os metacarpale alulare; **pfadM**, caudal prominence of facies articularis digitalis major; **pp**, processus pisiformis; **si**, sulcus interosseus; **smd**, symphysis metacarpalis distalis; **vpm3**, ventral protuberance of os metacarpale minus; **vr**, ventral ridge.

Femur: **lca**, linea intermuscularis caudalis; **lcr**, linea intermuscularis cranialis; **tf**, triangular facet; **tgl**, tuberculum musculi gastrocnemialis lateralis.

Tibiotarsus: **cf**, crista fibularis; **cl**, condylus lateralis; **cm**, condylus medialis; **ctr**, cristae trochleae; **faf**, facies articularis fibularis; **fal**, facies articularis lateralis; **ilcm**, impressio ligamenti collateralis medialis; **lf**, lineae musculi fibularis; **sf**, sulcus musculi fibularis; **tp**, tuberositas poplitea; **trel**, lateral tuberositas retinaculi extensori; **trem**, medial tuberositas retinaculi extensori.

Tarsometatarsus: **ch**, canalis hypotarsi; **clh**, crista lateralis hypotarsi; **cmh**, crista medialis hypotarsi; **cmp**, crista medianoplantaris; **cpl**, crista plantaris lateralis; **cpm**, crista plantaris medialis; **eet2**, external edge of trochlea metatarsi II; **eet4**, external edge of trochlea metatarsi IV; **ei**, eminentia intercotylaris; **fvd**, foramen vasculare distale; **h**, hypotarsus; **ppcm**, plantar prominence of cotyla medialis; **ppt2**, plantar process of trochlea metatarsi II; **ppt4**, plantar process of trochlea metatarsi IV; **sh**, sulcus hypotarsi; **sl**, sulcus ligamentosus; **t2**, trochlea metatarsi II; **t3**, trochlea metatarsi III; **t4**, trochlea metatarsi IV; **tfb**, tuberculum musculi fibularis brevis; **ttc**, tuberositas musculi tibialis cranialis.

Complete lists of all issues of *Novitates* and *Bulletin* are available on the web (http://digitallibrary.amnh.org/dspace). Inquire about ordering printed copies via e-mail from scipubs@amnh.org or via standard mail from:

American Museum of Natural History—Scientific Publications
Central Park West at 79th Street
New York, NY 10024

♾ This paper meets the requirements of ANSI/NISO Z39.48-1992 (permanence of paper).